Physiological Functions of Acyl-CoA: Monoacylglycerol Acyltransferase

by

Ting-Ni Huang

A dissertation submitted in partial fulfillment of
the requirements for the degree of

Doctor of Philosophy

(Nutritional Sciences)

at the

University of Wisconsin-Madison

2017

Date of final oral examination: 8/16/2017

The dissertation is approved by the following members of the Final Oral Committee:

Caroline Alexander, Professor, Oncology
Guy Groblewski, Professor, Nutritional Sciences
Laura Hernandez, Associate Professor, Dairy Science
Linda Schuler, Professor, Comparative Biosciences
Eric Yen, Associate Professor, Nutritional Sciences

Abstract

Mogat1 and *Mogat2* are cloned based on their sequence homology with acyl-CoA: diacylglycerol acyltransferase 2 (DGAT2), and they belong to a gene family of 7 members, including *Mogat3.* Enzymes encoded by *Mogat1*, *Mogat2,* and *Mogat3* are shown to exhibit acyl-CoA: monoacylglycerol acyltransferase activity *in vitro*, catalyzing the synthesis of diacylglycerol, the precursor of triacylglycerol; thus, they are named MGAT1, MGAT2, and MGAT3, respectively. Whereas *Mogat3* is a pseudogene not expressed in mice, *Mogat1* and *Mogat2* are expressed in both humans and mice. MGAT2 is highly expressed in the small intestine, where it mediates the absorption of dietary fat. Mice lacking MGAT2 show changes in the kinetics, but not the quantity of fat absorption. These mice have increased energy expenditure and are protected from diet- and genetically induced obesity. The physiological functions of MGAT1, on the other hand, are not clear. In this dissertation, I used genetically engineered mice to explore the physiological roles of MGAT1 in systemic energy metabolism and the roles of MGAT2 in female reproduction and mammary gland functions. Unexpectedly, I found that *Mogat1* and *Mogat2* play divergent roles in systemic energy metabolism. While *Mogat2* deficiency increases energy expenditure and protects mice from metabolic disorders, *Mogat1* deficiency reduces energy expenditure and promotes adiposity in response to excess calories. Mice lacking *Mogat1* have normal thermogenic brown adipose tissue; their decreases in energy expenditure are associated with increased thermal insulation in a cold environment or decreased physical activity at room temperature and thermoneutrality. In addition, I found that MGAT2 is specifically required for female reproduction and milk synthesis. Loss of MGAT2 in females reduces the rate in achieving or carrying a pregnancy to term. MGAT2 deficient dams also have prolonged gestation, smaller litter size, and a high neonatal mortality in their offspring. Those MGAT2 deficient dams that deliver and nurse pups successfully have reduced milk

quality and quantity. These studies uncover novel functions of MGAT1 and MGAT2 and open new areas of research in lipid metabolism.

Table of Contents

Chapter 1. Physiological functions of lipid metabolism mediated by acyl-CoA: monoacylglycerol acyltransferases

Triacylglycerol (TAG) is the most energy rich nutrient in the body and plays a pivotal role in cellular and systemic metabolism. TAG synthesis in cells is essential for multiple processes including, but not limited to, dietary fat absorption, lipid droplet formation, and milk fat production. Acyl-CoA: monoacylglycerol acyltransferase (MGAT) uses monoacylglycerol (MAG) and fatty acyl-CoA to synthesize diacylglycerol (DAG), the precursor of TAG. Two isoforms of genes coding for MGAT, *Mogat1* and *Mogat2*, show differential tissue expression and divergent functions in mice where transgenic studies indicate *Mogat1* deficiency promotes adiposity while *Mogat2* deficiency protects mice from metabolic disorders in response to excess calories. As this thesis investigates potential roles of *Mogat1* in promoting adiposity and *Mogat2* in the processes of parturition and milk fat synthesis in mice, this chapter provides a comprehensive overview of what is known of the potential role of TAG metabolism and the *Mogat* genes in regulating these processes.

Physiological functions of acyl-CoA: monoacylglycerol acyltransferase (MGAT)

Acyl-CoA: monoacylglycerol acyltransferase (MGAT) catalyzes one of the major triacylglycerol (TAG) synthesis pathways, using monoacylglycerol (MAG) and fatty acyl-CoA to synthesize diacylglycerol (DAG), the precursor of TAG. MGAT is well-characterized for dietary fat absorption in the enterocytes, where it resynthesizes TAG for chylomicron secretion using sn-2 MAG and fatty acids, which are digested from dietary fat in the intestinal lumen by pancreatic lipase (Fig 1-1 (Yen and Farese, 2003)).

Discovery of Mogat genes and identification of their MGAT activity

Mogat1 and *Mogat2* were cloned based on their sequence homology with acyl-CoA: diacylglycerol acyltransferase (DGAT) 2. They are part of the gene family that includes *Mogat3* and wax synthases. However, *Mogat* coded enzymes, produce far less TAG than *Dgat* coded enzymes, when using oleoyl-CoA or DAG as a substrate (Cheng et al., 2003; Yen and Farese, 2003; Yen et al., 2002). Instead, they mainly produce DAG when using oleoyl-CoA or MAG as a substrate. *Mogat* coded enzymes exhibit increased MGAT activity depending on the level of the gene expressed as well as the concentration of the substrates (Cheng et al., 2003; Yen and Farese, 2003; Yen et al., 2002). *Mogat1* and *Mogat2*, the original DGAT candidates, were therefore identified as MGAT.

Most of the genes within the DGAT2 family exhibit more than one acyltransferase activities *in vitro* (Yen et al., 2005). *Mogat1* and *Mogat2* coded enzymes not only catalyze MGAT activity but also some DGAT activity (Yen et al., 2005; Yen et al., 2002). *Mogat1*, additionally, exhibits weak but detectable acyl-CoA: fatty acyl alcohol acyltransferase (wax synthase) and acyl-CoA: retinol acyltransferase (ARAT) activities (Yen et al., 2005). Both *Mogat1* and *Mogat2* preferentially exhibit MGAT activity on MAG containing the fatty acyl moiety at the sn-2 position, although the activity is detected on sn-1 and sn-3 MAG (Yen and Farese, 2003; Yen et al., 2002). In addition, both *Mogats* prefer MAG and fatty acyl-CoA containing long chain unsaturated fatty acids rather than long chain saturated fatty acids (Yen and Farese, 2003).

Tissue expression patterns of Mogat genes

Mogat1-Mogat3 genes are expressed in both humans and rodents (Cao et al., 2003a; Cao et al., 2003b; Cheng et al., 2003; Yen and Farese, 2003; Yen et al., 2002; Yue et al., 2011).

However, these genes exhibit different tissue expression patterns. In humans, *Mogat1* is expressed in liver and kidney (Yen and Farese, 2003). *Mogat2* is highly detected in liver, small intestine, colon, stomach, and kidney (Yen and Farese, 2003). *Mogat3* is present in the gastrointestinal tract with the highest level found in the ileum (Cheng et al., 2003). In mice, *Mogat1* is detected mainly in stomach and kidney, with a relatively lower level in white adipose tissue (WAT), brown adipose tissue (BAT), liver, and uterus, but not in small intestine (Yen et al., 2002). *Mogat2* is highly expressed in small intestine (Yen et al., 2009; Yen and Farese, 2003), with a much lower level in stomach, kidney, and BAT (Yen et al., 2009). *Mogat3* is expressed in humans and rats and is likely involved in lipid metabolism in the intestine, where it is expressed (Cheng et al., 2003; Yue et al., 2011). *Mogat3* is not expressed in mice and thus not examined in this dissertation.

Implication of Mogat1 in hepatic lipid metabolism

Hepatic expression of *Mogat1* mRNA is induced in several mouse models of fatty liver disease, including diet-induced obesity (Lee et al., 2012), lipodystrophic *Agpat2*$^{-/-}$ (Cortés et al., 2009), leptin deficient *ob/ob* (Agarwal et al., 2016), and mice with alcoholic-induced hepatic steatosis (Yu et al., 2016). Therefore, *Mogat1* has been proposed to be involved in hepatic lipogenesis. Inactivation of *Mogat1* gene might be of potential in the treatment for hepatic steatosis. However, inactivation of *Mogat1* using different strategies on different mouse models exhibit inconsistent results. Lee et al. and Yu et al. reported that *Mogat1* mRNA induced by liver PPARγ is critical for the development of non-alcoholic (Lee et al., 2012) and alcoholic fatty livers (Yu et al., 2016), respectively. Knocking down *Mogat1* in mice using short hairpin RNA after 12 weeks of high fat feeding improves glucose metabolism, alleviates hepatic steatosis, and

reduces diet-induced obesity (Lee et al., 2012). Knocking down *Mogat1* in mice using short hairpin RNA after 3 weeks of ethanol diet also suppresses alcohol-induced hepatic steatosis (Yu et al., 2016). Hall et al. reported that knocking down *Mogat1* in mice using anti-sense oligonucleotide after 14 weeks of high fat feeding or in 6 week-old *ob/ob* mice improves glucose metabolism and hepatic insulin signaling, but not hepatic steatosis or obesity (Hall et al., 2014). Agarwal et al., however, reported that global *Mogat1* deletion does not ameliorate hepatic steatosis in either *Agpat2*$^{-/-}$ or *ob/ob* mice, and has no effects on their body weight or glucose metabolism (Agarwal et al., 2016). Interestingly, the MGAT activity tested on either *Agpat2*$^{-/-}$ or *Mogat1* deficient *Agpat2*$^{-/-}$ mice is not different compared to wild-type despite the difference of *Mogat1* mRNA expression (Agarwal et al., 2016). Therefore, both physiological significance of *Mogat1* and the biochemical reaction it catalyzes *in vivo* remains unclear.

Physiological function of Mogat2 in intestinal fat absorption

While *Mogat1* is not expressed in the small intestine and *Mogat3* is a pseudogene in mice, *Mogat2* is believed to be the isoform responsible for the highest MGAT activity detected in the mouse small intestine for dietary fat absorption. Indeed, mice lacking a functional *Mogat2* gene have greatly reduced intestinal MGAT activity (Yen et al., 2009). These mice show delayed fat absorption (Yen et al., 2009) and increased energy expenditure (Nelson et al., 2011; Yen et al., 2009). Consequently, they are protected from diet-induced obesity (Nelson et al., 2011; Yen et al., 2009) and related comorbidities (Yen et al., 2009).

The physiological function of *Mogat2* in tissues other than small intestine is not clear. Mouse models targeting *Mogat2* specifically in the small intestine imply that extra-intestinal *Mogat2* may modulate energy metabolism. Intestinal specific *Mogat2* deficient mice do not have the

same levels of increased energy expenditure and protection from obesity as global deficient *Mogat2* mice (Nelson et al., 2014). Re-introducing intestinal MGAT activity in global *Mogat2* deficient mice by expression of the human *MOGAT2* gene does not exhibit a sufficient level of recovery in metabolic efficiency and weight gain as control mice (Gao et al., 2013).

Potential physiological functions of Mogats

MGAT activity has been reported in tissues where degradation and re-synthesis of TAG are prominent, such as WAT in migratory birds (Mostafa et al., 1994). Migratory birds hydrolyze fat from adipose tissues for β-oxidation as a fuel for flight muscles, and resynthesize fat using essential fatty acids to sustain reproduction after the spring migration (Mostafa et al., 1994). This is consistent with the finding that *Mogat* encoded enzymes preferentially use unsaturated long chain fatty acids for TAG esterification *in vitro* (Yen and Farese, 2003).

Physiological role of TAG metabolism and adiposity

TAG is synthesized and stored as the main lipid in adipose tissues, where its metabolism is associated with systemic energy balance. When calories are consumed in excess, TAG synthesis is increased; whereas TAG is mobilized when energy is needed. Significant increases in adipose tissue size, termed adiposity, may eventually affect systemic energy metabolism and can lead to an array of chronic diseases.

TAG metabolism

TAG esterification includes the glycerol-3-phosphate (G3P) and MAG pathways (Fig 1-2 (Coleman and Mashek, 2011)). The G3P pathway, identified by Kennedy more than 50 years ago (Kennedy, 1961), exists in most mammalian cell types. G3P is mainly synthesized from the glycolysis intermediate, dihydroxyacetone phosphate (DHAP). The initial reaction uses G3P, catalyzed by glycerol-3-phosphate acyltransferase (GPAT), to produce lysophosphatidic acid (LPA). LPA can also be synthesized from the acylated DHAP. It is further esterified by 1-acylglycerol-3-phosphate acyltransferase (AGPAT) to produce phosphatidic acid (PA). PA is then hydrolyzed by lipin, the PA phosphatase (PAP), to form DAG. DAG esterification is catalyzed by DGAT as the final step in TAG synthesis.

TAG degradation, or lipolysis, is a process existing mainly in the adipose tissue that hydrolyzes TAG stored in the lipid droplets into glycerol and free fatty acids (Fig 1-3 (Watt and Steinberg, 2008)). At basal state, adipose triacylglycerol lipase (ATGL) present on lipid droplets performs lipolysis at a slow rate. The fatty acids released are either resynthesized into lipids or oxidized locally in the mitochondria. Stimulation such as fasting, cold challenge, stress, glucagon, or noradrenaline trigger the cAMP–PKA signaling pathway in adipocytes. PKA activation leads to the phosphorylation of both perilipin1 (Peri A) and hormone sensitive lipase (HSL). Phosphorylated Peri A releases CGI-58 (comparative gene identification-58), the protein that tightly binds to non-phosphorylated Peri A. CGI-58 subsequently binds to ATGL for rapid TAG hydrolysis. Phosphorylated HSL translocates from cytoplasm to lipid droplets, associates with phosphorylated Peri A, and degrades DAG into MAG. Monoacylglycerol lipase (MGL) cleaves MAG to produce glycerol and the final fatty acid. Fatty acids and glycerol generated are released to the blood and act as systemic energy substrates in non-adipose tissues.

Functions of various adipose tissues

White adipose tissue (WAT) is the main storage for energy deposits and spared fuels. Each fat depot possesses specific functions. Visceral fat, including the gonadal fat pad (GWAT), mesenteric fat pad (MWAT), and perirenal fat pad (PWAT), serves as a cushion to protect internal organs. The subcutaneous fat pad, or inguinal fat (IWAT), is the white fat depot that becomes brown under cold stimulation. Intradermal fat (dWAT), the fat depot embedded in the skin below the dermis, is responsible for insulation as part of thermoregulation, defense against bacterial infection, and support for hair growth and wound healing (Alexander et al., 2015).

Brown adipose tissue (BAT) performs non-shivering thermogenesis in response to cold to maintain body temperature. Brown adipocytes, distinct from white ones, have abundant mitochondria that are enriched with uncoupling protein 1 (UCP1). UCP1 allows protons to bypass ATP production at the end of the electron transport chain thereby generating heat. BAT therefore requires a high rate of substrate uptake and metabolism. It was originally thought that the existence of BAT is only in mice and human babies but not human adults. However, functional BAT has been observed in healthy human adults in recent years (Virtanen et al., 2009). Cervical fat in human adults also has similar molecular markers as the BAT of mice and human babies (Peirce et al., 2014).

Beige fat, the white fat depots that becomes brown under cold stimulation, has the characteristics of both WAT and BAT. It has the same origin as WAT (Peirce et al., 2014). Without stimulation, beige possess similar molecular markers as WAT (Peirce et al., 2014). Once activated in response to cold, beige fat become enriched with UCP1 similar to BAT and performs thermogenesis.

Adipose tissue helps nutrient partition into adipose tissue itself and other tissues/organs by secreting adipokines, which modulate systemic energy metabolism. In WAT, the hormone leptin regulates satiety, and both leptin and adiponectin control glucose homeostasis. The cytokines IL-6, TNFα, and resistin released are associated with hyperglycemia. Circulating free fatty acids reduce adipocyte and muscle glucose uptake, promote hepatic glucose output, and may lead to lipotoxicity and insulin resistance (Rosen and Spiegelman, 2006). In BAT and beige fat, the adipokines are also named batokines (Villarroya et al., 2017). Bone morphogenetic protein 8B (BMP8b), acting as an autocrine factor, enhances BAT activation in response to both cold exposure and high fat feeding (Whittle et al., 2012). Vascular endothelial growth factor A (VEGFA), acting as a paracrine factor, increases vascularization of the endothelial cells in BAT which promotes thermogenesis under cold challenge (Asano et al., 1999; Xue et al., 2009). Neuregulin 4 (Nrg4), acting as an endocrine factor, promotes a healthy adipokine profile in WAT and ameliorates diet-induced metabolic disorders (Chen et al., 2017).

Dysfunctional adipose tissue leads to systemic metabolic disorders

WAT with functional lipid metabolism plays a pivotal role in metabolic health; while BAT performing thermogenesis is a potential target for body weight control. Visceral fat accumulation, or central / apple-shaped obesity, is associated with an increased susceptibility to metabolic diseases. In contrast, subcutaneous fat accumulation in the thighs and the hips, or peripheral / pear-shaped obesity, is less detrimental (Kissebah and Krakower, 1994). Although WAT has its flexibility to adapt and expand in response to chronic excess calorie consumption, such flexibility is not unlimited. When the capacity of WAT function is overloaded, lipids will accumulate in non-adipose tissues and eventually lead to lipotoxicity. BAT, on the other hand, is critical in nutrient

partition and utilization because of its high glucose and lipid metabolism, which carries a high potential in the elimination of extra calories. BAT in mice increases its capacity to be activated in response to high fat feeding (Cannon and Nedergaard, 2004; Feldmann et al., 2009; Rothwell and Stock, 1983). Activated BAT has been shown to ameliorate hyperglycemia and hyperlipidemia in mouse models of diabetes (Arbeeny et al., 1995) and dyslipidemia (Bartelt et al., 2011).

Lipid metabolism during parturition

Parturition is the process of delivering the fetus from the womb to the extrauterine environment. Initiation of parturition involves a coordination of signals from both the fetus and the mother (Challis JRG et al., 2000). Successful parturition requires the maturation of fetal organs necessary for extrauterine survival, and the release of pulmonary surfactant immediately following birth. Additionally, the mother undergoes a switching of the myometrium from a quiescent state of maintaining pregnancy to an active state of contraction. This includes a decrease in maternal circulating progesterone concentration (Virgo and Bellward, 1974) or the withdrawal of progesterone function (Challis JRG et al., 2000; Virgo and Bellward, 1974), and an increase in prostaglandins $PGF_{2}\alpha$ and PGE_2 from the myometrium (Challis JRG et al., 2000). Bioactive lipids, derived from phospholipids, cholesterol, and fatty acids, appear to be some of the key factors in the initiation of parturition, including the synthesis of pulmonary surfactant by the fetus, as well as maternal progesterone and prostaglandins.

Fetal release of pulmonary surfactant

Pulmonary surfactant is composed of 10% surfactant proteins and 90% phospholipids with dipalmitoyl phosphatidylcholine (DPPC) as the major species (Schmitz and Müller, 1991). Secretion of the pulmonary surfactant from the fetus to the amniotic fluid signals the maturation of fetal respiratory and immune systems which are required for survival in the extrauterine environment. Low levels of phospholipids and DPPC in the lung and amniotic fluid cause respiratory distress syndrome in preterm birth infants (Ekelund et al., 1973). Fetal pulmonary surfactant synthesis is modulated by maternal nutrition, as DPPC production in the lung of the fetus is stimulated by supplementing fish oil in mouse dams (Blanco et al., 2004).

Maternal withdrawal of the function in progesterone

Progesterone is a steroid hormone derived from cholesterol. During pregnancy, progesterone maintains uterine quiescence by down-regulating prostaglandin production and oxytocin receptor expression in the myometrium (Kota et al., 2013). During parturition, the effects of progesterone must be overcome by factors that coordinate myometrial contraction. Estrogen is one such factor that promotes a series of myometrial changes by increasing the production of prostaglandins $PGF_{2}\alpha$ and PGE_2 as well as the expression of prostaglandin receptors and oxytocin receptors (Kota et al., 2013). Progesterone functional withdrawal and estrogen functional activation are mediated by their concentration in the circulation in most species (Challis JRG et al., 2000), but not in humans. As the human myometrium nears parturition, the responsiveness to progesterone is mediated by the expression of different subtypes of progesterone receptors (PR): an increase in the expression of PR-A: PR-B ratio implies the

functional withdrawal (Mesiano et al., 2002). Estrogen functional activation is indicated by the increased expression of estrogen receptor (ER) α (Mesiano et al., 2002).

Maternal prostaglandin synthesis

Prostaglandins $PGF_{2}\alpha$ and PGE_{2} are derivatives of arachidonic acid (AA, C20:4 (n-6)), released from membrane phospholipids (Schildknecht et al., 2008) when they act locally to stimulate myometrial contractility (Challis JRG et al., 2000). Biosynthesis of prostaglandin involves multiple enzymes, including phospholipases, cylcooxygenase, and prostaglandin synthases (Fig 1-4 (Schildknecht et al., 2008)). These enzymes in the uterus are thus important for labor induction. Phospholipase A2 (PLA2), an enzyme responsible for the release of AA from glycerophospholipids, as well as cyclooxygenase-1 (COX-1), an enzyme involved in converting AA to prostaglandins, are both expressed in the uterine epithelium (Brown et al., 2009; Gross et al., 1998). Deletion of either enzyme in mice leads to reduced prostaglandin production in the uterus on the day of anticipated delivery, in turn leading to prolonged gestation and an increased mortality rate of neonates (Brown et al., 2009; Gross et al., 1998).

Lipid metabolism during milk production

Milk is required for the thriving of mammalian neonates. It contains all the essential nutrients and regulatory components for neonatal growth and development. Macronutrients in the milk provide energy and building blocks for tissue growth. Vitamins and minerals facilitate the energy yielding processes and other critical biochemical reactions. Regulatory components such as lactoferrin and immunoglobulin assist in the immune response. Among the milk constituents, fat

provides newborns with a concentrated energy source of up to 50% of calorie intake (Uauy and Castillo, 2003), and acts as a carrier of lipid soluble vitamins and bioactive components including conjugated linoleic acids.

Structure of mammary glands

Milk fat is synthesized in the mammary epithelial cells. Mammary gland is composed of two major tissue compartments, the epithelium and the stroma (Anderson et al., 2007; Hennighausen and Robinson, 2005). A single layer of epithelial cells forming a ball-shaped structure with a central lumen is termed the mammary alveoli (Fig 1-5 (Inman et al., 2015)). The alveolar epithelial cells synthesize and secrete milk into the central lumen for delivery. Milk is delivered by mammary ducts containing ductal epithelial cells. Both alveolar and ductal epithelial cells are surrounded by basal myoepithelial cells, containing smooth muscle actin that contracts in response to oxytocin to mediate milk let-down through the ducts to the nipple. The stroma is composed of mostly adipocytes as well as extracellular matrix, fibroblasts, immune cells, blood vessels, and neurons that may locally secrete hormones and growth factors or coordinate systemic signals to support mammary gland development.

Mammary gland development

Mammary gland development can be divided into 5 stages after the rudimentary ductal structure is established in the embryo (Hens and Wysolmerski, 2005): puberty, mature virgin, pregnancy, lactation, and involution (Fig 1-5 (Inman et al., 2015)).

The onset of puberty in mice is defined as the time when ovulation first occurs (Silver, 1995). At puberty, ductal elongation is stimulated by estrogen, progesterone, epidermal growth factor, and insulin-like growth factor (IGF) 1, directing the proliferative terminal end buds (Anderson et al., 2007). Elongation ends when the ducts reach the margin of the fat pad and the terminal end buds regress to form terminal ducts (Anderson et al., 2007).

In the mature virgin, the fad pad is filled with branching ducts and the alveolar buds are formed (Hennighausen and Robinson, 2005). Alveolar bud formation is under the control of progesterone (Anderson et al., 2007). Its formation and disappearance therefore follow the estrous cycle (Anderson et al., 2007).

At pregnancy, the epithelial compartment gradually expands. Ductal branching and alveolar bud formation accelerate with a large increase in DNA synthesis and cellular proliferation at early gestation (Anderson et al., 2007). The alveolar buds then differentiate into secretory lobes near parturition, under the control of prolactin (Anderson et al., 2007).

At lactation, the alveoli are fully mature, and the alveolar epithelial cells synthesize and secrete milk into lumen. Milk production is largely increased in response to suckling, under the control of prolactin and oxytocin. With cessation of suckling stimulus upon weaning, the involution of mammary glands is triggered. In mice, the involution takes approximately 10 days and can be divided into 2 stages (Furth et al., 1997; Lund et al., 1996). The first stage lasts about 2 days after weaning and can be reversed back to the status of lactation. At the second stage, the basal membranes and extracellular matrix in the mammary glands are degraded, resulting in the destruction of secretory lobes. As involution progresses, mammary epithelial cells are removed and adipocytes appear again. Eventually, the mammary glands are remodeled back to the structure of a mature virgin.

Mammary gland development switching from pregnancy to lactation is the key to the success in milk synthesis. During this process, large lipid droplets in the cytoplasm of epithelial cells at late gestation are replaced by small lipid droplets at the apical surface of the epithelium (Fig 1-6 (Anderson et al., 2007)). The successful lactation switch is determined by the functional withdrawal of progesterone and prolactin secretion at late gestation (Anderson et al., 2007). From pregnancy to lactation, genes involved in milk fat synthesis are highly regulated (Fig 1-7 (Anderson et al., 2007)).

Milk fat synthesis

Milk fat is composed of TAG as the major lipid species, accounting for over 98% (Anderson et al., 2007). Both fatty acids and glycerol in milk TAG are either sourced from dietary fat that stored in the tissues or *de novo* lipogenesis in the mammary glands (Barber et al., 1997). The source of milk fat depends on the availability of substrates in the blood, which in turn is determined by dietary components and feeding status (Fig 1-8 (Anderson et al., 2007)). Under high fat feeding, both fatty acids and glycerol are mostly derived from the breakdown of the dietary fat in the chylomicrons by lipoprotein lipase (LPL). During fasting, fatty acids can be transferred directly from adipose tissue in an albumin-bound form directly to the alveoli, or indirectly from the liver in the form of VLDL following hydrolysis by LPL. Under high carbohydrate feeding, both substrates are mainly synthesized from glucose: G3P is derived from DHAP by glycolysis; fatty acids are made endogenously in the mammary glands. The fatty acids synthesized by mammary glands are mostly medium-chained (MCFAs, C8:0-C14:0) because of the thioesterase II unique to the mammary epithelium (Barber et al., 1997). This enzyme hydrolyzes the thioester bond from the elongating acyl chains in the fatty acid synthase and release as MCFAs (Barber et al., 1997). Milk TAG is then synthesized via G3P pathway.

Lipid synthesis enzymes are involved in milk production

Lipid synthesis enzymes are required for milk production. GPAT4, glycerol-3-phosphate acyltransferase, one of the enzymes catalyzing the formation of LPA by acylation on G3P, is highly expressed in the mammary epithelium but not in the surrounding adipose tissue. Lacking a functional GPAT4 globally, mouse mammary glands are underdeveloped with reduced size and number of alveoli in the lactating mammary glands. This results in the depletion of TAG in the milk and pups nursed by GPAT4 deficient dams die perinatally (Beigneux et al., 2006). DGAT1, the enzyme catalyzing the formation of TAG from DAG, is expressed in both mammary epithelium and stroma. DGAT1 in both compartments are required for mammary gland development. Mouse dams deficient in DGAT1 globally have less mammary ducts at mid-gestation, reduced epithelial cells and small lumen at peripartum. Therefore, these dams cannot produce milk (Cases et al., 2004).

In this dissertation, this overview of lipid metabolism in adiposity, parturition, and milk production is applied to the exploration of physiological mechanisms in the newly identified MGAT functions. Specifically, how *Mogat1* deficiency promotes adiposity in response to excess calories (Chapter 2), and how *Mogat2* deficiency impairs female reproduction (Chapter 3) and mammary gland functions (Chapter4) are delineated in the following chapters.

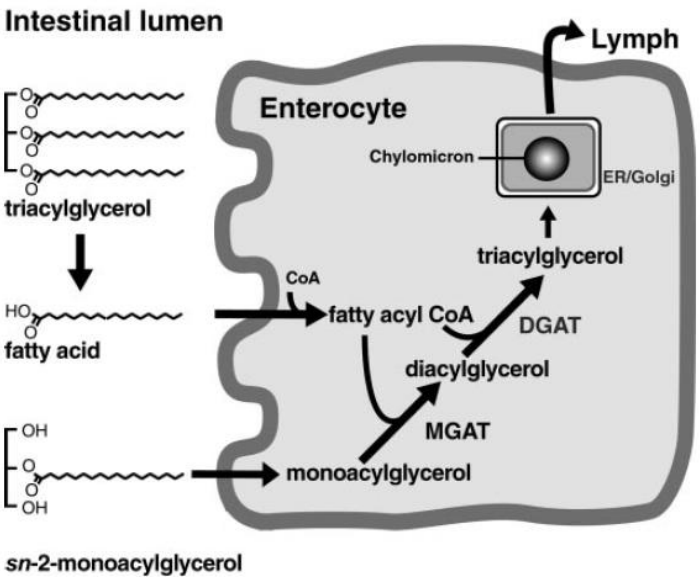

Figure 1-1. MGAT catalyzes the reassembling of digested dietary TAG during fat absorption in the enterocyte (Yen and Farese, 2003).

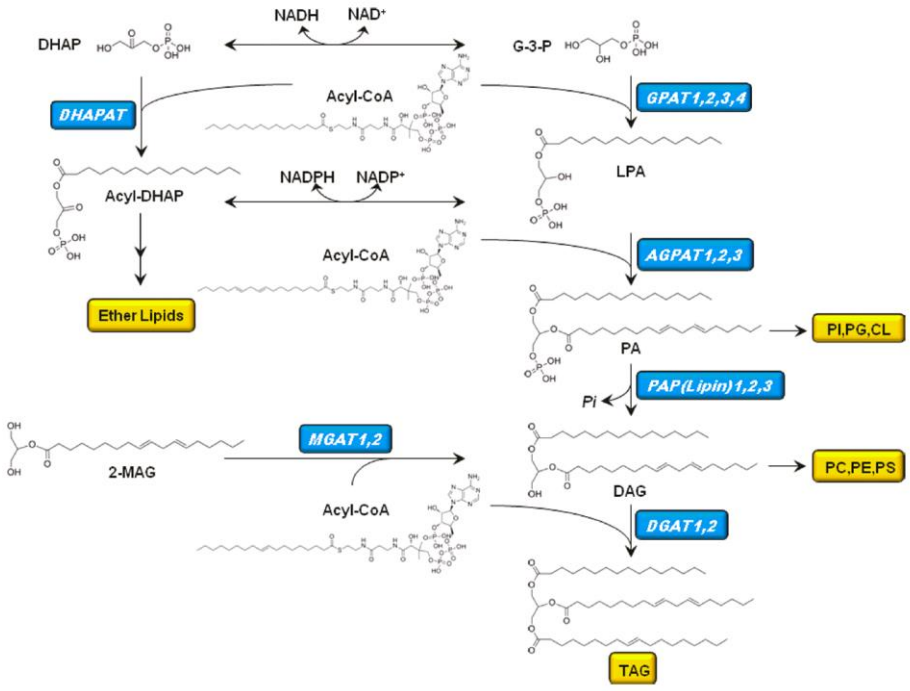

Figure 1-2. TAG esterification involves G3P and MAG pathways (Coleman and Mashek, 2011).

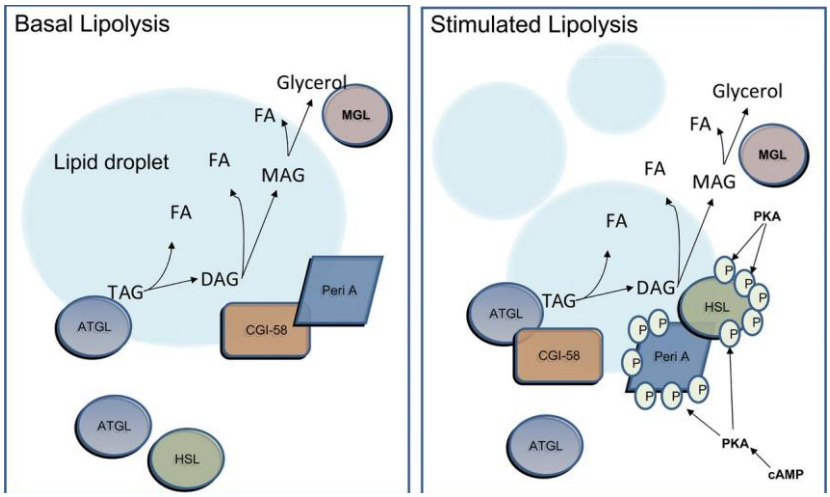

Figure 1-3. Lipolysis is the hydrolysis of TAG stored in the lipid droplets into glycerol and free fatty acids (Watt and Steinberg, 2008).

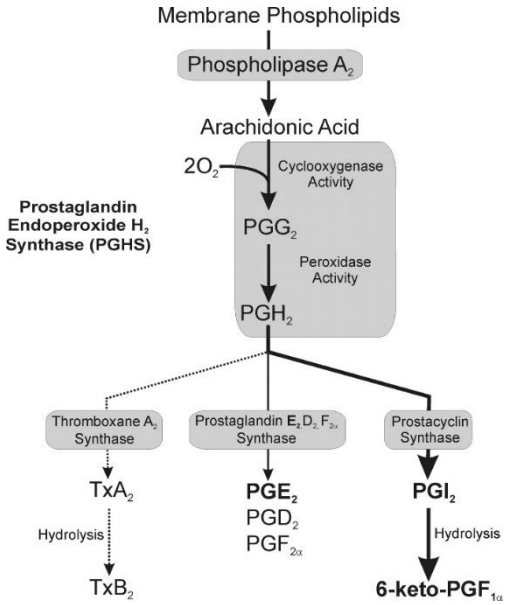

Figure 1-4. Prostaglandin synthesis involves multiple enzymes, including phospholipases, cylcooxygenase, and prostaglandin synthases (Schildknecht et al., 2008).

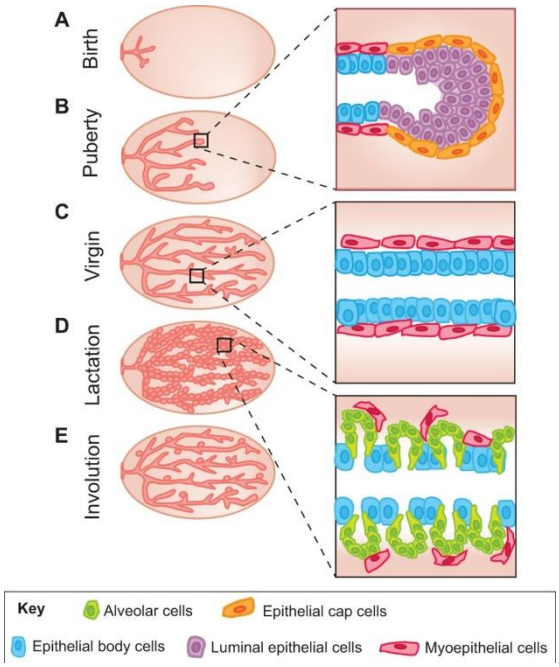

Figure 1-5. Mammary glands develop from the rudimentary ductal structure established in the embryo, puberty, mature virgin, pregnancy, lactation, to involution (Inman et al., 2015).

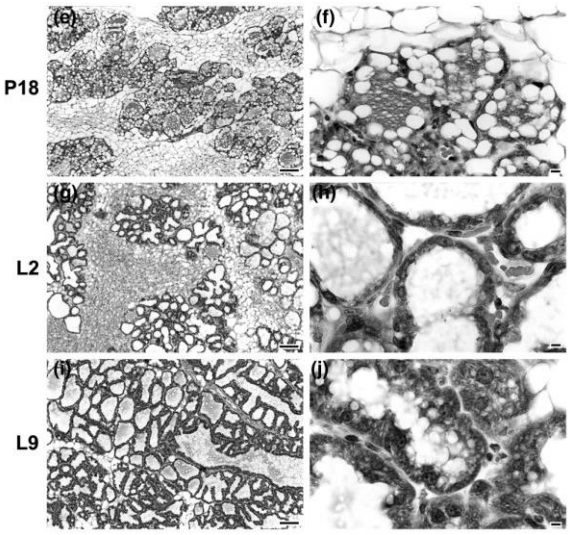

Figure 1-6. From pregnancy (P) to lactation (L), large lipid droplets in the cytoplasm of epithelial cells at late gestation are replaced by small lipid droplets at the apical surface of the epithelium (Anderson et al., 2007).

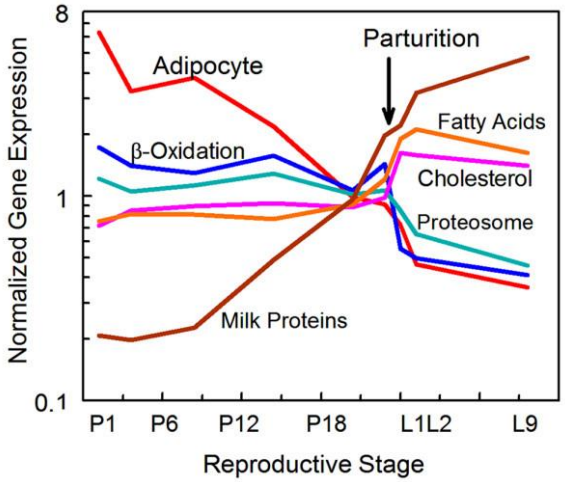

Figure 1-7. From pregnancy (P) to lactation (L), the genes tightly regulated are those involved in milk fat synthesis (Anderson et al., 2007).

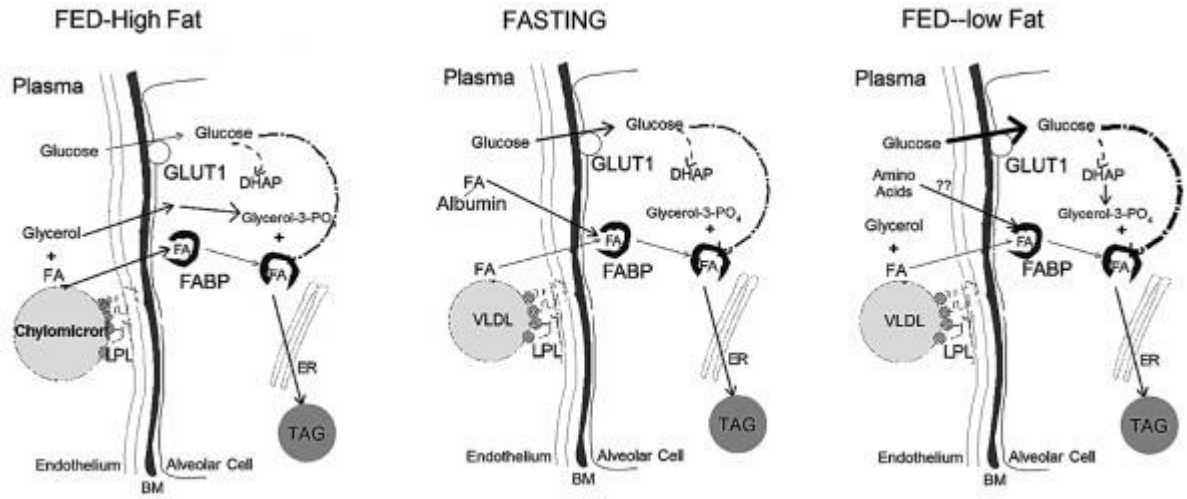

Figure 1-8. Milk fat synthesis is determined by the dietary components and the feeding status (Anderson et al., 2007).

References

Agarwal, A.K., Tunison, K., Dalal, J.S., Yen, C.L., Farese, R.V., Horton, J.D., and Garg, A. (2016). Mogat1 deletion does not ameliorate hepatic steatosis in lipodystrophic (Agpat2-/-) or obese (ob/ob) mice. J Lipid Res *57*, 616-630.

Alexander, C.M., Kasza, I., Yen, C.L., Reeder, S.B., Hernando, D., Gallo, R.L., Jahoda, C.A., Horsley, V., and MacDougald, O.A. (2015). Dermal white adipose tissue: a new component of the thermogenic response. J Lipid Res *56*, 2061-2069.

Anderson, S.M., Rudolph, M.C., McManaman, J.L., and Neville, M.C. (2007). Key stages in mammary gland development. Secretory activation in the mammary gland: it's not just about milk protein synthesis! Breast Cancer Res *9*, 204.

Arbeeny, C.M., Meyers, D.S., Hillyer, D.E., and Bergquist, K.E. (1995). Metabolic alterations associated with the antidiabetic effect of beta 3-adrenergic receptor agonists in obese mice. Am J Physiol *268*, E678-684.

Asano, A., Kimura, K., and Saito, M. (1999). Cold-induced mRNA expression of angiogenic factors in rat brown adipose tissue. J Vet Med Sci *61*, 403-409.

Barber, M.C., Clegg, R.A., Travers, M.T., and Vernon, R.G. (1997). Lipid metabolism in the lactating mammary gland. Biochim Biophys Acta *1347*, 101-126.

Bartelt, A., Bruns, O.T., Reimer, R., Hohenberg, H., Ittrich, H., Peldschus, K., Kaul, M.G., Tromsdorf, U.I., Weller, H., Waurisch, C., et al. (2011). Brown adipose tissue activity controls triglyceride clearance. Nat Med *17*, 200-205.

Beigneux, A.P., Vergnes, L., Qiao, X., Quatela, S., Davis, R., Watkins, S.M., Coleman, R.A., Walzem, R.L., Philips, M., Reue, K., et al. (2006). Agpat6--a novel lipid biosynthetic gene required for triacylglycerol production in mammary epithelium. J Lipid Res *47*, 734-744.

Blanco, P.G., Freedman, S.D., Lopez, M.C., Ollero, M., Comen, E., Laposata, M., and Alvarez, J.G. (2004). Oral docosahexaenoic acid given to pregnant mice increases the amount of surfactant in lung and amniotic fluid in preterm fetuses. Am J Obstet Gynecol *190*, 1369-1374.

Brown, N., Morrow, J.D., Slaughter, J.C., Paria, B.C., and Reese, J. (2009). Restoration of on-time embryo implantation corrects the timing of parturition in cytosolic phospholipase A2 group IVA deficient mice. Biol Reprod *81*, 1131-1138.

Cannon, B., and Nedergaard, J. (2004). Brown adipose tissue: function and physiological significance. Physiol Rev *84*, 277-359.

Cao, J., Burn, P., and Shi, Y. (2003a). Properties of the mouse intestinal acyl-CoA:monoacylglycerol acyltransferase, MGAT2. J Biol Chem *278*, 25657-25663.

Cao, J., Lockwood, J., Burn, P., and Shi, Y. (2003b). Cloning and functional characterization of a mouse intestinal acyl-CoA:monoacylglycerol acyltransferase, MGAT2. J Biol Chem *278*, 13860-13866.

Cases, S., Zhou, P., Shillingford, J.M., Wiseman, B.S., Fish, J.D., Angle, C.S., Hennighausen, L., Werb, Z., and Farese, R.V. (2004). Development of the mammary gland requires DGAT1 expression in stromal and epithelial tissues. Development *131*, 3047-3055.

Challis JRG, Matthews, S.G., Gibb, W., and Lye, S.J. (2000). Endocrine and paracrine regulation of birth at term and preterm. Endocr Rev *21*, 514-550.

Chen, Z., Wang, G.-X., Ma, S.L., Jung, D.Y., Ha, H., Altamimi, T., Zhao, X.-Y., Guo, L., Zhang, P., Hu, C.-R., et al. (2017). Nrg4 promotes fuel oxidation and a healthy adipokine profile to ameliorate diet-induced metabolic disorders. Molecular Metabolism *In press*.

Cheng, D., Nelson, T.C., Chen, J., Walker, S.G., Wardwell-Swanson, J., Meegalla, R., Taub, R., Billheimer, J.T., Ramaker, M., and Feder, J.N. (2003). Identification of acyl coenzyme A:monoacylglycerol acyltransferase 3, an intestinal specific enzyme implicated in dietary fat absorption. J Biol Chem *278*, 13611-13614.

Coleman, R.A., and Mashek, D.G. (2011). Mammalian triacylglycerol metabolism: synthesis, lipolysis, and signaling. Chem Rev *111*, 6359-6386.

Cortés, V.A., Curtis, D.E., Sukumaran, S., Shao, X., Parameswara, V., Rashid, S., Smith, A.R., Ren, J., Esser, V., Hammer, R.E., et al. (2009). Molecular mechanisms of hepatic steatosis and insulin resistance in the AGPAT2-deficient mouse model of congenital generalized lipodystrophy. Cell Metab *9*, 165-176.

Ekelund, L., Arvidson, G., and Astedt, B. (1973). Amniotic fluid lecithin and its fatty acid composition in respiratory distress syndrome. J Obstet Gynaecol Br Commonw *80*, 912-917.

Feldmann, H.M., Golozoubova, V., Cannon, B., and Nedergaard, J. (2009). UCP1 ablation induces obesity and abolishes diet-induced thermogenesis in mice exempt from thermal stress by living at thermoneutrality. Cell Metab *9*, 203-209.

Furth, P.A., Bar-Peled, U., and Li, M. (1997). Apoptosis and mammary gland involution: reviewing the process. Apoptosis *2*, 19-24.

Gao, Y., Nelson, D.W., Banh, T., Yen, M.I., and Yen, C.L. (2013). Intestine-specific expression of MOGAT2 partially restores metabolic efficiency in Mogat2-deficient mice. J Lipid Res *54*, 1644-1652.

Gross, G.A., Imamura, T., Luedke, C., Vogt, S.K., Olson, L.M., Nelson, D.M., Sadovsky, Y., and Muglia, L.J. (1998). Opposing actions of prostaglandins and oxytocin determine the onset of murine labor. Proc Natl Acad Sci U S A *95*, 11875-11879.

Hall, A.M., Soufi, N., Chambers, K.T., Chen, Z., Schweitzer, G.G., McCommis, K.S., Erion, D.M., Graham, M.J., Su, X., and Finck, B.N. (2014). Abrogating monoacylglycerol acyltransferase activity in liver improves glucose tolerance and hepatic insulin signaling in obese mice. Diabetes *63*, 2284-2296.

Hennighausen, L., and Robinson, G.W. (2005). Information networks in the mammary gland. Nat Rev Mol Cell Biol *6*, 715-725.

Hens, J.R., and Wysolmerski, J.J. (2005). Key stages of mammary gland development: molecular mechanisms involved in the formation of the embryonic mammary gland. Breast Cancer Res *7*, 220-224.

Inman, J.L., Robertson, C., Mott, J.D., and Bissell, M.J. (2015). Mammary gland development: cell fate specification, stem cells and the microenvironment. Development *142*, 1028-1042.

KENNEDY, E.P. (1961). Biosynthesis of complex lipids. Fed Proc *20*, 934-940.

Kissebah, A.H., and Krakower, G.R. (1994). Regional adiposity and morbidity. Physiol Rev *74*, 761-811.

Kota, S.K., Gayatri, K., Jammula, S., Krishna, S.V., Meher, L.K., and Modi, K.D. (2013). Endocrinology of parturition. Indian J Endocrinol Metab *17*, 50-59.

Lee, Y.J., Ko, E.H., Kim, J.E., Kim, E., Lee, H., Choi, H., Yu, J.H., Kim, H.J., Seong, J.K., Kim, K.S., et al. (2012). Nuclear receptor PPARγ-regulated monoacylglycerol O-acyltransferase 1 (MGAT1) expression is responsible for the lipid accumulation in diet-induced hepatic steatosis. Proc Natl Acad Sci U S A *109*, 13656-13661.

Lund, L.R., Rømer, J., Thomasset, N., Solberg, H., Pyke, C., Bissell, M.J., Danø, K., and Werb, Z. (1996). Two distinct phases of apoptosis in mammary gland involution: proteinase-independent and -dependent pathways. Development *122*, 181-193.

Mesiano, S., Chan, E.C., Fitter, J.T., Kwek, K., Yeo, G., and Smith, R. (2002). Progesterone withdrawal and estrogen activation in human parturition are coordinated by progesterone receptor A expression in the myometrium. J Clin Endocrinol Metab *87*, 2924-2930.

Mostafa, N., Bhat, B.G., and Coleman, R.A. (1994). Adipose monoacylglycerol:acyl-coenzyme A acyltransferase activity in the white-throated sparrow (Zonotrichia albicollis): characterization and function in a migratory bird. Lipids *29*, 785-791.

Nelson, D.W., Gao, Y., Spencer, N.M., Banh, T., and Yen, C.L. (2011). Deficiency of MGAT2 increases energy expenditure without high-fat feeding and protects genetically obese mice from excessive weight gain. J Lipid Res *52*, 1723-1732.

Nelson, D.W., Gao, Y., Yen, M.I., and Yen, C.L. (2014). Intestine-specific deletion of acyl-CoA:monoacylglycerol acyltransferase (MGAT) 2 protects mice from diet-induced obesity and glucose intolerance. J Biol Chem *289*, 17338-17349.

Peirce, V., Carobbio, S., and Vidal-Puig, A. (2014). The different shades of fat. Nature *510*, 76-83.

Rosen, E.D., and Spiegelman, B.M. (2006). Adipocytes as regulators of energy balance and glucose homeostasis. Nature *444*, 847-853.

Rothwell, N.J., and Stock, M.J. (1983). Luxuskonsumption, diet-induced thermogenesis and brown fat: the case in favour. Clin Sci (Lond) *64*, 19-23.

Schildknecht, S., Daiber, A., Ghisla, S., Cohen, R.A., and Bachschmid, M.M. (2008). Acetaminophen inhibits prostanoid synthesis by scavenging the PGHS-activator peroxynitrite. FASEB J *22*, 215-224.

Schmitz, G., and Müller, G. (1991). Structure and function of lamellar bodies, lipid-protein complexes involved in storage and secretion of cellular lipids. J Lipid Res *32*, 1539-1570.

Silver, L.M. (1995). Mouse genetics : concepts and applications. (New York: Oxford University Press).

Uauy, R., and Castillo, C. (2003). Lipid requirements of infants: implications for nutrient composition of fortified complementary foods. J Nutr *133*, 2962S-2972S.

Villarroya, F., Cereijo, R., Villarroya, J., and Giralt, M. (2017). Brown adipose tissue as a secretory organ. Nat Rev Endocrinol *13*, 26-35.

Virgo, B.B., and Bellward, G.D. (1974). Serum progesterone levels in the pregnant and postpartum laboratory mouse. Endocrinology *95*, 1486-1490.

Virtanen, K.A., Lidell, M.E., Orava, J., Heglind, M., Westergren, R., Niemi, T., Taittonen, M., Laine, J., Savisto, N.J., Enerbäck, S., et al. (2009). Functional brown adipose tissue in healthy adults. N Engl J Med *360*, 1518-1525.

Watt, M.J., and Steinberg, G.R. (2008). Regulation and function of triacylglycerol lipases in cellular metabolism. Biochem J *414*, 313-325.

Whittle, A.J., Carobbio, S., Martins, L., Slawik, M., Hondares, E., Vázquez, M.J., Morgan, D., Csikasz, R.I., Gallego, R., Rodriguez-Cuenca, S., et al. (2012). BMP8B increases brown adipose tissue thermogenesis through both central and peripheral actions. Cell *149*, 871-885.

Xue, Y., Petrovic, N., Cao, R., Larsson, O., Lim, S., Chen, S., Feldmann, H.M., Liang, Z., Zhu, Z., Nedergaard, J., et al. (2009). Hypoxia-independent angiogenesis in adipose tissues during cold acclimation. Cell Metab *9*, 99-109.

Yen, C.L., Brown, C.H., Monetti, M., and Farese, R.V. (2005). A human skin multifunctional O-acyltransferase that catalyzes the synthesis of acylglycerols, waxes, and retinyl esters. J Lipid Res *46*, 2388-2397.

Yen, C.L., Cheong, M.L., Grueter, C., Zhou, P., Moriwaki, J., Wong, J.S., Hubbard, B., Marmor, S., and Farese, R.V. (2009). Deficiency of the intestinal enzyme acyl CoA:monoacylglycerol acyltransferase-2 protects mice from metabolic disorders induced by high-fat feeding. Nat Med *15*, 442-446.

Yen, C.L., and Farese, R.V. (2003). MGAT2, a monoacylglycerol acyltransferase expressed in the small intestine. J Biol Chem *278*, 18532-18537.

Yen, C.L., Stone, S.J., Cases, S., Zhou, P., and Farese, R.V. (2002). Identification of a gene encoding MGAT1, a monoacylglycerol acyltransferase. Proc Natl Acad Sci U S A *99*, 8512-8517.

Yu, J.H., Song, S.J., Kim, A., Choi, Y., Seok, J.W., Kim, H.J., Lee, Y.J., Lee, K.S., and Kim, J.W. (2016). Suppression of PPARγ-mediated monoacylglycerol O-acyltransferase 1 expression ameliorates alcoholic hepatic steatosis. Sci Rep *6*, 29352.

Yue, Y.G., Chen, Y.Q., Zhang, Y., Wang, H., Qian, Y.W., Arnold, J.S., Calley, J.N., Li, S.D., Perry, W.L., Zhang, H.Y., et al. (2011). The acyl coenzymeA:monoacylglycerol acyltransferase 3 (MGAT3) gene is a pseudogene in mice but encodes a functional enzyme in rats. Lipids *46*, 513-520.

Inactivation of *Mogat1* exacerbates adiposity in mouse models of diet-induced and genetic obesity

Ting-Ni Huang[1], Mei-I Yen[1], Ildiko Kasza[2], David W. Nelson[1], Brian W. Parks[1], Caroline M. Alexander[2], and Chi-Liang E Yen[1*]

[1]Department of Nutritional Sciences, College of Agriculture and Life Sciences; [2]McArdle Laboratory for Cancer Research, School of Medicine and Public Health, University of Wisconsin–Madison, WI 53706

[*]Address for correspondence:

C.-L. Eric Yen
Department of Nutritional Sciences, University of Wisconsin–Madison
1415 Linden Drive
Madison, WI 53706

Fax: (608) 262-5860
E-mail: yen@nutrisci.wisc.edu

Running title: *Mogat1* deficiency and adiposity

Abstract

Mogat1 is cloned based on its sequence homology with acyl-CoA: diacylglycerol acyltransferase 2. The protein encoded by *Mogat1*, however, exhibit high acyl-CoA: monoacylglycerol acyltransferase (MGAT) activity *in vitro*, and thus was named MGAT1. The physiological function of MGAT1 is not clear, although the hepatic expression of *Mogat1* is induced in various mouse models of fatty liver. In this study, using datasets from genome-wide association studies, we identified an inverse relationship between the expression level of *Mogat1* in the adipose tissue and adiposity in both humans and mice. This relationship raises the question of whether *Mogat1* limits adiposity. Using mice lacking a functional *Mogat1* globally, we found that these mice grew normally during the suckling period and when fed a regular low-fat chow diet. When fed with the high-fat diet, these mice exhibited reduced energy expenditure and increased adiposity compared to wildtype mice. Mice lacking *Mogat1* had normal thermogenic brown adipose tissue; their decreases in energy expenditure were associated with increased thermal insulation in a cold environment or decreased physical activity at room temperature and thermoneutrality. When introduced into the hyperphagic Agouti mice, which become obese without high-fat feeding overtime, loss of *Mogat1* also exacerbates fat accumulation. Interestingly, none of the tissues examined from mice deficient in *Mogat1* exhibited reduction in MGAT activity. These findings reveal a novel physiological function of *Mogat1* in regulating systemic energy balance and adiposity through yet unidentified biochemical activities.

Key words: triacylglycerol, adiposity, energy expenditure, brown adipose tissue, thermal insulation, physical activity

Introduction

Adiposity is the fat accumulation in the adipose tissue. The extra calories that are stored as fat result from positive energy balance, either over-consumption of calories or reduction in energy expenditure. Adipose tissue plays integral roles in systemic energy metabolism. It is not only an energetic reservoir, but also an organ that secretes hormones, cytokines, and signaling lipids to communicate with other tissues.

Adipose tissue stores lipid primarily as triacylglycerol (TAG). TAG biosynthesis occurs through two major pathways, glycerol-3-phosphate (G3P) and monoacylglycerol (MAG) pathways. Both pathways generate diacylglycerol (DAG), the precursor of TAG. The G3P pathway (Kennedy, 1961), the predominant TAG synthesis pathway in most mammalian cell types, generates DAG from the dephosphorylation of phosphatidic acid, which is produced by the sequential acylation of G3P.

The MAG pathway (Lehner and Kuksis, 1996) is the predominant TAG synthesis pathway in cell types that are involved in lipid recycling, including enterocytes, hepatocytes, and adipocytes. The MAG pathway has been well-characterized for dietary fat absorption in the enterocytes (Phan and Tso, 2001; Yen and Farese, 2003), where it generates DAG from the fatty acids and sn-2 MAG digested from dietary fat (mostly TAG) in the intestinal lumen by pancreatic lipase. The rate limiting step of this process is catalyzed by acyl-CoA: monoacylglycerol acyltransferase (MGAT).

Mogat1 is the first identified gene that codes for MGAT. However, *Mogat1* is not responsible for the dietary fat absorption, because its mRNA is not expressed in the small intestine of humans or mice. Instead, *Mogat1* is expressed in tissues where MGAT activity is less prominent. In humans, *Mogat1* is detected in the liver and kidney (Yen and Farese, 2003). In

mice, *Mogat1* is expressed mainly in the stomach and kidney, with relatively lower levels in the adipose tissues, liver, and uterus (Yen et al., 2002).

The potential role of *Mogat1* in the development of hepatic steatosis has attracted attention recently. The hepatic expression of *Mogat1* mRNA is induced in various mouse models of fatty liver, including diet-induced obesity (Lee et al., 2012), lipodystrophic *Agpat2*$^{-/-}$ (Cortés et al., 2009), leptin deficient *ob/ob* (Agarwal et al., 2016), and mice with alcohol-induced hepatic steatosis (Yu et al., 2016). Therefore, inactivation of the *Mogat1* gene might be of potential in the treatment for fatty liver. However, using different strategies to inactivate *Mogat1* in different mouse models has yielded inconsistent results. For example, *Mogat1* mRNA induced by liver PPARγ is critical for the development of non-alcoholic (Lee et al., 2012) and alcoholic fatty livers (Yu et al., 2016). Knocking down *Mogat1* in mice using short hairpin RNA after 12 weeks of high-fat feeding improves glucose metabolism, alleviates hepatic steatosis, and reduces diet-induced obesity (Lee et al., 2012). Further, knocking down *Mogat1* in mice using short hairpin RNA after 3 weeks of ethanol diet also suppresses alcohol-induced hepatic steatosis (Yu et al., 2016). In contrast, Hall et al. reported that knocking down *Mogat1* in mice using anti-sense oligonucleotide after 14 weeks of high-fat feeding or on 6-week old *ob/ob* mice improves glucose metabolism and hepatic insulin signaling, but does not attenuate hepatic steatosis or obesity (Hall et al., 2014). Additionally, Agarwal et al. reported that global *Mogat1* deletion does not ameliorate hepatic steatosis in either *Agpat2*$^{-/-}$ or *ob/ob* mice, and has no effects on their body weight or glucose metabolism (Agarwal et al., 2016). Therefore, the physiological significance of *Mogat1* remains unclear.

In this study, using genome-wide association studies, we identified an inverse relationship between the expression level of *Mogat1* in the adipose tissue and adiposity in both humans and mice. Using mice lacking a functional *Mogat1* globally, we tested the hypothesis that *Mogat1* limits fat mass expansion.

Materials and Methods

Mice

All animal studies were approved by the University of Wisconsin-Madison Animal Care and Use Committee and were performed in accordance with the Public Health Service Policy on Human Care and Use of Laboratory Animals.

Mice globally deficient in *Mogat1* (*M1*$^{-/-}$) were generated at the Gladstone Institutes, University of California at San Francisco, as previously described (Agarwal et al., 2016). Mice used in our studies have been backcrossed into the C57BL/6J genetic background for 10 or more generations. The experimental mice and their wildtype littermate controls (WT) were generated by intercrossing the heterozygous *M1*$^{+/-}$ mice. *M1*$^{-/-}$ mice with the Agouti mutation and their controls were generated by first crossing *M1*$^{-/-}$ mice with Agouti yellow (*Ay/a*) mice in the C57BL/6J genetic background, originally from the Jackson Laboratory (Bar Harbor, ME), and then intercrossing the resulting heterozygotes with one carrying the Agouti mutation.

Mice were housed at 23ºC on a 12 hr light / 12 hr dark cycle where the dark phase was from 6 pm to 6 am. They were fed a standard chow diet (8604, Teklad, Madison, WI) after weaning unless further indicated.

Genotyping

Genotypes of mice were determined by PCR. Three primers were used to determine the *Mogat1* genotypes: forward primer between exon 1 and exon 2 of *Mogat1*, 5'-CTGGAGCAAGCAGGGCCAGAATGAG-3'; reverse primer between exon 2 and exon 3 of *Mogat1*, 5'-GGACCTAAGGCACGTTCTGTCTG-3'; reverse primer on *neo* cassette which

replaces the deleted exon 2, 5'-CGTTGACTCTAGAGGATCCGAC-3'. The PCR reaction produced a 586-bp amplicon and a ~300-bp amplicon for the wildtype and the *Mogat1*-targeted allele, respectively.

Tissue Mogat1 expression

Tissue *Mogat1* mRNA expression levels were determined by real time quantitative PCR. Total RNA was isolated using RiboZol reagent (AMRESCO N580) and 1 μg of RNA was reverse transcribed to cDNA (Bio-Rad 170-8891). *Mogat1* expression was assessed by Roche LightCycler 480 using SYBR FAST qPCR kit (KAPA Biosystem 07959494001). *36B4* was used as a housekeeping gene, and its expression level was not different between genotypes. The $2^{-\Delta\Delta Ct}$ method was used to calculate the fold change in gene expression. The primers detecting for *Mogat1* is: forward: AGCAAGGAGGCAGAAGATG; reverse: TGTGACCCGGATCCAAAT; for *36B4* is: forward: GCAGATCGGGTACCCAACTGTTG; reverse: CAGCAGCCGCAAATGCAGATG.

Tissue MGAT activity

Tissue MGAT activity was measured using total tissue homogenate as previously described (Yen and Farese, 2003). Tissues were homogenized with reaction buffer containing 50 mM Tris-HCl and 250 mM sucrose at pH 7.4 with protease inhibitor and monoacylglycerol lipase inhibitor (MAFP, BML-ST360, Enzo Life Science (Hoover et al., 2008)). The homogenate was centrifuged at 600 *g* for 10 min to precipitate cellular debris, leaving the enzyme-containing fraction in the supernatant. Reactions were started by adding 100 μL of supernatant into the substrate mixture (5 mM $MgCl_2$, 1.25 mg/mL BSA, 50 mM Tris-HCl, 250 mM sucrose, 100 μM

^{14}C-labeled 2-monooleoylglycerol, and 25 μM oleoyl-CoA), and stopped after 5 min by adding 3 mL chloroform: methanol (2:1, v/v) for enzyme inactivation and subsequent lipid extraction. The lipids were extracted, dried, and separated by thin-layer chromatography (TLC) on silica gel G-60 plates with the solvent system, hexane: diethyl ether: acetic acid (80:20:1, v/v/v). Lipid bands were visualized with iodine vapor, and the products were identified by comparison with the migration of known lipid standards. The incorporation of radioactive substrates into lipid products was visualized using a phosphorimaging scanner (Typhoon FLA 7000, GE Healthcare) and quantified by scraping and counting in a scintillation counter (Packard Tri-Carb 2200 CA liquid scintillation counter analyzer).

Metabolic phenotyping

To examine the effects of *Mogat1* deficiency in response to excess calories, two obese mouse models were used: diet-induced obese and hyperphagic Agouti mice. Non-Agouti *M1*$^{-/-}$ and WT control mice were fed with a regular chow diet after weaning and switched to the high-fat diet (60% calories from fat, D12492, Research Diets, New Brunswick, NJ) at 10-13 weeks old. Mice with the Agouti mutation were maintained on regular chow diet after weaning. Body weight and body composition (EchoMRI) were monitored weekly in diet-induced obese mice for 8 weeks and monthly in Agouti mice from 3-8 months old.

To examine the effects of *Mogat1* deficiency on glucose metabolism, glucose tolerance test (GTT), fasting insulin measurement, and insulin tolerance test (ITT) were performed. GTT and fasting insulin were measured in mice after 8-10 weeks of high-fat feeding and age-matched chow-fed mice, or in 4- and 6-month old Agouti mice. Mice were fasted for 4-6 hours and fasting blood was then collected in the early afternoon for glucose and insulin measurement. 1 mg/kg body weight of glucose was injected intraperitoneally afterwards for GTT. Blood glucose levels

were measured using a hand-held glucose meter before and 15, 30, 60, and 120 min after glucose administration. Plasma insulin was analyzed using an ELISA kit (Crystal Chem 90080). ITT was performed in 7-month old Agouti mice. Mice were fasted for 4-6 hours and in the early afternoon 1.5 U/kg body weight of insulin was injected intraperitoneally. Blood glucose levels were measured using a hand-held glucose meter before and 15, 30, 60, and 120 min after insulin administration.

Tissues were harvested for weighing, biochemical, and histological analysis from 12-14-week old high-fat fed mice and 8-month old Agouti mice in the early afternoon after fasting for 4-6 hours.

Hepatic triacylglycerol (TAG) levels

30-50 mg frozen liver was homogenized in 1 mL PBS, and lipids were extracted with 3 mL chloroform: methanol (2:1, v/v). 10% lipid extract was resuspended with chloroform containing 1% Triton X-100 to help dissolve in water-soluble reagents for TAG assay and evaporated to dryness. Dried lipid extract was resuspended in ddH_2O for TAG analysis by an enzymatic and colorimetric assay (Wako 461-08992/461-09092).

Histology

1 cm^3 adipose tissue samples were fixed in 4% paraformaldehyde overnight. The subsequent paraffin embedding, sectioning, and hematoxylin and eosin (H&E) staining were processed at the UW Department of Surgery Histology Core Facility. Images were taken with an optical

microscope. Quantification of adipocyte size was performed using Adiposoft-ImageJ (Galarraga et al., 2012).

1 cm^2 skin sections were fixed in 4% paraformaldehyde overnight. The subsequent paraffin embedding, sectioning, and H&E staining were processed at the UW Carbone Cancer Center Experimental Pathology Laboratory.

Systemic energy balance

To examine systemic energy balance, a metabolic phenotyping system (LabMaster modular animal monitoring system; TSE Systems, Chesterfield, MO) was used as previously described (Nelson et al., 2011). The metabolic phenotyping chambers have similar housing, wood chip bedding, temperature, and humidity as the home cage environment. Mice were acclimatized to individual housing and metabolic cages for 1 week before experiment. During the experiment, mice were sequentially fed with standard chow, the semi-purified defined diets containing 10% (D12450B, Research Diets, New Brunswick, NJ), and 60% calories from fat (high fat diet; D12492, Research Diets, New Brunswick, NJ) for 3 days each diet at room temperature (23ºC). Body weight and body composition were measured at the beginning and the end of each diet treatment. Consumption of food and drink were monitored. As indicators of energy expenditure, oxygen consumption and carbon dioxide production were measured, and the metabolic rate was calculated from a modified Weir equation: kcal = 3.941 x V_{O2} (L) + 1.106 x V_{CO2} (L) (Weir, 1949) and analyzed before and after adjusting for body weight. To examine whether there was a genotype effect on energy expenditure, average oxygen consumption per day was plotted against body weight for each mouse after each diet treatment.

To assess the components involved in energy expenditure, core body temperature and physical activity were monitored continuously in a subset of mice equipped with a wireless telemeter implanted in the abdominal cavity. Following surgical implantation of the telemeters, the mice were allowed to recover for 3-4 weeks before experiment. To examine the effect of thermoregulation from brown adipose tissue (BAT) in energy expenditure, mice were further maintained on 60% diet but the cage temperature was set as 32^{o}C. To test the BAT function, mice were further housed at mild cold 16^{o}C and extreme cold 4^{o}C for 1-3 days each temperature. To examine diet-induced thermogenesis, mice were fasted for 12 hours at 4^{o}C during the day after maintained at 16^{o}C or 4^{o}C for 1-2 days.

Assessment of BAT function in vivo

To evaluate BAT function, maximal thermogenic capacity targeting β-adrenergic signaling was examined. 17-23-week old WT and *M1*$^{-/-}$ females were either acclimatized to chow or high-fat diet 3 days at thermoneutrality (32^{o}C). Mice were then administered 1 mg/kg body weight of the β3-adrenergic receptor agonist, CL316,243 (Sigma C5976) through intraperitoneal injection at noon. 2-3 hours both before and after drug administration, oxygen consumption and carbon dioxide production were measured under thermoneutrality using the metabolic phenotyping system.

Statistical Analysis

All data are presented as mean ± SEM. To determine the effects of *Mogat1* deficiency, data from *M1*$^{-/-}$ mice and their WT littermates were compared using the Student's *t*-test. When time in addition to genotype was involved, two-way ANOVA was used to determine the effects of

time, genotype, and interaction, followed by the Bonferroni post-test to assess differences between groups (Prism 5.01, GraphPad Inc.; La Jolla, CA). For average consumption per day, the EE ANCOVA analysis done for this work was provided by the NIDDK Mouse Metabolic Phenotyping Centers (MMPC, www.mmpc.org) using their Energy Expenditure Analysis page (http://www.mmpc.org/shared/regression.aspx) and supported by grant DK076169. $p<0.05$ is considered statistically significant.

Results

MOGAT1 expression in the adipose tissue is inversely correlated with adiposity in humans

To identify a potential physiological function of *MOGAT1*, we took advantage of the published dataset from a human genome wide association study (Civelek et al., 2017) in which abdominal subcutaneous adipose tissues were biopsied from extensively phenotyped participants for profiling mRNA levels. The dataset provides opportunities to identify genes that may be involved in adipose biology and in the regulation of cardio-metabolic traits (Civelek et al., 2017). With the gene-trait correlation analysis, we found that *MOGAT1* expression levels in the adipose tissue were inversely correlated with BMI in both men and women and that adipose *MOGAT1* levels were also negatively associated with the percentage of body fat, fasting plasma insulin level, and the insulin resistance index HOMA-IR in men (Table 2-1).

Mogat1 expression in the adipose tissue is inversely correlated with adiposity in mice

To determine if the expression of *Mogat1* is also inversely associated with adiposity in mice, we analyzed data from a mouse genome wide association study (Parks et al., 2015). In this dataset, a diverse population of more than 100 unique inbred strains of male and female mice were phenotyped for obesity related traits after feeding a diet rich in fat and refined carbohydrates, and their tissues were collected and profiled for mRNA levels. Using the gene-trait correlation analysis, we found *Mogat1* expression levels in the gonadal adipose tissue of both male and female mice were inversely correlated with body weight and fat mass before and after the diet treatment (Table 2-2). Adipose *Mogat1* expression was also negatively associated with the mass of various fat depots collected, including subcutaneous, visceral, gonadal, mesenteric, and retroperitoneal fat (Table 2-2). Although there was no significant association

with the fasting blood glucose levels, adipose *Mogat1* expression levels were inversely associated with the fasting plasma insulin levels and HOMA-IR (Table 2-2).

Mogat1 deficient mice accrue more fat mass when fed a high-fat diet

Based on the inverse relationship between *Mogat1* expression in the adipose tissue and adiposity in both humans and mice, we hypothesize that *Mogat1* limits fat mass expansion. To test the hypothesis, we examined if mice lacking a functional *Mogat1* globally (*Mogat1*$^{-/-}$; *M1*$^{-/-}$) are prone to accumulate excess body fat when fed a high-fat, high-refined carbohydrate diet. *M1*$^{-/-}$ mice grew normally during the suckling periods and had body weight similar to their wildtype (WT) littermates of corresponding sex when fed with a regular low-fat chow diet (*M1*$^{-/-}$ versus WT; when weaned at 3 weeks of age, female: 7.99 ± 0.33 g versus 8.24 ± 0.22 g and male: 8.46 ± 0.43 g vs 8.68 ± 0.20 g; at 6 months of age, female: 24.40 ± 1.33 g vs 24.30 ± 0.73 g and male: 31.58 ± 1.33 g vs 31.55 ± 1.24 g), although *M1*$^{-/-}$ females appeared to have a higher lean mass than WT at 3 months of age (Fig 2-1B). When fed a high-fat diet, both *M1*$^{-/-}$ females (Fig 2-1A) and *M1*$^{-/-}$ males (Fig 2-2A) gained significantly more body weight than their WT littermate controls. The body weight gain was due to the expansion of fat mass (Fig 2-1B and 2-2B) with enlarged lipid droplets in the adipocytes (Fig 2-1C and D). *M1*$^{-/-}$ mice had significantly more large adipocytes in inguinal fat pads (IWAT) (80-100 μm of diameter) and less small adipocytes in both IWAT (40-60 μm of diameter) and gonadal fat pads (GWAT) (60-80 μm of diameter) compared to WT littermates (Fig 2-1D). Excessive fat accumulation in *M1*$^{-/-}$ females after high-fat feeding was associated with glucose intolerance (Fig 2-1E) and elevated plasma insulin (Fig 2-1F). Comparing to WT females (Fig 2-1E and F), WT males developed more severe dysfunctional glucose metabolism after high-fat feeding (Fig 2-2C and D) and there was no further deterioration with the loss of *Mogat1* (Fig 2-2C and D).

Mogat1 deficient mice exhibit reduced energy expenditure

To explore the physiological mechanisms by which *Mogat1* deficiency promotes adiposity, systemic energy balance was examined in *M1*$^{-/-}$ female using metabolic phenotyping chambers. Mice were sequentially fed for 3 days at room temperature on each of three diets: a mixed-meal chow or a semi-purified diet containing 10% or 60% calories from fat. Both genotypes gained weight and *M1*$^{-/-}$ mice had more fat mass than WT throughout the study (Fig 2-3A and B). After 3 days of short-term high-fat feeding, *M1*$^{-/-}$ females exhibited significantly greater fat mass than WT (Fig 2-3B). Both *M1*$^{-/-}$ and WT mice exhibited a clear circadian rhythm in calorie intake (Fig 2-3C and 2-4C), respiratory exchange ratio (RER) (Fig 2-3D and 2-4D), and oxygen consumption (VO_2) (Fig 2-3E and 2-4E), as expected.

Both *M1*$^{-/-}$ and WT females showed similar patterns of calorie intake throughout the study (Fig 2-3C), suggesting that the body fat accumulation in *M1*$^{-/-}$ females was not due to the differences in feeding behaviors. This lack of difference in dietary intake was further supported by a lack of significant difference in RER between genotypes, even though RER changed during the light / dark cycle as well as under different diet treatments (Fig 2-3D).

M1$^{-/-}$ females exhibited a decrease in oxygen consumption compared to WT on each of the three diets (Fig 2-3E). When daily average of oxygen consumption was plotted against the body weight of each mouse after each diet treatment, the regression line of *M1*$^{-/-}$ mice was significantly lower than that of WT fed the same diet (Fig 2-3F). Based on the ANCOVA analysis, *M1*$^{-/-}$ mice exhibited an approximately 9% reduction in oxygen consumption compared to WT (Fig 2-3F), suggesting that excessive fat accumulation in *M1*$^{-/-}$ mice is due to a decrease in energy expenditure.

Mogat1 deficient mice have functioning brown adipose tissue

To test if reduced energy expenditure in *M1*$^{-/-}$ mice is due to impaired thermogenic brown adipose tissue, we first assessed the maximal thermogenic capacity by acclimatizing mice fed a chow or high-fat diet, under thermoneutrality (32^{o}C) and activating the β-adrenergic system. After injecting the β3-adrenergic receptor agonist CL316,243, mice showed a decrease in RER (Fig 2-5A) and an increase in oxygen consumption (Fig 2-5B) under both diet condition, as expected from increased fatty acid oxidation to maximize the heat production. The rectal temperature of all mice rose to approximately 39^{o}C. Compared to WT, *M1*$^{-/-}$ females showed similar RER and oxygen consumption after activating β-adrenergic signaling (Fig 2-5), suggesting that the brown adipose tissues of *M1*$^{-/-}$ mice have the same maximal thermogenic capacity.

Mogat1 deficient mice can tolerate cold despite reduced energy expenditure

Largely contributed by the thermogenesis of BAT (Feldmann et al., 2009), mice increase their thermogenesis to defend their body temperature under room-temperature housing (Golozoubova et al., 2004). At thermoneutrality, the cold stress is eliminated and the thermogenic effect from BAT is turned off. *M1*$^{-/-}$ mice still expended less energy at 32^{o}C (Fig 2-6C), suggesting that the reduced energy expenditure in *M1*$^{-/-}$ mice is not due to the decreased thermogenesis from BAT. We next examined if *M1*$^{-/-}$ mice fed a high-fat diet can tolerate increasing degrees of cold challenge at 16^{o}C and then 4^{o}C (with or without food for 12 hours). Both genotypes of mice could tolerate either temperature. As expected, mice expended more energy at cold – the energy expenditure was inversely correlated with the cage temperature (Fig 2-6C). Interestingly, except at 16^{o}C, *M1*$^{-/-}$ mice had statistically significant reductions in energy expenditure (Fig 2-6C) and yet they could maintain core body temperature (Fig 2-6D), as

monitored by intraperitoneal telemeters, under various ambient temperatures. In fact, *M1*$^{-/-}$ mice had an increased core body temperature during the day when housed at 32^{o}C (Fig 2-6D). Taken together, these data would suggest that *M1*$^{-/-}$ mice are better thermally insulated than WT mice. Indeed, when we examined the thickness of skin-embedded adipose tissue (dermal white adipose tissue; dWAT) (Alexander et al., 2015), *M1*$^{-/-}$ mice exhibited thicker dWAT under dorsal skin than did WT mice (Fig 2-7).

Mogat1 deficient mice have reduced ambulatory activity

The intraperitoneal telemeters, used to monitor core body temperature, also measure ambulatory activity. We observed that *M1*$^{-/-}$ mice had reduced ambulatory activity when fed a semi-purified diet at room temperature (23^{o}C) and under thermoneutrality (32^{o}C) (Fig 2-8). Both groups of mice were equally active at 16^{o}C and both decreased activity at 4^{o}C, suggesting that reduction in physical activity may also contribute to the reduction in energy expenditure under certain conditions.

The levels of Mogat1 expression do not correlate with MGAT activities in mouse tissues

To determine if *Mogat1* is expressed in skeletal muscles – and thus may modulate physical activity in a tissue autonomous manner, we examined MGAT activity and the expression levels of *Mogat1* and several related enzymes that have shown MGAT activity *in vitro*, including *Mogat2*, *Dgat1*, and *Dgat2*. The assessment of MGAT activity *in vitro* does not distinguish acyltransferases that possess MGAT activity, and as expected, the highest MGAT activities were found in the intestine, where *Mogat2* is expressed. While the genotype of *M1*$^{-/-}$ mice was confirmed with no detectable *Mogat1* mRNA in all tissues examined (Fig 2-9A), there was no

reduction of MGAT activity in tissues from *M1*$^{-/-}$ mice (Fig 2-9B and C). This finding suggests that, unlike MGAT2, the protein encoded by *Mogat1* is not a major MGAT enzyme *in vivo*.

Loss of Mogat1 exacerbates fat accumulation in genetically obese Agouti mice

To test if the effect of *Mogat1* inactivation requires high-fat feeding, we crossed *M1*$^{-/-}$ mice with the genetically obese, hyperphagic Agouti mice and monitored body weight and body composition of the Agouti mice with or without a functional *Mogat1* gene. We found that, without a functional *Mogat1*, both Agouti females (Fig 2-10A) and males (Fig 2-11A) gained more weight and more fat mass over time (Fig 2-10B, fat mass in 7-month old females, p=0.104, by Student's *t* test; Fig 2-11B). The accretion of body fat in Agouti *M1*$^{-/-}$ mice was also associated with impaired glucose metabolism, as indicated by glucose intolerance in 6-month old females (Fig 2-11C, genotype effect by repeated measures analysis of variance, p=0.057) and impaired blood glucose in response to insulin in 7-month old males (Fig 2-11E).

Discussion

Mogat1 has been cloned (Cases et al., 2001) and identified (Yen et al., 2002) since early 2000. Its potential role in hepatic lipid metabolism has attracted research interest, as the hepatic expression of *Mogat1* is induced in various mouse models of fatty liver (Agarwal et al., 2016; Cortés et al., 2009; Lee et al., 2012; Yu et al., 2016). However, whether the encoded enzyme causes hepatic steatosis remains controversial (Agarwal et al., 2016; Hall et al., 2014; Lee et al., 2012; Yu et al., 2016). In this study, we identified an inverse relationship between the expression levels of *Mogat1* in the adipose tissue and adiposity, using datasets from gene-trait correlation studies, in both human (Civelek et al., 2017) (Table 2-1) and mouse (Parks et al., 2015) (Table 2-2). In addition, mice lacking a functional *Mogat1* globally exhibited reduced energy expenditure (Fig 2-3E and 2-6C) and accrued even more fat mass when fed a high-fat or when had the Agouti mutation causing hyperphagia (Fig 2-1, 2-2, 2-10, and 2-11). These mice were not protected from fatty liver (Fig 2-1G and 2-2E); thus, the role of *Mogat1* in hepatic lipid metabolism is not clear. Instead, we found that *Mogat1* plays an essential role in regulating adiposity and systemic energy metabolism.

The physiological mechanism by which *Mogat1* deficiency promotes positive energy balance and increases adiposity involves reduced energy expenditure. The possibility of increased energy intake is excluded, because *M1*$^{-/-}$ mice exhibited normal feeding behaviors and had the same patterns and quantities of calorie intake as wildtype littermates under all conditions examined (Fig 2-3C). Although we cannot exclude the possibility that *Mogat1*, which is most highly expressed in the stomach (Yen et al., 2002) (Fig 2-9A), may enhance nutrient absorption, this possibility is discounted because the digestion and the absorption for the semi-purified 10% and 60% diet in wildtype mice are almost complete – it's unlikely *M1*$^{-/-}$ mice can absorb even more.

Mice expend a significant portion of metabolic energy to maintain body temperature under regular housing condition at 23ºC. They can generate heat to maintain body temperature in response to low ambient temperature by activating thermogenesis in the brown adipose tissues (BAT), increasing muscle shivering, or thickening a layer of intradermal fat for thermal regulation (Alexander et al., 2015).

M1$^{-/-}$ mice exhibited reduced energy expenditure and had enlarged lipid droplets in the BAT after long-term high-fat feeding, raising the possibility of impaired BAT activation. However, when their BAT thermogenic capacity was examined by acclimatization to thermoneutrality and then maximally activated with a β3-adrenergic agonist, *M1*$^{-/-}$ mice responded to the same extent as WT mice did. In addition, *M1*$^{-/-}$ mice had reduced energy expenditure and at the same time maintained the core body temperature when challenged with cold. Thus, BAT-induced thermogenesis does not contribute the reduction in energy expenditure of *M1*$^{-/-}$ mice. Consistently, *M1*$^{-/-}$ mice still expended less energy than WT mice did under thermoneutrality when the cold stress is eliminated and the thermogenic effect from BAT is inactivated (Fig 2-6C). Muscle shivering could also produce heat to maintain core body temperature and has been shown to fully compensate for thermogenesis in BAT of mice lacking uncoupling protein 1 (UCP1) (and thus the ability to generate heat). The possibility that muscle shivering contributes to thermoregulation of *M1*$^{-/-}$ mice (Fig 2-8) is also low, because *M1*$^{-/-}$ mice did not expended more energy under cold challenge.

The mechanisms underlying reduced energy expenditure of *M1*$^{-/-}$ mice likely involve thermal insulation, like how arctic mammals adapt to extreme cold (SCHOLANDER et al., 1950a; SCHOLANDER et al., 1950b). *Mogat1* regulates the expansion of fat mass and its deficiency results in accumulation of more fat in various depots, including a thicker intradermal fat (Fig 2-7). Because of better insulation from a layer of adipose tissue in the skin, *M1*$^{-/-}$ mice may not need to expend energy to the same extent as WT (Fig 2-6C) to maintain body temperature.

Consistent with the idea, *M1*$^{-/-}$ mice had a higher core body temperature under thermoneutrality, suggesting that the thickened intradermal fat may impede dissipation of body heat.

Reduced ambulatory activity may also contribute to the reduction of energy expenditure in *M1*$^{-/-}$ mice. It is not clear if the reduced physical activity is due to systemic or tissue-specific factors, because *Mogat1* expression is low yet detectable in the calf (Fig 2-9A). Thus, we cannot exclude the possibility that local muscle *Mogat1* deficiency impairs muscle functions and causes the decrease in physical activity, which in turn results in reduced energy expenditure and increased adiposity.

Although the protein encoded by *Mogat1* catalyzes TAG synthesis *in vitro* (Yen et al., 2002), it may not catalyze MGAT activity *in vivo*, as supported by the observation that mice lacking a functional *Mogat1* did not show a reduction in MGAT activity in any tissues examined (Fig 2-9). This is consistent with the finding that the hepatic MGAT activities tested in *Agpat2*$^{-/-}$, *Mogat1* deficient *Agpat2*$^{-/-}$, and WT mice are not different from each other despite the different levels of *Mogat1* mRNA expression in the liver (Agarwal et al., 2016).

Most of the genes within the DGAT2 family, which *Mogat1* belongs to, exhibit more than one acyltransferase activity *in vitro* (Yen et al., 2005). Within the same family, a human skin multifunctional acyltransferase can catalyze the synthesis of acylglycerols, waxes, and retinyl ester. *Mogat1* and *Mogat2* coded enzymes not only catalyze MGAT activity but also some DGAT activity (Yen et al., 2005; Yen et al., 2002). *Mogat1*, additionally, exhibits weak but detectable acyl-CoA: fatty acyl alcohol acyltransferase (wax synthase) and acyl-CoA: retinol acyltransferase (ARAT) activities (Yen et al., 2005). In our study, additionally, we found *Mogat1* encoded enzymes also utilized acyl acceptors including monoalkylglycerol ethers, acetyl

monoalkylglycerol ethers, LPC, and LPC-plasmalogen in the test tube (data not shown). It is likely that *Mogat1* limits adiposity through yet unidentified biochemical activities.

In summary, we have identified *Mogat1* as a factor modulating adiposity. Loss of *Mogat1* reduces energy expenditure, likely through enhanced thermal insulation and reduced physical activity. *Mogat1* encoded enzyme may not catalyze MGAT activities *in vivo*. The biochemical reaction of *Mogat1* in the regulation of systemic energy balance and adiposity warrant further investigation.

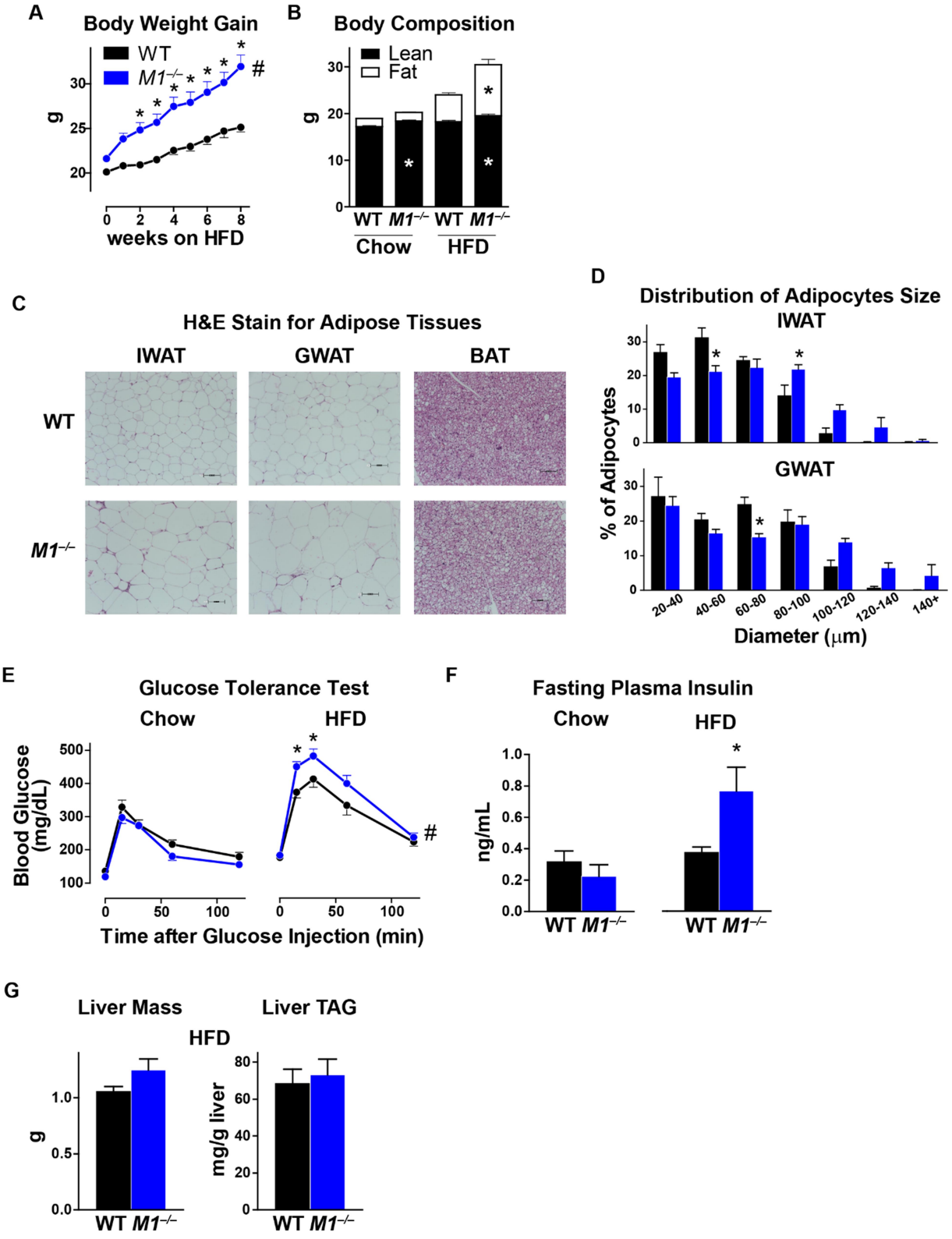
A
Body Weight Gain
WT
M1−/−
g
weeks on HFD
B
Body Composition
Lean
Fat
g
WT M1−/− WT M1−/−
Chow
HFD
C
H&E Stain for Adipose Tissues
IWAT
GWAT
BAT
WT
M1−/−
D
Distribution of Adipocytes Size
IWAT
GWAT
% of Adipocytes
20-40
40-60
60-80
80-100
100-120
120-140
140+
Diameter (μm)
E
Glucose Tolerance Test
Chow
HFD
Blood Glucose (mg/dL)
Time after Glucose Injection (min)
F
Fasting Plasma Insulin
Chow
HFD
ng/mL
WT M1−/−
WT M1−/−
G
Liver Mass
Liver TAG
HFD
g
mg/g liver
WT M1−/−
WT M1−/−

Figure 2-1. *M1*$^{-/-}$ female mice accrue more fat mass when fed a high-fat diet.

A. Body weight gain on high-fat diet. n=13-18/genotype.

B. Body composition before and 8 weeks after high-fat feeding. Mice were fed with a regular chow diet after weaning and switched to the high-fat diet at 10-13 weeks old. n=13-18/genotype.

C. Representative H&E stains on adipose tissues. IWAT, inguinal fat pads; GWAT, gonadal fat pads; BAT, brown adipose tissue. The bottom scale represents 100 μm.

D. Distribution of adipocyte size in IWAT and GWAT quantified by Adiposoft-ImageJ. n=4-5/genotype. There is an interaction between size and genotype effect by repeated measures analysis of variance.

E. Glucose tolerance test after fasting for 4-6 hours. Glucose was challenged through intraperitoneal injection (1 g/kg of body weight, 10% glucose in PBS). n=13-18/genotype for 8 weeks of high-fat fed mice.

F. Fasting plasma insulin level after fasting for 4-6 hours. n=6/genotype for chow fed mice; n=8/genotype for 8 weeks of high-fat fed mice.

G. Liver mass and hepatic TAG levels after 12-14 weeks of high-fat feeding. Liver was harvested after fasting for 4-6 hours. n=7-13/genotype.

Data are presented as mean ± SEM. WT, black circles/lines/bars; *M1*$^{-/-}$, blue circles/lines/bars. **p*<0.05 versus WT littermate controls by the Student's *t* test or the Bonferroni posttests after repeated measures analysis of variance. #p<0.05, genotype effect by repeated measures analysis of variance.

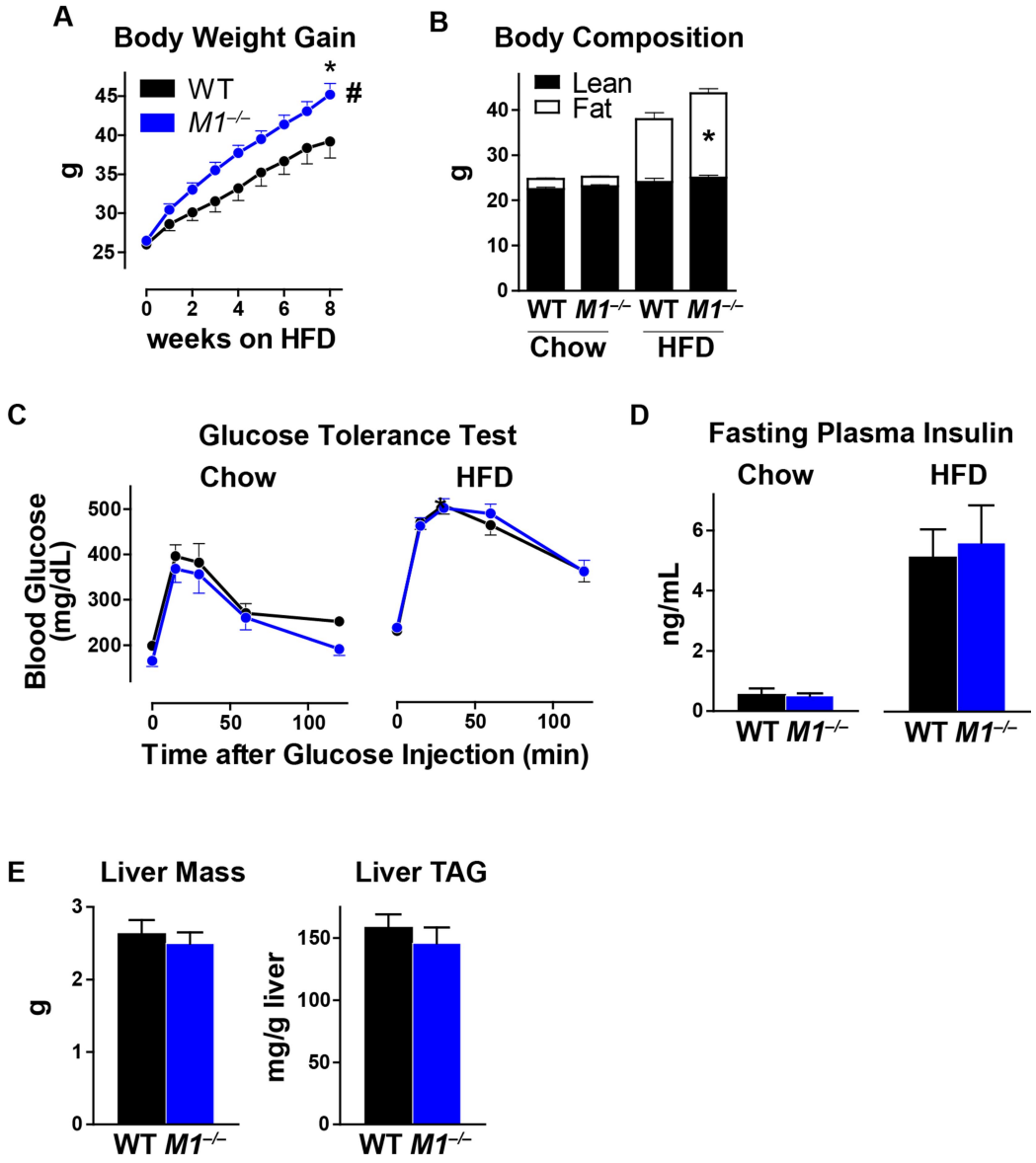

Figure 2-2. *M1*$^{-/-}$ male mice accrue more fat mass when fed a high-fat diet.

A. Body weight gain on high-fat diet. n=8-14/genotype.

B. Body composition before and 8 weeks after high-fat feeding. Mice were fed with a regular chow diet after weaning and switched to the high-fat diet at 10-13 weeks old. n=8-14/genotype.

C. Glucose tolerance test after fasting for 4-6 hours. Glucose was challenged through

intraperitoneal injection (1 g/kg of body weight, 10% glucose in PBS). n=6-7/genotype for chow fed mice; n=18-19/genotype for 8 weeks of high-fat fed mice.

D. Fasting plasma insulin level after fasting for 4-6 hours. n=6-7/genotype for chow fed mice; n=14-15/genotype for 8 weeks of high-fat fed mice.

E. Liver mass and hepatic TAG levels after 12-14 weeks of high-fat feeding. Liver was harvested after fasting for 4-6 hours. n=13-16/genotype.

Data are presented as mean ± SEM. WT, black circles/lines/bars; *M1*$^{-/-}$, blue circles/lines/bars. *p<0.05 versus WT littermate controls by the Student's t test or the Bonferroni posttests after repeated measures analysis of variance. #p<0.05, genotype effect by repeated measures analysis of variance.

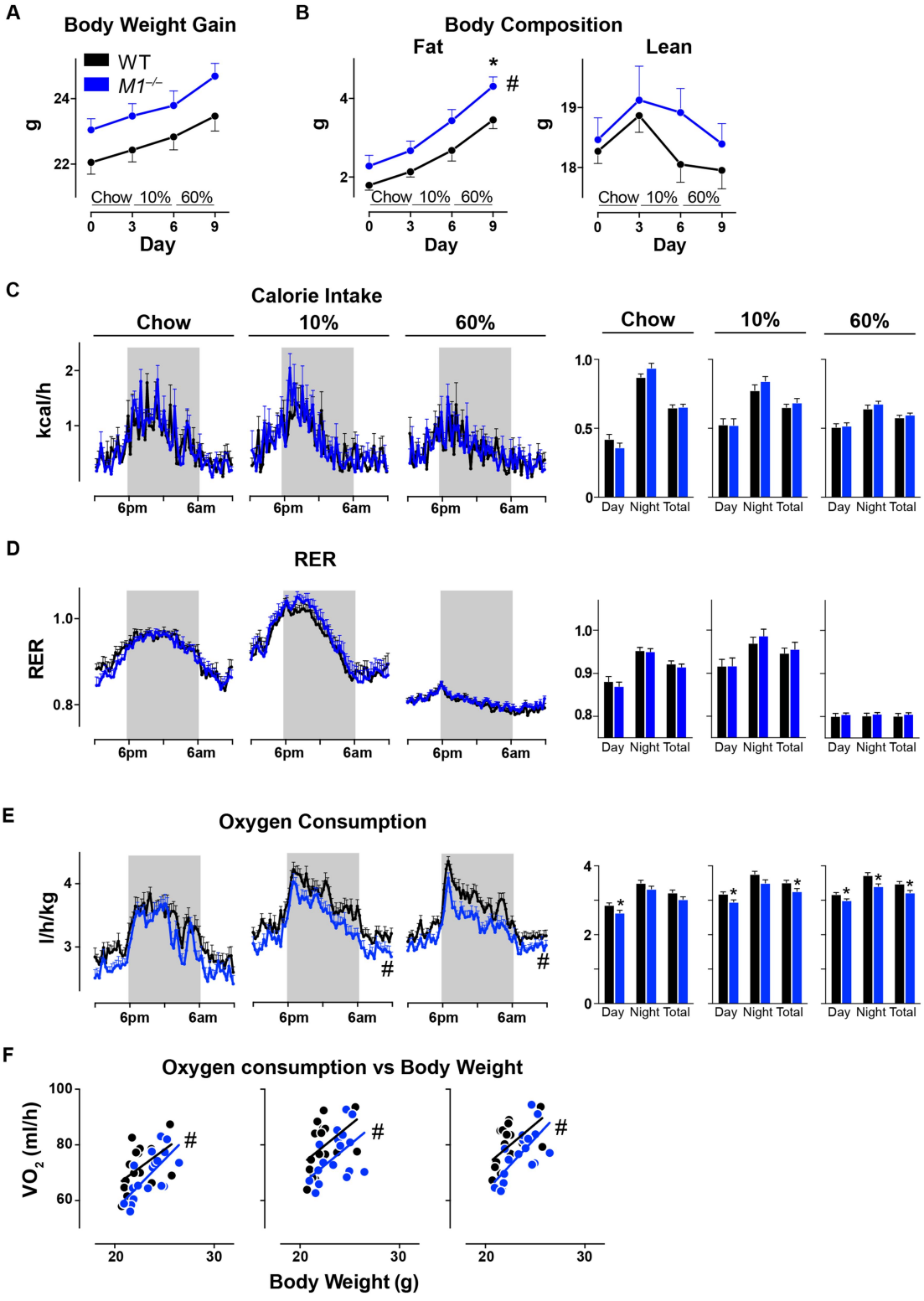
A
Body Weight Gain
WT
M1-/-
g
24
22
Chow 10% 60%
0 3 6 9
Day
B
Body Composition
Fat
Lean
g
4
2
19
18
*
#
Chow 10% 60%
0 3 6 9
Day
C
Calorie Intake
Chow
10%
60%
kcal/h
2
1
6pm 6am
1.0
0.5
0
Day Night Total
D
RER
RER
1.0
0.8
0.9
E
Oxygen Consumption
l/h/kg
4
3
2
F
Oxygen consumption vs Body Weight
VO2 (ml/h)
100
80
60
20 30
Body Weight (g)

Figure 2-3. *M1*$^{-/-}$ female mice exhibit reduced energy expenditure.

10-22-week old *M1*$^{-/-}$ females and WT littermates were individually housed in metabolic phenotyping chambers and sequentially fed with standard chow, the semi-purified defined diets containing 10%, and 60% calories from fat for 3 days each diet at room temperature (23^{o}C).

A. Body weight gain. n=17-18/genotype.

B. Body composition. n=9-10/genotype.

C. Calorie intake. Total calorie intake is presented as bar graphs. n=16-18/genotype.

D. RER (Respiratory Exchange Ratio) calculated by dividing carbon dioxide production with oxygen consumption. Average RER is presented as bar graphs. n=16-18/genotype.

E. Oxygen consumption adjusted by body weight. Average oxygen consumption is presented as bar graphs. n=16-18/genotype.

F. Regression analysis of oxygen consumption versus body weight of mice. Daily average oxygen consumption is plotted against the body weight of each mice after each diet treatment (r^2= 0.22-0.48 for each regression). n=16-18/genotype.

Data are presented as mean ± SEM. Graphs represent the average of two days. Gray areas mark dark phase of the light cycle (6 PM to 6 AM). WT, black circles/lines/bars; *M1*$^{-/-}$, blue circles/lines/bars. *p<0.05 versus WT littermate controls by the Student's *t* test or the Bonferroni posttests after repeated measures analysis of variance. #p<0.05 in line graphs represents genotype effect by repeated measures analysis of variance. #p<0.05 in regression analysis represents the difference between two linear regression lines by ANCOVA.

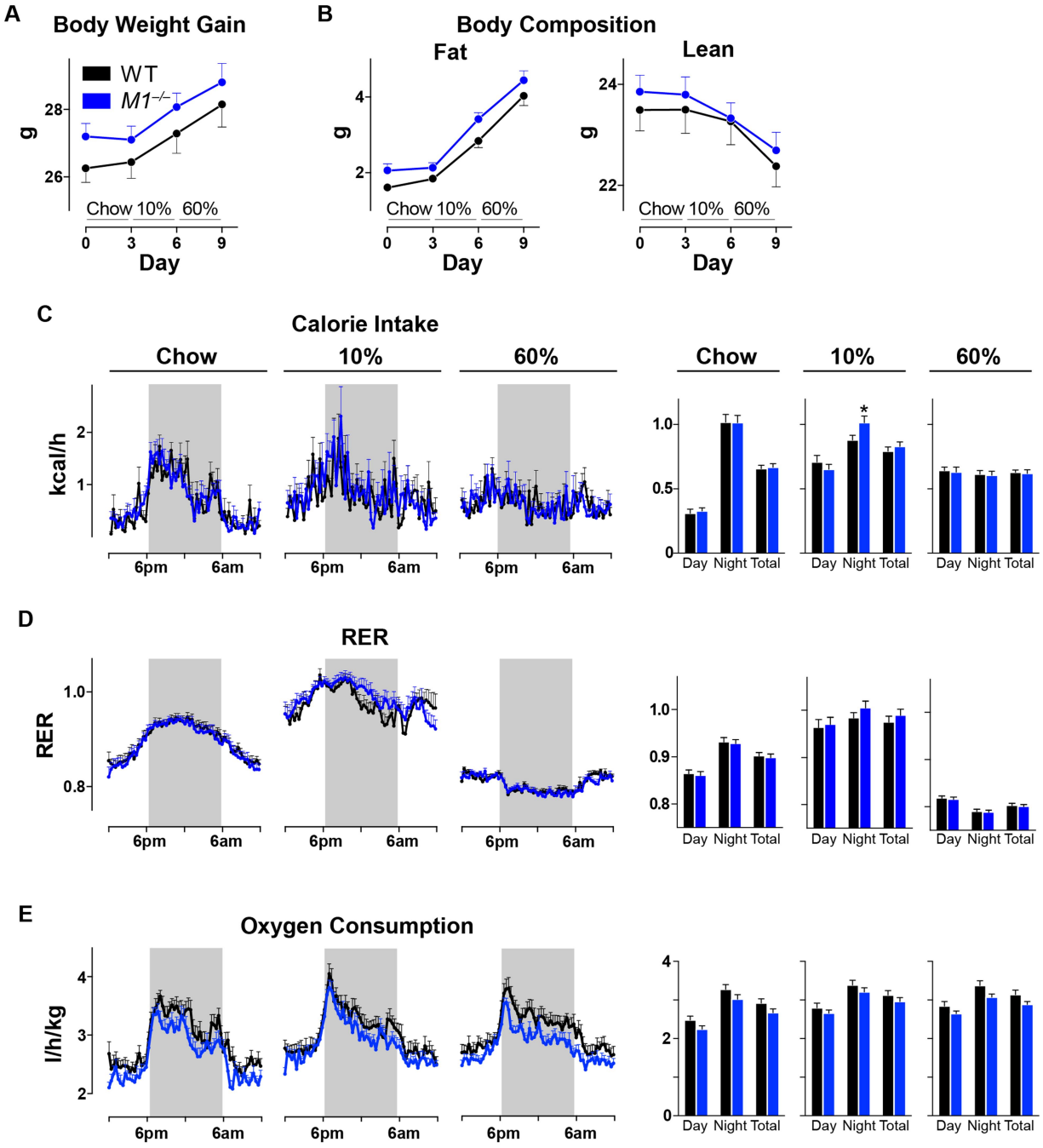

Figure 2-4. *M1*$^{-/-}$ male mice have reduced energy expenditure.

10-15-week old *M1*$^{-/-}$ males and WT littermates were individually housed in metabolic phenotyping chambers and sequentially fed with standard chow, the semi-purified defined diets containing 10%, and 60% calories from fat for 3 days each diet at room temperature (23^{o}C).

A. Body weight gain. n=12-14/genotype.

B. Body composition. n=12-14/genotype.

C. Calorie intake. Total calorie intake is presented as bar graphs. n=12-14/genotype.

D. RER (Respiratory Exchange Ratio) calculated by dividing carbon dioxide production with oxygen consumption (V_{CO2}/V_{O2}). Average RER is presented as bar graphs. n=12-14/genotype.

E. Oxygen consumption adjusted by body weight. Average oxygen consumption is presented as bar graphs. n=12-14/genotype.

Data are presented as mean ± SEM. Graphs represent the average of two days. Gray areas mark dark phase of the light cycle (6 PM to 6 AM). WT, black circles/lines/bars; *M1*$^{-/-}$, blue circles/lines/bars.

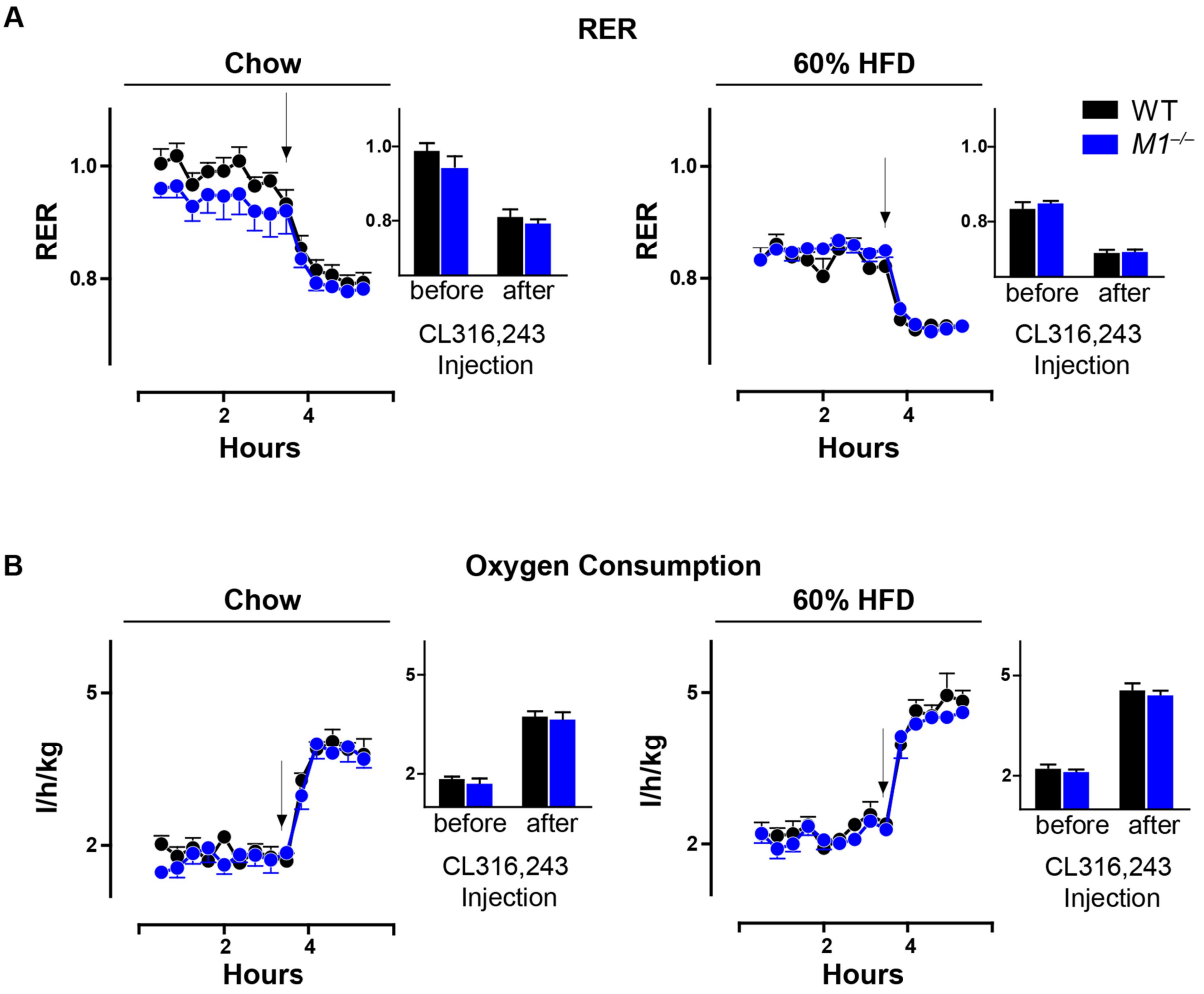

Figure 2-5. *M1*$^{-/-}$ mice have functioning brown adipose tissue

17-23-week old of WT and *M1*$^{-/-}$ females were either acclimatized to chow or high-fat diet 3 days at 32°C. Mice were then administered with 1 mg/kg body weight of CL316,243 through intraperitoneal injection at noon. 2-3 hours both before and after drug administration, the oxygen consumption and carbon dioxide production were measured under thermoneutrality by the metabolic phenotyping system.

A. RER (Respiratory Exchange Ratio) calculated by dividing carbon dioxide production with oxygen consumption (V_{CO2}/V_{O2}). Average RER before and after CL316,243 administration are presented as bar graphs. n=4/genotype.

B. V_{O2} (Oxygen consumption). Average V_{O2} before and after CL316,243 administration are presented as bar graphs. n=4/genotype.

Arrows represent the time of CL316,243 injection. Data are presented as mean ± SEM. WT, black circles/lines/bars; *M1*$^{-/-}$, blue circles/lines/bars.

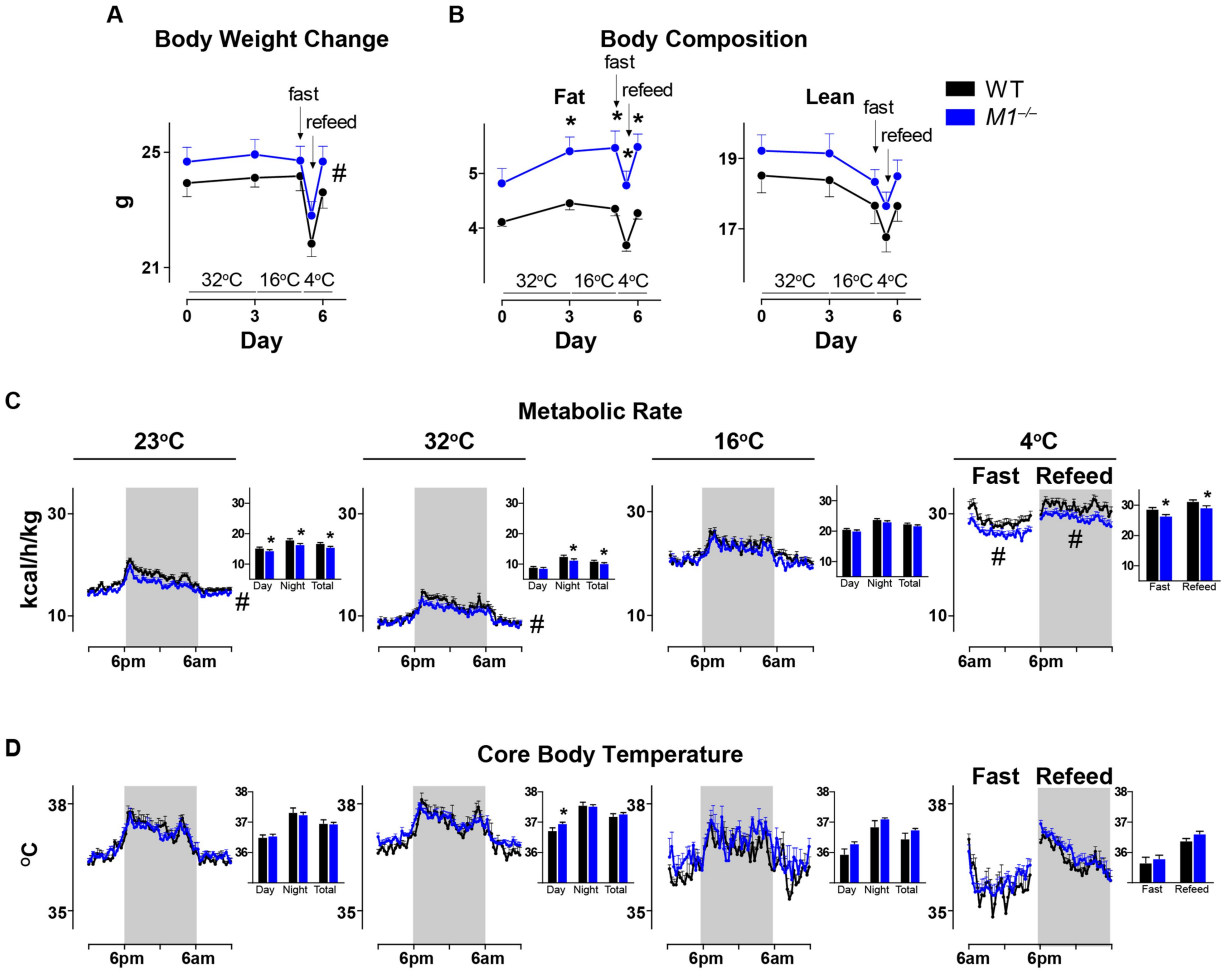

Figure 2-6. *M1*$^{-/-}$ mice can tolerate cold despite reduced energy expenditure.

10-22-week old *M1*$^{-/-}$ females and WT littermates were individually housed in metabolic phenotyping chambers sequentially at 32°C,16°C, and 4°C after acclimatized to 60% diet for 3 days at room temperature. At 4°C, mice were fasted 12 hours during the day and refed at night. Part of the mice were equipped with a wireless telemeter so core body temperature was monitored continuously.

A. Body weight change. n=7-9/genotype.

B. Body composition. n=4/genotype.

C. Metabolic rate calculated by a modified Weir equation (metabolic rate= 3.941 x V_{O2} + 1.106 x

V_{CO2}) and adjusted by body weight. Average metabolic rate is presented as bar graphs. n=7-18/genotype.

D. Core body temperature. Average body temperature is presented as bar graphs. n=7-8/genotype.

Data are presented as mean ± SEM. *p<0.05 versus WT littermate controls by the Student's t test or the Bonferroni posttests after repeated measures analysis of variance. #p<0.05, genotype effect by repeated measures analysis of variance.

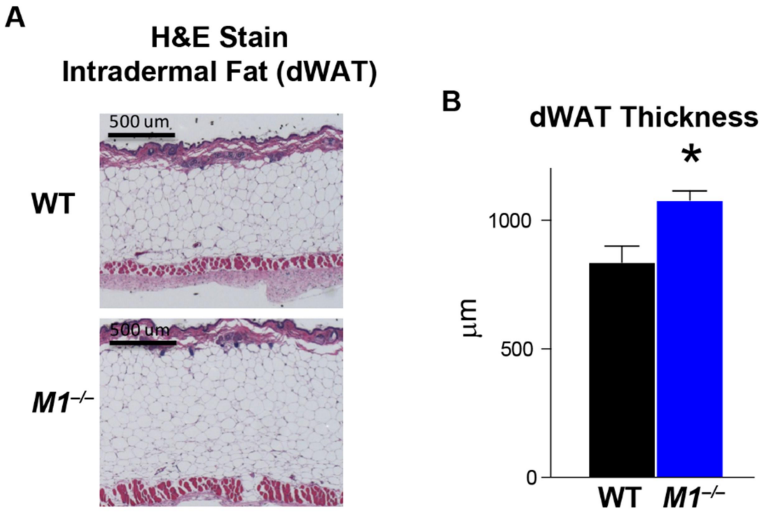

Figure 2-7. *M1*$^{-/-}$ mice are better thermally insulated than WT.

Paraffin-embedded dorsal skin samples collected from *M1*$^{-/-}$ females and WT littermates housed at room temperature after 12 weeks of high-fat feeding. The skin samples were sectioned, H&E stained, and the thickness of intradermal fat (dWAT) was quantified by measuring from muscle to dermis, n=3-4/genotype. Data are presented as mean ± SEM. WT, black bars; *M1*$^{-/-}$, blue bars. *p<0.05 versus WT littermate controls by the Student's *t* test.

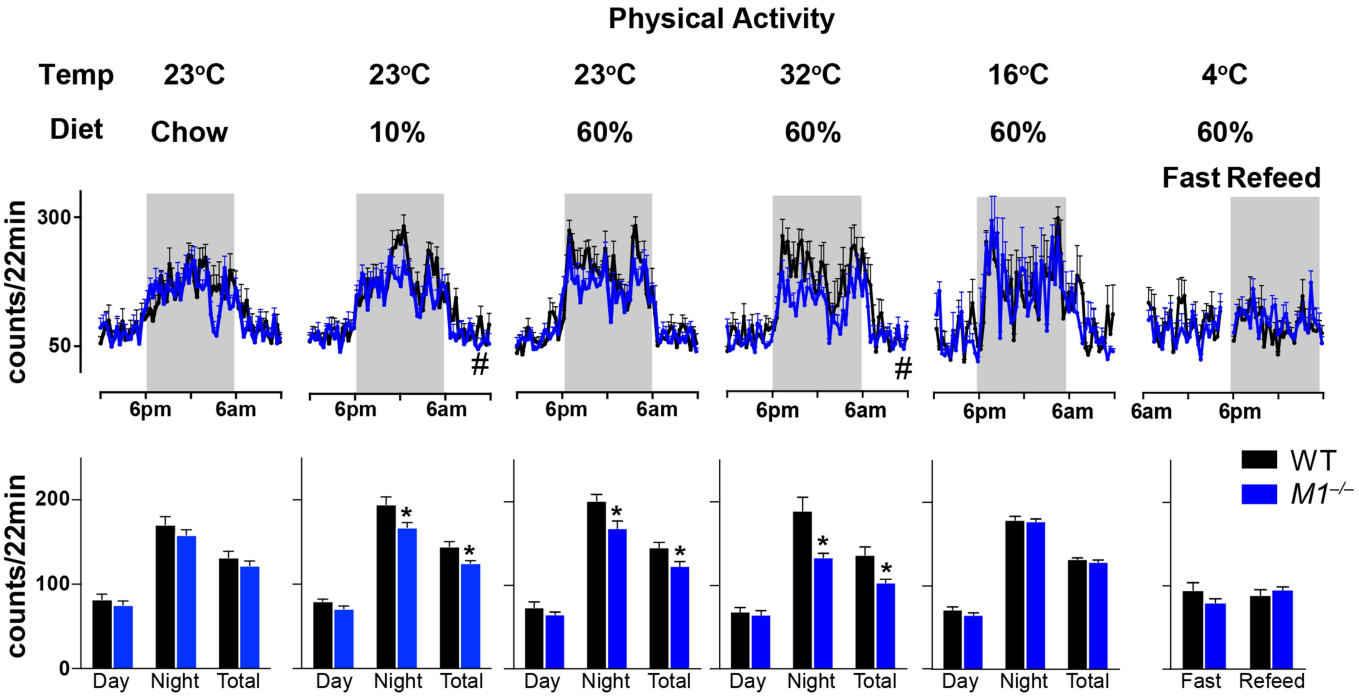

Figure 2-8. *M1*$^{-/-}$ mice have reduced ambulatory activity.

10-22-week old *M1*$^{-/-}$ females and WT littermates were individually housed in metabolic phenotyping chambers sequentially at 32°C,16°C, and 4°C after acclimatized to 60% diet for 3 days at room temperature. At 4°C, mice were fasted 12 hours during the day and refed at night. Physical activity was monitored continuously in mice equipped with a wireless telemeter. Average physical activity is represented as bar graphs. n=7-8/genotype. Data are presented as mean ± SEM. *p<0.05 versus WT littermate controls by the Student's t test. #p<0.05, genotype effect by repeated measures analysis of variance.

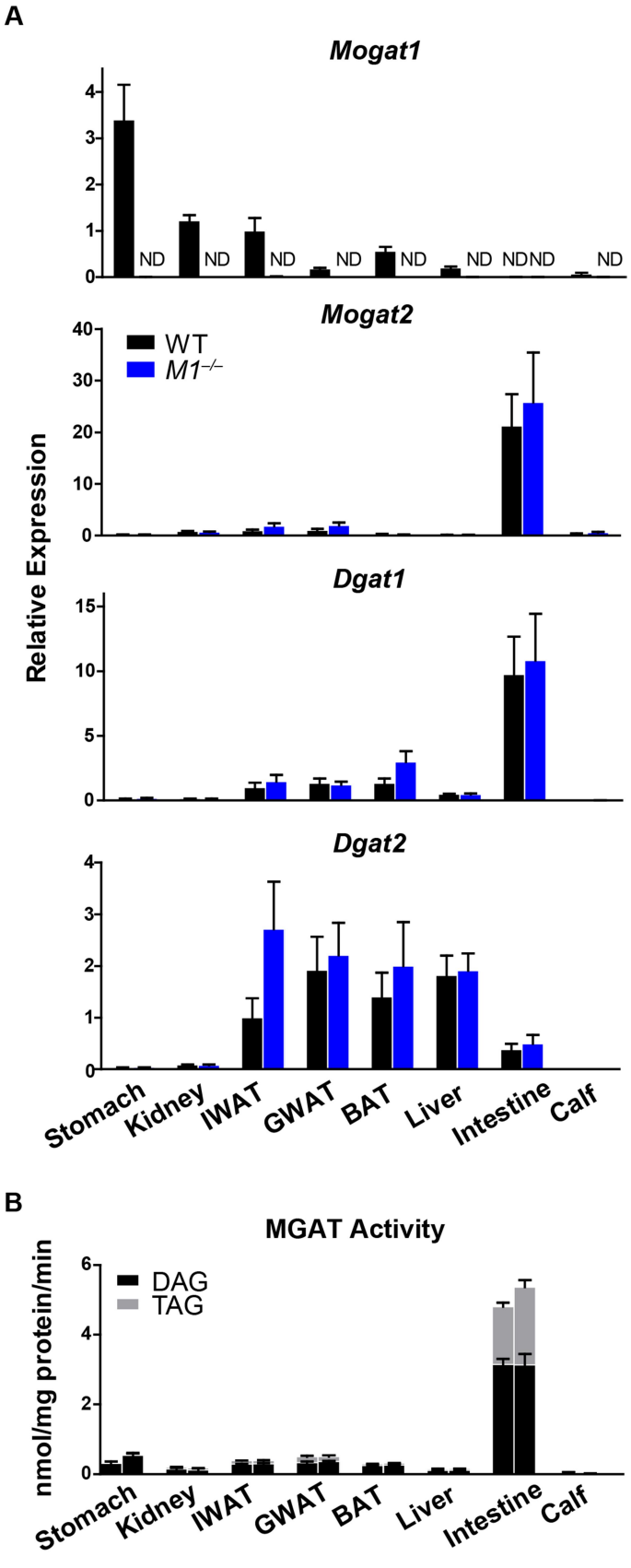
A
Mogat1
ND
Mogat2
WT
M1-/-
Relative Expression
Dgat1
Dgat2
Stomach
Kidney
IWAT
GWAT
BAT
Liver
Intestine
Calf
B
MGAT Activity
DAG
TAG
nmol/mg protein/min

Figure 2-9. The levels of *Mogat1* expression do not correlate with MGAT activities in mouse tissues.

A. *Mogat1*, *Mogat2*, *Dgat1*, and *Dgat2* mRNA expression levels in stomach, kidney, white adipose tissue from inguinal fat pad (IWAT), white adipose tissue from gonadal fat pad (GWAT), brown adipose tissue (BAT), liver, jejunum (intestine), and calf of high-fat fed wildtype (WT) and *M1*$^{-/-}$ female mice. The expression level of each gene in IWAT of WT mice was taken as 1. n= 3-8/genotype. ND, not detected. Data are presented as mean ± SEM. WT, black bars; *M1*$^{-/-}$, blue bars.

B. MGAT activity was measured in the above mouse tissues. Incorporation of ^{14}C-sn-2 monooleoylglycerol into both diacylglycerol (DAG, black bars) and triacylglycerol (TAG, gray bars) represents total MGAT activity. n=3-4/genotype. Data are presented as mean ± SEM.

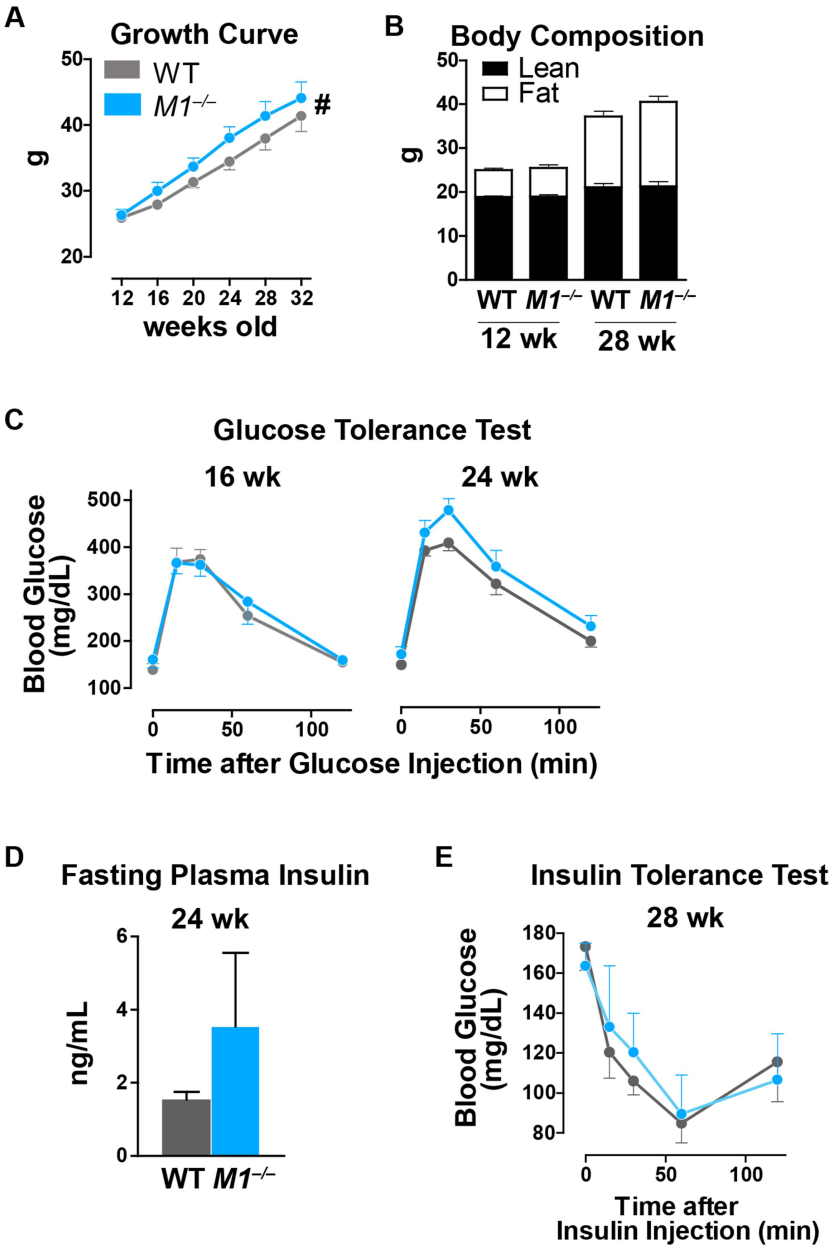

Figure 2-10. Loss of *Mogat1* exacerbates fat accumulation in genetically obese Agouti female mice.

A. Growth curve. n=12-16/genotype

B. Body composition at 12 and 28 weeks old. Mice were fed with chow diet after weaning. n=7-12/genotype.

C. Glucose tolerance test after fasting for 4-6 hours at 16 and 24 weeks old. Glucose was challenged through intraperitoneal injection (1 g/kg of body weight, 10% glucose in PBS). n=4/genotype for 16-week old mice; n=9-16/genotype for 24-week old mice.

D. Fasting plasma insulin levels after fasting for 4-6 hours. n=7/genotype.

E. Insulin tolerance test after fasting for 4-6 hours at 28 weeks old. Insulin was challenged through intraperitoneal injection (1.5 U/kg of body weight, 0.3 U/mL in PBS). n=9-10/genotype.

Data are presented as mean ± SEM. Agouti WT, gray circles/lines/bars; Agouti *M1*$^{-/-}$, light blue circles/lines/bars. #$p<0.05$, genotype effect by two-way ANOVA.

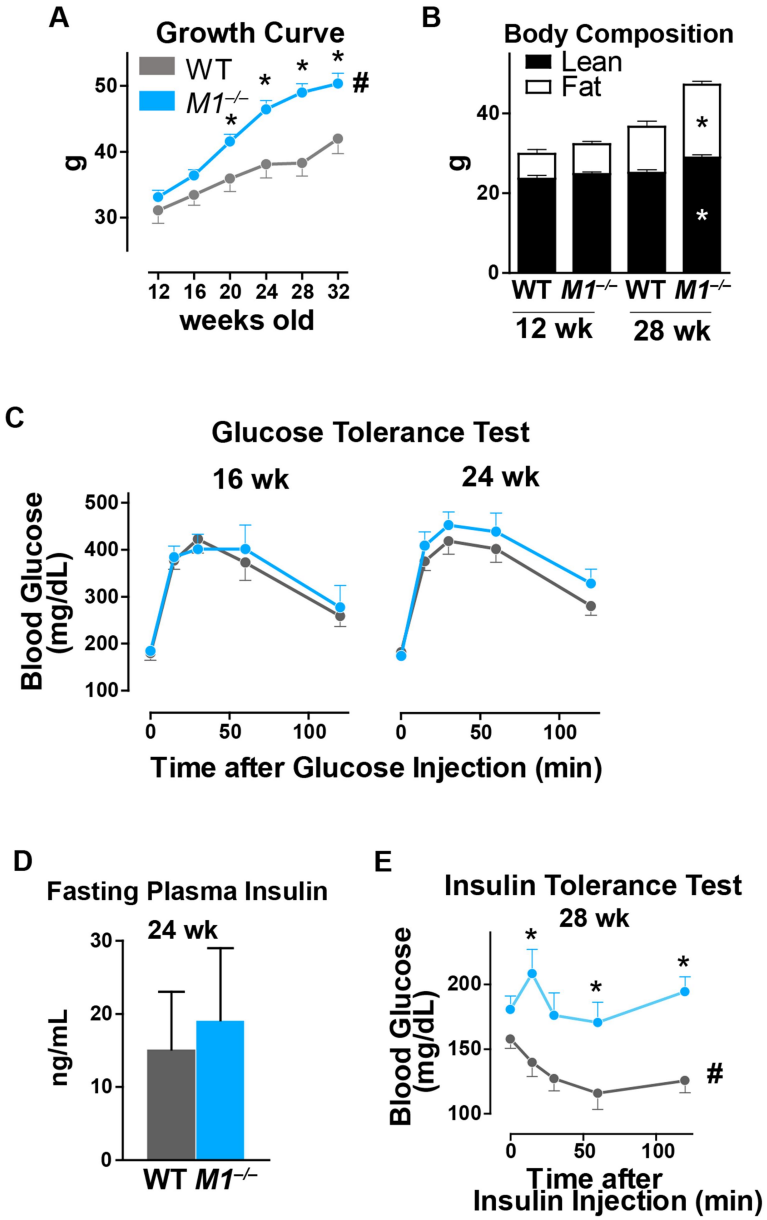

Figure 2-11. Loss of *Mogat1* exacerbates fat accumulation in genetically obese Agouti male mice.

A. Growth curve. n=12-21/genotype

B. Body composition at 12 and 28 weeks old. Mice were fed with chow diet after weaning. n=7-14/genotype.

C. Glucose tolerance test after fasting for 4-6 hours at 16 and 24 weeks old. Glucose was

challenged through intraperitoneal injection (1 g/kg of body weight, 10% glucose in PBS). n=8-9/genotype for 16-week old mice; n=15/genotype for 24-week old mice.

D. Fasting plasma insulin levels after fasting for 4-6 hours. n=10/genotype.

E. Insulin tolerance test after fasting for 4-6 hours at 28 weeks old. Insulin was challenged through intraperitoneal injection (1.5 U/kg of body weight, 0.3 U/mL in PBS). n=10-14/genotype.

Data are presented as mean ± SEM. Agouti WT, gray circles/lines/bars; Agouti *M1*$^{-/-}$, light blue circles/lines/bars. *p<0.05 versus WT littermate controls by the Student's t test or the Bonferroni posttests after repeated measures analysis of variance. #p<0.05, genotype effect by two-way ANOVA.

Table 2-1. Human adipose *Mogat1* gene-trait correlation

	Men		Women	
Trait	*r*	*p* value	*r*	*p* value
BMI	-0.157	3.56E-09	-0.149	5.66E-06
% Fat mass	-0.134	5.15E-07	-0.055	0.098
HOMA-IR	-0.134	4.99E-07	-0.062	0.061
Insulin	-0.128	1.69E-06	-0.053	0.108
Glucose	-0.045	0.096	-0.032	0.338

The data is analyzed from a human genome wide association study in which abdominal subcutaneous adipose tissues were biopsied from extensively phenotyped participants for profiling mRNA levels (Civelek et al., 2017). HOMA-IR, homeostasis model assessment-estimated insulin resistance index. *r*, biweight midcorrelation.

Table 2-2. Mouse adipose *Mogat1* gene-trait correlation

	Males		Females	
Trait	*r*	*p* value	*r*	*p* value
Weight before HF/HS diet	-0.191	0.006	-0.360	5.37E-07
Fat mass before HF/HS diet	-0.533	3.92E-18	-0.515	1.02E-15
Weight after 8 weeks HF/HS diet	-0.553	6.76E-18	-0.709	1.11E-31
Fat mass after 8 weeks HF/HS diet	-0.615	4.54E-25	-0.767	3.31E-42
Subcutaneous fat weight	-0.601	9.79E-24	-0.721	5.24E-35
Visceral fat weight	-0.494	2.13E-15	-0.697	6.99E-32
Gonadal fat weight	-0.423	2.74E-11	-0.662	5.42E-28
Mesenteric fat weight	-0.564	1.52E-20	-0.646	3.10E-26
Retroperitoneal fat weight	-0.148	0.025	-0.633	5.15E-25
HOMA-IR	-0.503	4.15E-14	-0.554	5.93E-15
Insulin	-0.550	4.72E-17	-0.553	6.02E-15
Glucose	-0.001	0.984	-0.130	0.092

The data is analyzed from a mouse genome wide association study (Parks et al., 2015). In this dataset, a diverse population of more than 100 unique inbred strains of male and female mice were phenotyped for obesity related traits after feeding a diet rich in fat and refined carbohydrates, and their tissues were collected and profiled for mRNA levels. HOMA-IR, homeostasis model assessment-estimated insulin resistance index. *r*, biweight midcorrelation.

Acknowledgement

We thank Dr. Yu Gao and Dr. David W. Nelson for pioneering this study. The authors' responsibilities were as follows–TNH and EY: designed the research and wrote the manuscript; BWP: analyzed data from gene-trait correlation studies; TNH and DWN: conducted metabolic studies; CMA and IK: designed and conducted intradermal fat analysis; TNH and MY: analyzed data from mice studies; TNH: conducted most of the experiments and had primary responsibility for the final content of the manuscript. This work was funded by U.S. National Institutes of Health (DK088210) and U.S. Department of Agriculture (WIS01442).

References

Agarwal, A.K., Tunison, K., Dalal, J.S., Yen, C.L., Farese, R.V., Horton, J.D., and Garg, A. (2016). Mogat1 deletion does not ameliorate hepatic steatosis in lipodystrophic (Agpat2-/-) or obese (ob/ob) mice. J Lipid Res *57*, 616-630.

Alexander, C.M., Kasza, I., Yen, C.L., Reeder, S.B., Hernando, D., Gallo, R.L., Jahoda, C.A., Horsley, V., and MacDougald, O.A. (2015). Dermal white adipose tissue: a new component of the thermogenic response. J Lipid Res *56*, 2061-2069.

Cases, S., Stone, S.J., Zhou, P., Yen, E., Tow, B., Lardizabal, K.D., Voelker, T., and Farese, R.V. (2001). Cloning of DGAT2, a second mammalian diacylglycerol acyltransferase, and related family members. J Biol Chem *276*, 38870-38876.

Civelek, M., Wu, Y., Pan, C., Raulerson, C.K., Ko, A., He, A., Tilford, C., Saleem, N.K., Stančáková, A., Scott, L.J., et al. (2017). Genetic Regulation of Adipose Gene Expression and Cardio-Metabolic Traits. Am J Hum Genet *100*, 428-443.

Cortés, V.A., Curtis, D.E., Sukumaran, S., Shao, X., Parameswara, V., Rashid, S., Smith, A.R., Ren, J., Esser, V., Hammer, R.E., et al. (2009). Molecular mechanisms of hepatic steatosis and insulin resistance in the AGPAT2-deficient mouse model of congenital generalized lipodystrophy. Cell Metab *9*, 165-176.

Feldmann, H.M., Golozoubova, V., Cannon, B., and Nedergaard, J. (2009). UCP1 ablation induces obesity and abolishes diet-induced thermogenesis in mice exempt from thermal stress by living at thermoneutrality. Cell Metab *9*, 203-209.

Galarraga, M., Campión, J., Muñoz-Barrutia, A., Boqué, N., Moreno, H., Martínez, J.A., Milagro, F., and Ortiz-de-Solórzano, C. (2012). Adiposoft: automated software for the analysis of white adipose tissue cellularity in histological sections. J Lipid Res *53*, 2791-2796.

Golozoubova, V., Gullberg, H., Matthias, A., Cannon, B., Vennström, B., and Nedergaard, J. (2004). Depressed thermogenesis but competent brown adipose tissue recruitment in mice devoid of all hormone-binding thyroid hormone receptors. Mol Endocrinol *18*, 384-401.

Golozoubova, V., Hohtola, E., Matthias, A., Jacobsson, A., Cannon, B., and Nedergaard, J. (2001). Only UCP1 can mediate adaptive nonshivering thermogenesis in the cold. FASEB J *15*, 2048-2050.

Hall, A.M., Soufi, N., Chambers, K.T., Chen, Z., Schweitzer, G.G., McCommis, K.S., Erion, D.M., Graham, M.J., Su, X., and Finck, B.N. (2014). Abrogating monoacylglycerol acyltransferase activity in liver improves glucose tolerance and hepatic insulin signaling in obese mice. Diabetes *63*, 2284-2296.

Hoover, H.S., Blankman, J.L., Niessen, S., and Cravatt, B.F. (2008). Selectivity of inhibitors of endocannabinoid biosynthesis evaluated by activity-based protein profiling. Bioorg Med Chem Lett *18*, 5838-5841.

KENNEDY, E.P. (1961). Biosynthesis of complex lipids. Fed Proc *20*, 934-940.

Lee, Y.J., Ko, E.H., Kim, J.E., Kim, E., Lee, H., Choi, H., Yu, J.H., Kim, H.J., Seong, J.K., Kim, K.S., et al. (2012). Nuclear receptor PPARγ-regulated monoacylglycerol O-acyltransferase 1 (MGAT1) expression is responsible for the lipid accumulation in diet-induced hepatic steatosis. Proc Natl Acad Sci U S A *109*, 13656-13661.

Lehner, R., and Kuksis, A. (1996). Biosynthesis of triacylglycerols. Prog Lipid Res *35*, 169-201.

Nelson, D.W., Gao, Y., Spencer, N.M., Banh, T., and Yen, C.L. (2011). Deficiency of MGAT2 increases energy expenditure without high-fat feeding and protects genetically obese mice from excessive weight gain. J Lipid Res *52*, 1723-1732.

Parks, B.W., Sallam, T., Mehrabian, M., Psychogios, N., Hui, S.T., Norheim, F., Castellani, L.W., Rau, C.D., Pan, C., Phun, J., et al. (2015). Genetic architecture of insulin resistance in the mouse. Cell Metab *21*, 334-346.

Phan, C.T., and Tso, P. (2001). Intestinal lipid absorption and transport. Front Biosci *6*, D299-319.

SCHOLANDER, P.F., HOCK, R., WALTERS, V., and IRVING, L. (1950a). Adaptation to cold in arctic and tropical mammals and birds in relation to body temperature, insulation, and basal metabolic rate. Biol Bull *99*, 259-271.

SCHOLANDER, P.F., WALTERS, V., HOCK, R., and IRVING, L. (1950b). Body insulation of some arctic and tropical mammals and birds. Biol Bull *99*, 225-236.

WEIR, J.B. (1949). New methods for calculating metabolic rate with special reference to protein metabolism. J Physiol *109*, 1-9.

Yen, C.L., Brown, C.H., Monetti, M., and Farese, R.V. (2005). A human skin multifunctional O-acyltransferase that catalyzes the synthesis of acylglycerols, waxes, and retinyl esters. J Lipid Res *46*, 2388-2397.

Yen, C.L., and Farese, R.V. (2003). MGAT2, a monoacylglycerol acyltransferase expressed in the small intestine. J Biol Chem *278*, 18532-18537.

Yen, C.L., Stone, S.J., Cases, S., Zhou, P., and Farese, R.V. (2002). Identification of a gene encoding MGAT1, a monoacylglycerol acyltransferase. Proc Natl Acad Sci U S A *99*, 8512-8517.

Yu, J.H., Song, S.J., Kim, A., Choi, Y., Seok, J.W., Kim, H.J., Lee, Y.J., Lee, K.S., and Kim, J.W. (2016). Suppression of PPARγ-mediated monoacylglycerol O-acyltransferase 1 expression ameliorates alcoholic hepatic steatosis. Sci Rep *6*, 29352.

Loss of acyl-CoA: monoacylglycerol acyltransferase (MGAT) 2 impairs female reproduction in mice

Ting-Ni Huang, Feng-Chun Miao, and Chi-Liang E Yen*

Department of Nutritional Sciences, University of Wisconsin–Madison, WI 53706

*Address for correspondence:

C.-L. Eric Yen

Department of Nutritional Sciences, University of Wisconsin–Madison

1415 Linden Drive

Madison, WI 53706

Fax: (608) 262-5860

E-mail: yen@nutrisci.wisc.edu

Running title: MGAT2 and female reproduction

Abstract

Acyl-CoA: monoacylglycerol acyltransferase (MGAT) 2 is known for its role in reassembling digested triacylglycerol in the enterocytes during the absorption of dietary fat. Other physiological functions of MGAT2 are not clear. In this study, we unexpectedly observed that female mice lacking MGAT2 exhibited defects in reproduction. These mice had a reduced pregnancy rate after mating (14.8%, compared to 4% in wildtype littermates). For those pregnant MGAT2 deficient dams, more of them had delayed parturition (45.8%, compared to 10% in wildtypes) or dystocia (14.9%, compared to 5.1% in wildtypes). Associated with the delayed parturition, the litter size born to these dams was smaller (6.73 compared to 7.5 pups from wildtype) and the pups suffered from a high neonatal mortality (68% died within 3 days, compared 29% in those born to wildtypes). MGAT2 deficient dams had dysregulated progesterone metabolism and uterine prostaglandin synthesis required for parturition. Bypassing the potential impaired maternal myometrial contraction using Caesarean section delivery, however, failed in rescuing the pups, suggesting that these pups were not fully developed. These findings reveal a novel physiological function of MGAT2 in female reproduction and highlight the potential effect of lipid metabolism on maternal-fetal communication.

Key words: lipid metabolism, female reproduction, pregnancy, parturition, maternal-fetal communication

Introduction

Female reproduction involves the processes of achieving pregnancy and carrying a pregnancy to live birth. Parturition, one of the critical timepoints determining the success in female reproduction, is the process of delivering the fetus from the womb to the extrauterine environment. Initiation of parturition involves the signals from both the fetus and the mother, and the coordination in between (Challis JRG et al., 2000). Successful parturition requires the maturation of fetal organs necessary for extrauterine survival, as well as the maternal myometrium switching from a quiescent state of maintaining pregnancy to an active state of contraction.

Parturition before the maturation of the fetus and parturition beyond the full-term are both associated with health risks. In humans, births occur before 37 weeks are considered preterm (Ferré et al., 2016). The rate of preterm births in the United States is about 10% (Hamilton et al., 2015), which is linked to one-third of infant mortality (Blencowe et al., 2013; Liu et al., 2012). Infants born prematurely may also be compromised with lifelong disabilities (Behrman et al., 2007). On the other hand, pregnancies not delivered after 42 weeks of gestation, two weeks beyond full-term, are considered post-term (Galal et al., 2012). The rate of post-term pregnancy in the United States is about 3%-12%, based on the ultrasound dating or the last menstrual period (Buck and Platt, 2011). Prolonged gestation can put both the fetus and the mother at risk, and it often requires Caesarean delivery (C section) or other strategies for labor induction (Galal et al., 2012).

The causes of preterm birth and post-term pregnancy are multi-factorial and remain poorly understood. Bioactive lipids, derived from phospholipids, cholesterol, and fatty acids, appear to be some of the key factors. For example, parturition is initiated with the fetal maturation signals, such as the release of pulmonary surfactant by the fetus (Mendelson and Condon, 2005). The

process continues with subsequent maternal myometrium contraction, which requires the decrease in maternal circulating progesterone concentration (Virgo and Bellward, 1974) or the withdrawal of progesterone function (Challis JRG et al., 2000; Virgo and Bellward, 1974), as well as myometrial stimulants including prostaglandins $PGF_{2}\alpha$ and PGE_{2} (Challis JRG et al., 2000). Thus, lipid metabolism plays a role in parturition by modulating the levels of pulmonary surfactant, progesterone, and prostaglandins.

Pulmonary surfactant is composed of 10% surfactant proteins and 90% phospholipids with dipalmitoyl phosphatidylcholine (DPPC) as the major species (Schmitz and Müller, 1991). Secretion of the pulmonary surfactant from the fetus to the amniotic fluid signals the maturation of fetal respiratory and immune systems which are required for survival in the extrauterine environment. Low levels of phospholipids and DPPC in the lung and amniotic fluid cause respiratory distress syndrome in preterm birth infants (Ekelund et al., 1973). Fetal pulmonary surfactant synthesis is modulated by maternal nutrition, as DPPC production in the lung of the fetus is stimulated by supplementing fish oil in mouse dams (Blanco et al., 2004).

Progesterone is a steroid hormone derived from cholesterol. During pregnancy, progesterone maintains uterine quiescence by down-regulating prostaglandin production and oxytocin receptors expression in the myometrium (Kota et al., 2013). During parturition, the effects of progesterone must be overcome by factors that coordinate myometrial contraction. Estrogen is one such factor that promotes a series of myometrial changes by increasing the production of prostaglandins $PGF_{2}\alpha$ and PGE_{2} as well as the expression of prostaglandin receptors and oxytocin receptors (Kota et al., 2013).

Prostaglandins $PGF_{2}\alpha$ and PGE_{2} are derivatives of arachidonic acid (AA, C20:4 (n-6)), released from membrane phospholipids (Schildknecht et al., 2008). They are the local stimulants that provoke myometrial contractility (Challis JRG et al., 2000). Biosynthesis of

prostaglandin involves multiple enzymes, including phospholipases, cylcooxygenase, and prostaglandin synthases (Schildknecht et al., 2008). These enzymes in the uterus are thus important for labor induction. Phospholipase A2 (PLA2), an enzyme responsible for the release of AA from glycerophospholipids, as well as cyclooxygenase-1 (COX-1), an enzyme involved in converting AA to prostaglandins, are both expressed in the uterine epithelium (Brown et al., 2009; Gross et al., 1998). Deletion of either enzyme in mice leads to reduced prostaglandin production in the uterus on the day of anticipated delivery, in turn leading to prolonged gestation and an increased mortality rate of litters (Brown et al., 2009; Gross et al., 1998).

Acyl-CoA: monoacylglycerol acyltransferase 2 (MGAT2) catalyzes the synthesis of diacylglycerol, a precursor of the major neutral lipid triacylglycerol. The enzyme is highly expressed in the small intestine and thought to mediate the absorption of dietary fat. Mice lacking a functional MGAT2 globally have greatly reduced intestinal MGAT activity and delayed fat absorption (Yen et al., 2009). Interestingly, these mice absorb normal quantitation of dietary fat but exhibit increased energy expenditure. As a result, these mice are protected from diet-induced as well as genetic obesity and related comorbidities (Nelson et al., 2011; Yen et al., 2009). The physiological function of MGAT2 beyond the regulation of energy balance is not clear.

MGAT2 exhibits relatively high activity with the monoacylglycerol (MAG) containing polyunsaturated fatty acyl groups (Yen and Farese, 2003), including 2-arachidonoylglycerol (2-AG). The enzyme competes with monoacylglycerol lipase (MGL) for MAG substrate. 2-AG hydrolyzed by MGL has been shown to provide AA for PGE_2 synthesis in the brain and in the nervous system to regulate neuroinflammation (Nomura et al., 2011) and fever response (Sanchez-Alavez et al., 2015). MGAT2 may thus modulate 2-AG metabolism and prostaglandin synthesis.

In this study, we made the unexpected observation that MGAT2 deficient female mice exhibited failures in achieving pregnancy, parturition, and neonatal survival. These observations suggest that mouse models of MGAT2 deficiency may help delineate the role of lipid metabolism in female reproduction.

Materials and Methods

Mice

All animal studies were approved by the University of Wisconsin-Madison Animal Care and Use Committee and were performed in accordance with the Public Health Service Policy on Human Care and Use of Laboratory Animals.

Mice globally deficient in *Mogat1* (*M1*$^{-/-}$) (Agarwal et al., 2016), *Mogat2* (*M2*$^{-/-}$) (Yen et al., 2009), and *Dgat1* (*D1*$^{-/-}$) (Smith et al., 2000) were generated at the Gladstone Institutes, University of California at San Francisco, as previously described. These lines of mice used in our studies have been backcrossed into the C57BL/6J genetic background for 10 or more generations. The experimental mice and their wildtype littermate controls were generated by intercrossing heterozygous mice of each genotype. *M1*$^{-/-}$, *M2*$^{-/-}$, and *D1*$^{-/-}$ mice were born at Mendelian ratios, as reported.

To generate mice lacking both *Mogat1* and *Mogat2* globally (*M1*$^{-/-}$*M2*$^{-/-}$ (*M12*$^{-/-}$)), we first produced double-heterozygotes (*M1*$^{+/-}$*M2*$^{+/-}$) as breeders by intercrossing *M1*$^{-/-}$ females with *M2*$^{-/-}$ males, given that *M2*$^{-/-}$ females had difficulties in reproduction (Chapter 3) and in lactation (Chapter 4). However, the number of produced experimental *M1*$^{-/-}$*M2*$^{-/-}$ mice was low as expected (Table 3-1). To increase the probability of generating *M1*$^{-/-}$*M2*$^{-/-}$ mice, we intercrossed *M1*$^{-/-}$*M2*$^{+/-}$ mice. Nonetheless, in the context of MGAT1 deficiency, the additional MGAT2 deficiency appeared detrimental, because the number of the *M1*$^{-/-}$*M2*$^{-/-}$ pups born was only half that of *M1*$^{-/-}$*M2*$^{+/+}$ pups (Table 3-1).

To generate mice without a functional *Mogat2* specifically in the enterocytes (*M2*^{IKO}) or in the adipocytes (*M2*^{AKO}) as well as their littermate controls (*M2*$^{f/f}$), mice possessing the “floxed” *Mogat2* allele (*M2*$^{f/f}$) were bred with mice expressing the Cre transgene under the control of villin

1 (Nelson et al., 2014) or aP2 promoter (B6.Cg-Tg(Fabp4-cre)1Rev/J; The Jackson Laboratory), respectively. Both *M2*^{IKO} and *M2*^{AKO} mice were born at Mendelian ratios.

Mice were housed at 23^{o}C on a 12 hr light / 12 hr dark cycle where the dark phase was from 6 pm to 6 am. They were fed a standard chow diet (8604, Teklad, Madison, WI) after weaning.

Genotyping

Genotypes of mice were determined by PCR. To determine the *Mogat1* genotypes, three primers were used: forward primer between exon 1 and exon 2 of *Mogat1*, 5'-CTGGAGCAAGCAGGGCCAGAATGAG-3'; reverse primer between exon 2 and exon 3 of *Mogat1*, 5'-GGACCTAAGGCACGTTCTGTCTG-3'; reverse primer on *neo* cassette which replaces the deleted exon 2, 5'-CGTTGACTCTAGAGGATCCGAC-3'. The PCR reaction produced a 586-bp amplicon and a ~300-bp amplicon for the wild-type and the *Mogat1*-targeted allele, respectively. To determine the *Mogat2* genotypes, three primers were used: forward primer, 5'-CCTTTAGCCTGGTCTAGGCAGAG-3'; reverse primer, 5'-CAGCAAAGCCCCCTCCTGAATCTCTC-3'; reverse primer on *neo* cassette which replaces the deleted exon 1, 5'-CGTTGACTCTAGAGGATCCGAC-3'. The PCR reaction produced a 381-bp amplicon and a ~200-bp amplicon for the wild-type and the *Mogat2*-targeted allele, respectively. To determine the *Dgat1* genotypes, three primers were used: forward primer, 5'-ACTCCTGTCTCAATGCTGTGG-3'; reverse primers, 5'-TGTGCACGGGGATATTCCAG-3' and 5'-TACCGGTGGATGTGGAATGTGTGC-3'. The PCR reaction produced a 194-bp amplicon and a ~300-bp amplicon for the wild-type and the *Dgat1*-targeted allele, respectively.

To determine the presence of Cre recombinase transgene and an internal control (*Mogat1*), four primers were used: forward primer for Cre, 5'-CCCGGCAAAACAGGTAGTTA-3'; reverse

primer for Cre, 5'-TGCCAGGATCAGGGTTAAG-3'; forward and reverse primers for *Mogat1*, as described above. The PCR reaction produced a 374-bp amplicon and a 586-bp amplicon for transgene and internal control, respectively. To determine the presence of the floxed *Mogat2* allele, two primers were used: forward for *Mogat2*, 5'-GTATGCCACCTGGTGGTAC-3'; reverse for *Mogat2*, 5'-GCAGTCCTATACCAGTACAG-3'. The PCR reaction produced a 478-bp amplicon and a 512-bp amplicon for the wild-type allele and the allele with the addition of a 34-bp *loxP* site, respectively.

Mating and Gestation Timing

8-20-week old virgin female mice were used for breeding experiments, because C57BL/6J females become sexually mature between 6-8 weeks of age and have best reproductive performance before 6 months of age for the first 5 litters (Silver, 1995). 3-6-month old proven fertile male mice were used as breeders (Silver, 1995). Females and males were housed separately until the day of pairing. Mice were paired consecutively 5 nights per week for up to 5 weeks until plugged. To time the gestation more precisely and to increase the chance of a successful copulation, one male and two female mice were housed together right before dark phase between 5-6 pm. The following morning before 10 am, the females were separated from the male and examined for a vaginal plug, which indicates a successful copulation. The presence of a vaginal plug was considered as gestation day 0.5. Females with a vaginal plug were weighed immediately and again two weeks later. A weight gain of 5 g or more and an apparent lateral bulge in the abdomen were considered indicative of a confirmed pregnancy. The number of pairings until observing a vaginal plug and whether the plugged females became pregnant were recorded. After 18 days of pregnancy, the dams were monitored twice a day, in the early morning before 10 am and in the late afternoon after 5 pm. The time when mouse

dams finished giving birth to the whole litter was considered the end of gestation. The date of birth and the litter size born alive or dead were recorded, and in some experiments, the weight of alive pups was measured. Dystocia in mice – a pup is visible in the vaginal canal but cannot pass and/or the dam delivers for an extended period without pushing out additional pups – was also recorded.

When studying the effect of MGAT2 deficiency in dams on parturition, we paired the *M2*$^{-/-}$ females and their WT littermate controls with WT and *M2*$^{-/-}$ males, respectively. With this breeding scheme, all pups have the same genotype so we can examine the genotype effects specifically on the dams.

Caesarean section and the subsequent fostering

Caesarean section (C section) was performed as a terminal study (Murphy, 1993). Following CO_2 euthanasia and cervical dislocation, each dam was placed on her back and her abdomen was sprayed with 70% ethanol. The abdominal cavity was opened with sterile surgery instruments. Uterus was excised by pulling on the extremity of one horn and cutting the ovary and uterine ligaments. Vagina was transected and the other horn of the uterus was excised. The whole uterus with fetuses was placed in a petri dish on a heat pad. Pups were removed by tearing or cutting the uterus with scissors and yolk sac and placenta were cleaned carefully, so that pups were not hurt. Pups were then placed on a paper towel with heat pad. The amniotic fluid in the nostrils and mouth were cleared with cotton swabs. Pups were gently massaged until they resuscitated and started to move and breathed on their own. If the pups took at least one breath on their own, we defined them as alive at birth. We continued stimulating each pup for at least 1 hour or until they were revived and continuously breathed on their own.

Foster moms were separated from their original litters right before fostering. Pups from C section were placed in a nest after mixing them with bedding from the cage used to house the litter from the foster mom. The foster mother was then transferred to the cage with her new litter. The survival of the fostered litter was monitored daily until weaning at 3 weeks of age.

Plasma progesterone and uterine prostaglandin assay

Plasma progesterone (Cayman No. 582601) and uterine $PGF_{2\alpha}$ (Cayman No. 516011) were analyzed using EIA kits with the blood and the uterus collected from dams at pregnancy day 15 and 19, which represent the mid- and late gestation, respectively. Half of the uterus was homogenized in 100% ethanol. The extract was dried and resuspended with the buffer provided in the kit for measurement. Prostaglandins, including $PGF_{2\alpha}$, PGE_2, 6-keto-$PGF_{1\alpha}$, PGD_2, and thromboxane B2, in 50-100 mg of uterus collected at 19 days of gestation were also analyzed using mass spectrometric assays by Dr. Ginger Milne at the Eicosanoid Core Laboratory, Vanderbilt University.

Statistical analysis

All data are presented as mean ± SEM. For determining the effects of MGAT2 deficiency – our primary research goal – data were compared between two groups, *i.e*. $M2^{-/-}$ mice and their WT littermates, using the Student's *t*-test, if the data were normally distributed, and the Mann-Whitney rank sum test, if not. When additional genotypes were included for comparison, one-way ANOVA was first used to determine if there is a genotype effect. If so, the Dunnett's post hoc test was used to determine if the data from each group were different compared to those of their respective controls (*i.e*. WT or $M2^{f/f}$). When time in addition to genotype was involved, two-

way ANOVA was used to determine the effects of time, genotype, and interaction, followed by the Bonferroni post-test to assess differences between groups (Prism 5.01, GraphPad Inc.; La Jolla, CA). To determine the statistical significance of the differences between observed frequencies and expected frequencies, i.e. genotypes of mice produced with certain breeding scheme, plugged, pregnant, or dystocia, the chi-squared test was used. $p<0.05$ is considered statistically significant.

Results

Loss of MGAT2 in female mice reduces the rate of pregnancy

WT female mice required an average of 5.6 pairings to show a vaginal plug (Table 3-2), indicating successful copulation. Six out of 106 females paired repetitively did not exhibit a vaginal plug after 25 or more attempts, and 4 out of 100 (4%) successfully copulated females were not pregnant (Table 3-2). Similar to WT females, mice deficient in MGAT2 globally (*Mogat2*$^{-/-}$; *M2*$^{-/-}$) required an average of 6.2 pairings for successful copulation, and 2 out of 83 females paired did not exhibit a vaginal plug after repetitive attempts (Table 3-2). The copulation-related phenotypic differences were not statistically significant between these two genotypes. In contrast, 12 out of 81 (14.8%) successfully copulated *M2*$^{-/-}$ females were not pregnant. The number was significantly higher than would have been expected from that of WT littermates (p<0.05 by chi-squared test, Table 3-2).

To determine if the effect on pregnancy is specific to MGAT2 deficiency, females lacking a functional MGAT1 (*Mogat1*$^{-/-}$ (*M1*$^{-/-}$)), an enzyme that shares 52% amino acid sequence homology (Yen et al., 2002) and also catalyzes MGAT activity *in vitro*, were mated and examined following the same process. *M1*$^{-/-}$ mice required an average of 5.8 pairings for a successful copulation (Table 3-2). One out of 9 *M1*$^{-/-}$ females paired did not exhibit a vaginal plug, and 1 out of 8 copulated females were not pregnant (Table 3-2). The numbers of *M1*$^{-/-}$ mice were not different statistically from those of WT (Table 3-2). Females deficient in both *Mogat1* and *Mogat2* globally (*Mogat12*$^{-/-}$ (*M12*$^{-/-}$)), on the other hand, exhibited phenotypes like *M2*$^{-/-}$ females. *M12*$^{-/-}$ mice required an average of 5.1 pairings to show a vaginal plug (Table 3-2). All females paired were successful in copulation (Table 3-2), but a higher than expected number of successfully copulated *M12*$^{-/-}$ females were not pregnant (29.4%, 5 out of 17 observations; p<0.05 by chi-squared test; Table 3-2).

M2$^{-/-}$ mice exhibit increased energy expenditure (Nelson et al., 2011; Yen et al., 2009). To explore if the failure in pregnancy is due to the systemic metabolic inefficiency, global DGAT1 deficient (*Dgat1*$^{-/-}$; *D1*$^{-/-}$), which also exhibit increased energy expenditure and are protected from diet-induced obesity (Chen et al., 2002; Nelson et al., 2014; Smith et al., 2000) were examined. These *D1*$^{-/-}$ females required an average of 5.1 pairings to show a vaginal plug, and all females paired successfully copulated (Table 3-2). Like *M2*$^{-/-}$ females, a higher than expected number of successfully copulated *D1*$^{-/-}$ females were not pregnant (36.4%, 4 out of 11 observations; $p<0.05$ by chi-squared test; Table 3-2), suggesting systemic metabolic inefficiency may contribute to the failure in pregnancy.

To explore if the loss of MGAT2 specifically in the adipose tissue or in the intestine recapitulate these phenotypes of global MGAT2 deficiency, adipocyte- (*M2*^{AKO}) and intestine-specific MGAT2 deficient (*M2*^{IKO}) females were examined. Both groups of *M2*^{AKO} and *M2*^{IKO} females had average numbers of pairings to observe a plug as well as high rates of successful copulation and pregnancy similar to their wildtype *M2*$^{f/f}$ controls (Table 3-2).

Loss of MGAT2 in dams impairs parturition

Most of the WT dams in our colony had a gestation period of 19.5 days (52 out of 60 observations; Fig 3-1 and Table 3-3). *M2*$^{-/-}$ dams, however, had a 46% incidence of prolonged gestation; 27 out of 59 dams had parturition later after 19.5 days (Fig 3-1) with an average of 20.18 days of gestation (Table 3-3). In addition to delayed parturition, more *M2*$^{-/-}$ than WT dams had dystocia (when a pup was visible in the vaginal canal but cannot pass, or the dam delivered for an extended period of time and showed weakness in pushing out additional pups); 11 out of 74 *M2*$^{-/-}$ dams as compared to 4 out of 79 WT dams ($p<0.05$ by chi-square test). Like *M2*$^{-/-}$ mice, *M12*$^{-/-}$ dams also had prolonged gestation more frequently with an average of 20.60 days

(Table 3-3), and 2 out of 12 dams had dystocia. In contrast, *M1*$^{-/-}$ and *D1*$^{-/-}$ dams both had gestation periods similar to WT dams.

The initiation of parturition in mice requires a decrease in plasma progesterone and increases in uterine $PGF_{2}\alpha$ and PGE_2 (Challis JRG et al., 2000). Associated with the prolonged gestation, *M2*$^{-/-}$ dams showed abnormal levels in circulating progesterone (Fig 3-3A) and in uterine prostaglandins (Fig 3-3B & Table 3-4), with WT dams exhibiting approximately 70 % reduced progesterone levels (Fig 3-3A) and 6-fold elevated $PGF_{2}\alpha$ levels (Fig 3-3B) from mid- to late gestation. *M2*$^{-/-}$ dams had changes in the same direction, but not to the same extent as WT dams (Fig 3-3). As a result, *M2*$^{-/-}$ dams had a significantly higher level of circulating progesterone (Fig 3-3A) and a lower level of uterine $PGF_{2}\alpha$ (Fig 3-3B), measured by EIA assays, compared to WT at late gestation. Using mass spectrometric assay as an alternative method to quantify tissue prostaglandins, *M2*$^{-/-}$ dams had approximately 28% and 47% reduction in uterine $PGF_{2}\alpha$ and PGE_2 levels, respectively (Table 3-4).

Loss of MGAT2 in dams reduces litter size and survival rate of offspring

The litters born to WT dams had an average size of 7.50 pups and an average survival rate of 96.4% at birth (Fig 3-2 and Table 3-3). The litters born to *M2*$^{-/-}$ dams, however, were smaller with an average size of 6.73 pups and a significantly reduced survival rate of 79.3% at birth (Fig 3-2 and Table 3-3). In addition, 68% of pups born to *M2*$^{-/-}$ dams died within 3 days (Fig 3-2). The high neonatal mortality of *M2*$^{-/-}$ dams was mostly associated with the delayed parturition (Fig 3-1). Compared to those born to WT dams, those of *M12*$^{-/-}$ dams also had a reduced litter size of 4.8 pups and a reduced survival rate of 66.19% at birth (Table 3-3). In contrast, those from *M1*$^{-/-}$ and *D1*$^{-/-}$ dams had normal litter sizes and survival rates (Table 3-3).

Delivery through Caesarean section does not reduce the mortality of neonates from M2$^{-/-}$ dams

To determine whether the delayed parturition in *M2*$^{-/-}$ dams causes the high neonatal mortality at birth, Caesarean section (C section) was performed to deliver neonates at 19 days of gestation. Most neonates (95%) from WT dams were alive at birth, moving and breathing on their own after stimulation, 85% remained alive one hour after C section, and 55% survived throughout the suckling period of 21 days (Fig 3-4), indicating that most fetuses were ready to survive in the extrauterine environment at least a half day before the average gestation period. The neonates from *M2*$^{-/-}$ dams, however, did not survive after the C section delivery on gestation day 19 (Fig 3-4). All their neonates appeared alive immediately after removal from the uterus, but the survival rate dropped to 16% within one hour and none survived over 2 days (Fig 3-4).

Discussion

The gene codes for MGAT2 has been cloned (Cases et al., 2001) and identified (Yen and Farese, 2003) since early 2000. Its physiological function is well-characterized in the small intestine for dietary fat absorption (Yen and Farese, 2003). In other tissues, however, the physiological significance of MGAT2 is not clear. In this study, we identified that MGAT2 is required for female reproduction. Specifically, we observed that female mice with global MGAT2 deficiency exhibited a reduced rate of pregnancy. For those MGAT2 deficient dams with successful pregnancy, they showed failures in parturition including delayed birth and dystocia. These dams also possessed reduced litter size and their litters exhibited a high neonatal mortality.

Female reproduction involves the processes of achieving pregnancy to live birth (Chandra et al., 2013). Achieving pregnancy requires ovulation, copulation, and embryo implantation. In mice, the copulation occurs at the late proestrus or early estrus stage of the estrous cycle, usually with an ovulation. Following copulation, the observation of pregnancy represents the success in ovulation and embryo implantation. We counted numbers of pairings until observing plug formation to represent the length and the existence of estrous cycles, and recorded the subsequent success in pregnancy. MGAT2 deficient females exhibited normal copulation related phenotypes, but a high rate of failure in achieving pregnancy (Table 3-2). These failures might be caused from impaired ovulation or embryo implantation.

Successful ovulation requires the regression of corpus luteum, associated with a reduction in circulating progesterone levels (Harrison and Braunwald, 1987). Thus, it is likely that the dysregulated progesterone metabolism in *M2*$^{-/-}$ dams resulted in a failure in ovulation. Lack of embryo implantation may lead to either reduced pregnancy or litter size. The small litter size observed in *M2*$^{-/-}$ dams may also be a consequence of abnormal embryo implantation, as we

did not observe a clear resorption in the uterus at late gestation. MGAT2 could conceivably be involved in implantation via endocannabinoid signaling. Endocannabinoids, both N-arachidonoylethanolamine (AEA) and 2-arachidonoylglycerol (2-AG), are present in the mouse uterus but with low levels specifically at the implantation site, which is thought to promote implantation (Sun and Dey, 2012; Wang et al., 2007). MGAT2 may use 2-AG as the major substrates because of its high enzyme activity with the MAG containing polyunsaturated fatty acyl groups (Yen and Farese, 2003). It is possible that MGAT2 deficiency leads to the accumulation of 2-AG at the implantation site and in turn decreases the successful rate of implantation resulting in either failures in pregnancy or small litter size.

MGAT2 deficient dams failed in parturition with half of the dams exhibiting delayed parturition (Fig 3-1; Table 3-3) and a high incidence in dystocia. Their prolonged gestation was associated with high neonatal mortality (Fig 3-1 & 3-2; Table 3-3). Delivery via C section immediately before the anticipated delivery to potentially bypass impaired maternal myometrial contraction, however, failed in rescuing the fetuses from *M2*$^{-/-}$ dams (Fig 3-4A). This implies that defective signals essential for maturation at the fetal side may also contribute the prolonged gestation.

Most surviving fetuses from *M2*$^{-/-}$ dams were maintained by the support of their mothers, and appeared to breathe on their own following removal from the uterus (Fig 3-4A). Although the body weight of the fetuses born to *M2*$^{-/-}$ dams by C section were lower compared to those born to WT dams (Fig 3-4B), the delayed growth of the fetuses may not be the cause of death. When allowing the fetuses to remain longer in the uterus for growth, high mortality remained (Fig 3-1). Similarly, C sections performed after prolonged gestation did not rescue the litters (data not shown). This implies that fetal organs may not have been fully developed to signal the mother for parturition and survive in the extrauterine environment.

Because the fetuses possessed the same genotype, their impaired development results from the genotype of dams. MGAT2 deficient mice exhibit increased energy expenditure and are thus protected from diet-induced as well as genetic obesity and related comorbidities (Nelson et al., 2011; Yen et al., 2009). The pregnant females need to increase their calorie intake to support the fetuses, and maternal nutrition can modulate the fetal organ development. For example, supplementing fish oil in mouse dams stimulates the production of dipalmitoyl phosphatidylcholine (DPPC), the major phospholipid species of pulmonary surfactant, in the lung of their fetuses (Blanco et al., 2004). This study provides a new mouse model to study the effects of maternal systemic energy and lipid metabolism on the fetus.

In addition to defective fetal maturation, litter size may also determine the length of gestation. In humans, mothers with twins or triplets have a greater chance in preterm birth than mothers with a single baby. In mice, which have big litter sizes tend to have shorter gestation (Murray et al., 2010; Silver, 1995). We observed litter size was inversely associated with the length of gestation, independent of the genotype in dams (data not shown). Less fetuses may accumulate weaker signals of maturation to communicate with the mother to initiate parturition compared to large litter sizes. Since *M2*$^{-/-}$ dams possessed smaller litter size (Table 3-3), this may have contributed to the prolonged gestation.

The initiation of parturition involves not only the fetal signals for maturation but also maternal signals for myometrial contraction. Myometrial contractions require $PGF_{2}\alpha$ and PGE_2 as stimulants in the uterus. Uterine *Mogat2* expression has been shown to increase upon progesterone stimulation (NCBI Gene Expression Omnibus (GEO)). Although the physiological and biochemical significance of this expression are not clear, it is likely that MGAT2 is involved in prostaglandin synthesis based on its biochemical characteristics. MGAT2 can indirectly provide membrane phospholipids as substrates because it generates DAG for phospholipid synthesis (Coleman and Mashek, 2011). However, we only observed the dysregulation of

$PGF_{2}\alpha$ and PGE_2 but not other eicosanoids such as 6-keto-PGF1α, PGD_2, and thromboxane B2 (Table 3-4). MGAT2 can also limit arachidonic acids (AA, 20:4 (n-6)) as a substrate for prostaglandin synthesis, because of its high enzyme activity with the polyunsaturated fatty acyl-CoA (Yen and Farese, 2003), suggesting MGAT2 deficient dams would possess more prostaglandins, contradictory to our findings.

The low $PGF_{2}\alpha$ and PGE_2 levels may also be a secondary effect of progesterone. Maternal myometrial contractions do not solely rely on one uterine prostaglandin, as $PGF_{2}\alpha$ injection alone was not able to induce the parturition for *M2*$^{-/-}$ dams (data not shown). It involves other components to coordinate the myometrial functional changes, such as the expression of prostaglandin receptors and oxytocin receptors on the myometrium near parturition. In fact, all the components coordinated for myometrial contraction during parturition must overcome the effect of progesterone, which maintains uterine quiescence. Consistent with our finding, *M2*$^{-/-}$ dams exhibited a high progesterone level in the circulation near the anticipated delivery (Fig 3-3A). How MGAT2 is involved in progesterone metabolism remains unclear and will require further investigation.

In summary, we have identified MGAT2 as being required for female reproduction and proposed possible mechanisms for how MGAT2 is involved in pregnancy, parturition, and neonatal survival. The biochemical significance of MGAT2 in the determination of pregnancy, litter size, maternal effects on the fetuses, and progesterone metabolism need further detailed characterization. Nonetheless, this study highlights the potential side effects of MGAT2 inhibitors on women, as MGAT2 is an important pharmaceutical target for treating obesity.

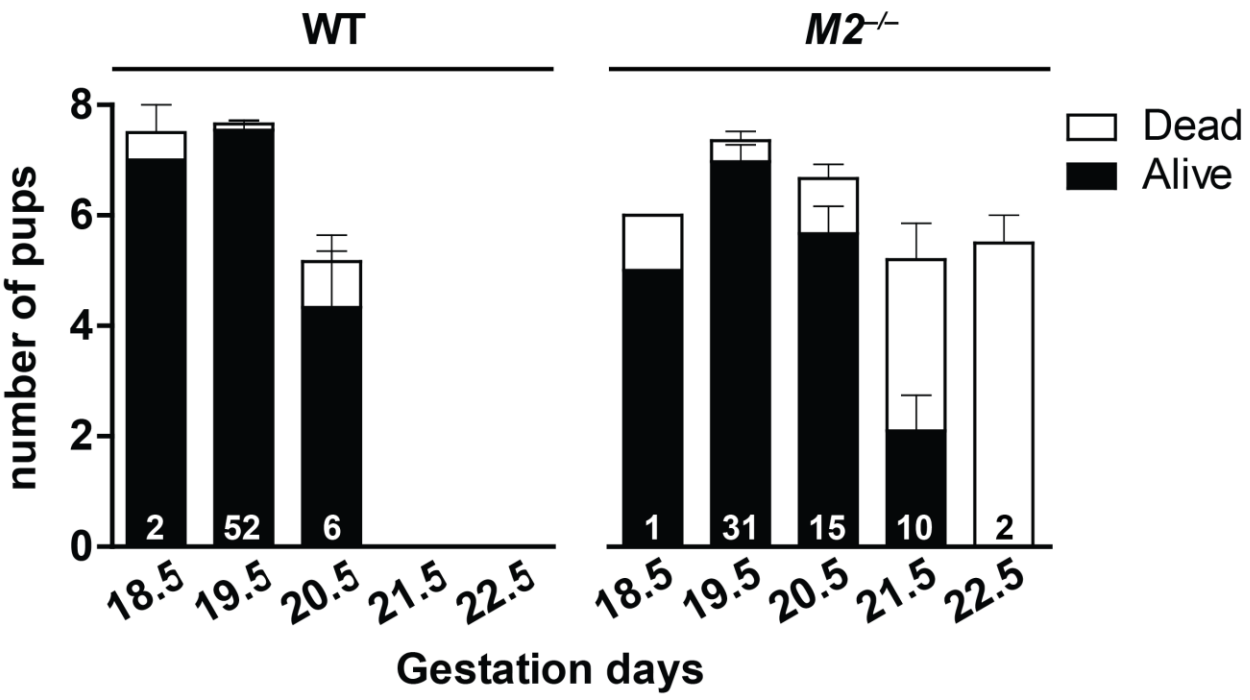

Figure 3-1. Loss of MGAT2 in dams delays parturition and increases mortality of pups at birth.

To determine the gestation days, the presence of a vaginal plug in the virgin female after mating with male mice overnight was considered as gestation day 0.5, and when mouse dams finished giving birth to the whole litter was considered the end of gestation. Data are presented as mean ± SEM. The number of litters observed was indicated as the number written on the bar (WT: 60; *M2*$^{-/-}$: 59 in total). The number of pups alive on the day of birth was represented as black bar; the number of pups dead on the day of birth was represented as white bar.

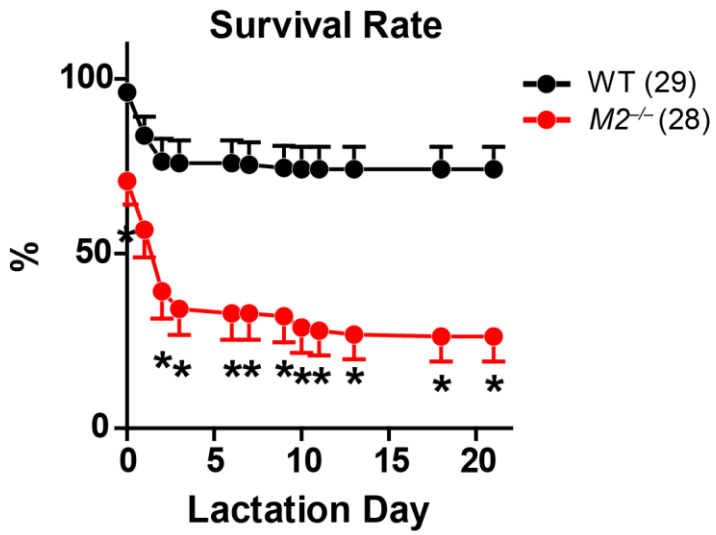

Figure 3-2. Pups born to MGAT2 deficient dams suffer from a high neonatal mortality. Survival curve of the litters born to *M2*$^{-/-}$ or WT dams (litter size in this experiment: 6.0 ± 0.4 in *M2*$^{-/-}$ dams and 7.5 ± 0.4 in WT dams, $p<0.05$). All the pups were the same genotype (*M2*$^{+/-}$) because we paired these first-time dams with male mice of the opposite genotype. The number of litters observed was indicated as the number written in the parentheses next to the genotype of dams. Data are presented as mean ± SEM. Litters born to WT dams were represented as black circles/lines; litters born to *M2*$^{-/-}$ dams were represented as red circles/lines. Repeated measures two-way ANOVA was used to determine the effects of lactation day, genotype and interaction, followed by the Bonferroni post-test to assess the differences versus day-matched controls. The effects of lactation day, genotype, and interaction are statistically significant. *$p<0.05$ is considered statistically significant.

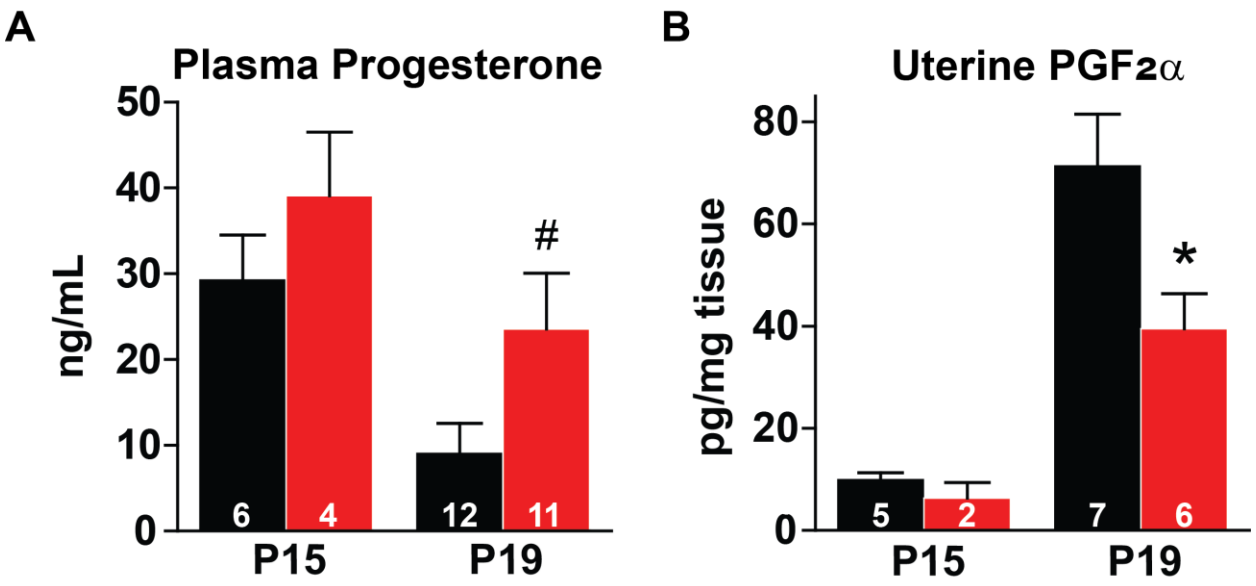

Figure 3-3. *M2*$^{-/-}$ dams do not decrease plasma progesterone or increase uterine PGF2α the day before expected parturition.

To determine the components required for initiation of parturition, progesterone and PGF2α were analyzed in the plasma and uterus collected from dams on gestation day 15 and 19 (P15 and P19). Data are presented as mean ± SEM. The number of dams analyzed was indicated as the number written on the bar. WT dams were represented as black bars; *M2*$^{-/-}$ dams were represented as red bars. Two-way ANOVA was used to determine the effects of gestation day, genotype, and interaction, followed by the Bonferroni post-test to assess differences between groups. *p<0.05 is considered statistically significant. The effects of gestational day on both progesterone and PGF2α are statistically significant. When comparing plasma progesterone at P19, Mann-Whitney rank sum test was used because the data is not normally distributed. #p<0.05 is considered statistically significant.

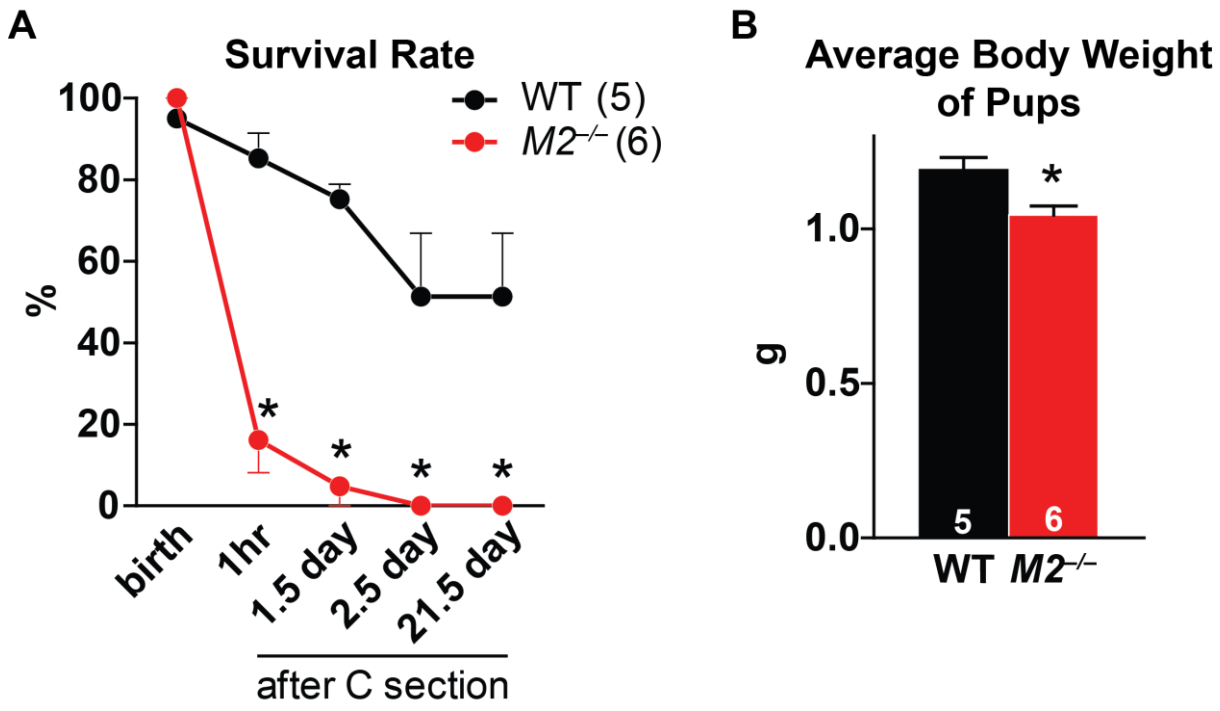

Figure 3-4. Pups born to *M2*$^{-/-}$ dams are not rescued by C section delivery on gestation day 19.

A. Survival rate and B. Body weight at birth of the litters from WT or *M2*$^{-/-}$ dams delivered by C section on gestation day 19. The litters were monitored every day until weaning at 3 weeks of age. Data are presented as mean ± SEM. The number of litters examined was indicated in the parentheses next to the genotype of dams or the number written on the bar. Litters from WT dams were represented as black circles/lines/bars; litters from *M2*$^{-/-}$ dams were represented as red circles/lines/bars. Repeated measures two-way ANOVA was used to determine the effects of time after C section, genotype, and interaction, followed by the Bonferroni post-test to assess differences between groups. The effects of time after C section, genotype, and interaction are statistically significant. Student's *t*-test was used to determine the differences between the average body weight of pups from WT or *M2*$^{-/-}$ dams. *p<0.05 is considered statistically significant.

Table 3-1. In the context of MGAT1 deficiency, mice with the additional MGAT2 deficiency are born at a reduced frequency.

	Offspring			
Parental cross	Genotype	# Expected	# Observed	*p* value
$M1^{-/-}M2^{+/-}$ x $M1^{-/-}M2^{+/-}$	$M1^{-/-}M2^{+/+}$	158.5	221	
	$M1^{-/-}M2^{+/-}$	317.0	309	
	$M1^{-/-}M2^{-/-}$	158.5	104	<0.01*

Chi-squared test was used to determine the significant differences between expected frequencies and observed frequencies of the genotypes. *$p<0.05$ is considered statistically significant.

Table 3-2. Successful copulation and the subsequent pregnancy

Genotype of females	Sample size	# Pairings until observing a plug	# Not plugged	# Not pregnant
WT	106	5.6 ± 0.4	6	4
M2$^{-/-}$	83	6.2 ± 0.5	2	12*
M1$^{-/-}$	9	5.8 ± 1.7	1	1
M12$^{-/-}$	17	5.1 ± 1.0	0	5*
D1$^{-/-}$	11	5.1 ± 0.9	0	4*
M2$^{f/f}$	25	6.6 ± 1.2	2	1
M2^{AKO}	9	6.7 ± 2.2	0	0
M2^{IKO}	14	5.9 ± 1.5	0	1

To determine a successful copulation, female mice were examined for a vaginal plug after pairing with the male overnight. Mice were paired consecutively 5 nights per week for up to 5 weeks until plugged. Females with a weight gain of 5 g or more and an apparent lateral bulge in the abdomen were considered indicative of a confirmed pregnancy. *M2*$^{-/-}$, *Mogat2*$^{-/-}$; *M1*$^{-/-}$, *Mogat1*$^{-/-}$; *M12*$^{-/-}$, *Mogat12*$^{-/-}$ (*M1*$^{-/-}$*M2*$^{-/-}$); *D1*$^{-/-}$, *Dgat1*$^{-/-}$; *M2*$^{f/f}$, *Mogat2*$^{f/f}$; *M2*^{AKO}, Cre driven by aP2 promoter; *M2*^{IKO}, Cre driven by villin 1 promoter. Number of pairings until observing a plug are presented as mean ± SEM. One-way ANOVA was used to determine if there is a genotype effect. Chi-squared test was used to determine if the differences between observed frequencies and expected frequencies (i.e. plugged and pregnant) are statistically significant (*p<0.05).

Table 3-3. Gestation time, litter size, and the survival rate at birth

Genotype of dams	Sample size	Gestation days	Litter size	Survival rate at birth (%)
WT	66	19.56 ± 0.00	7.50 ± 0.00	96.37 ± 0.00
M2$^{-/-}$	59	20.18 ± 0.00*	6.73 ± 0.00	79.31 ± 0.01*
M1$^{-/-}$	7	19.79 ± 0.18	7.29 ± 1.23	97.62 ± 2.38
M12$^{-/-}$	10	20.60 ± 0.28*	4.80 ± 0.85*	66.19 ± 12.85*
D1$^{-/-}$	4	19.50 ± 0.00	8.00 ± 0.41	97.22 ± 2.78

The presence of a vaginal plug in the virgin female after pairing with male mice overnight was considered as gestation day 0.5. The time when mouse dams finished giving birth to the whole litter was considered the end of gestation. *M2*$^{-/-}$, *Mogat2*$^{-/-}$; *M1*$^{-/-}$, *Mogat1*$^{-/-}$; *M12*$^{-/-}$, *Mogat12*$^{-/-}$ (*M1*$^{-/-}$*M2*$^{-/-}$); *D1*$^{-/-}$, *Dgat1*$^{-/-}$; *M2*$^{f/f}$, *Mogat2*$^{f/f}$; *M2*^{AKO}, Cre driven by aP2 promoter; *M2*^{IKO}, Cre driven by villin 1 promoter. Data are presented as mean ± SEM. One-way ANOVA was used to determine if there is a genotype effect. If so, the Dunnett's post hoc test was used to determine if the data from each group were different compared to those of their respective controls (*i.e*. WT or *M2*$^{f/f}$). *p<0.05, different from controls.

Table 3-4. Prostaglandin levels

Genotype of dams	Sample size	$PGF_{2}\alpha$	PGE_2	6-keto-$PGF_{1}\alpha$	PGD_2	Thromboxane B2
		(μg/mg tissue)				
WT	6	32 ± 2	168 ± 12	86 ± 7	347 ± 21	28 ± 2
M2$^{-/-}$	5	23 ± 2*	89 ± 6*	68 ± 10	311 ± 48	26 ± 7

Uterus was collected from dams at gestation day 19. Prostaglandin levels in the uterus was analyzed by mass spectrometric assays at the Eicosanoid Core Laboratory, Vanderbilt University. Data are presented as mean ± SEM. Student's *t*-test was used to determine the difference between WT and *M2*$^{-/-}$ dams. *p<0.05 is considered statistically significant.

Acknowledgement

We thank Dr. Ginger Milne at the Eicosanoid Core Laboratory, Vanderbilt University for performing uterine prostaglandin assay. The authors' responsibilities were as follows–TNH and EY: designed the research and wrote the manuscript; TNH and FCM: conducted breeding experiments and Caesarean section delivery; TNH: analyzed all the data and had primary responsibility for the final content of the manuscript. This work was funded by U.S. National Institutes of Health (DK088210) and U.S. Department of Agriculture (WIS01442).

References

Agarwal, A.K., Tunison, K., Dalal, J.S., Yen, C.L., Farese, R.V., Horton, J.D., and Garg, A. (2016). Mogat1 deletion does not ameliorate hepatic steatosis in lipodystrophic (Agpat2-/-) or obese (ob/ob) mice. J Lipid Res *57*, 616-630.

Behrman, R.E., Butler, A.S., and Institute of Medicine (U.S.). Committee on Understanding Premature Birth and Assuring Healthy Outcomes. (2007). Preterm birth : causes, consequences, and prevention. (Washington, D.C.: National Academies Press).

Blanco, P.G., Freedman, S.D., Lopez, M.C., Ollero, M., Comen, E., Laposata, M., and Alvarez, J.G. (2004). Oral docosahexaenoic acid given to pregnant mice increases the amount of surfactant in lung and amniotic fluid in preterm fetuses. Am J Obstet Gynecol *190*, 1369-1374.

Blencowe, H., Cousens, S., Chou, D., Oestergaard, M., Say, L., Moller, A.B., Kinney, M., Lawn, J., and Group, B.T.S.P.B.A. (2013). Born too soon: the global epidemiology of 15 million preterm births. Reprod Health *10 Suppl 1*, S2.

Brown, N., Morrow, J.D., Slaughter, J.C., Paria, B.C., and Reese, J. (2009). Restoration of on-time embryo implantation corrects the timing of parturition in cytosolic phospholipase A2 group IVA deficient mice. Biol Reprod *81*, 1131-1138.

Buck, G.M., and Platt, R.W. (2011). Reproductive and perinatal epidemiology. (Oxford: Oxford University Press.).

Cases, S., Stone, S.J., Zhou, P., Yen, E., Tow, B., Lardizabal, K.D., Voelker, T., and Farese, R.V. (2001). Cloning of DGAT2, a second mammalian diacylglycerol acyltransferase, and related family members. J Biol Chem *276*, 38870-38876.

Challis JRG, Matthews, S.G., Gibb, W., and Lye, S.J. (2000). Endocrine and paracrine regulation of birth at term and preterm. Endocr Rev *21*, 514-550.

Chandra, A., Copen, C.E., and Stephen, E.H. (2013). Infertility and impaired fecundity in the United States, 1982-2010: data from the National Survey of Family Growth. Natl Health Stat Report, 1-18, 11 p following 19.

Chen, H.C., Smith, S.J., Ladha, Z., Jensen, D.R., Ferreira, L.D., Pulawa, L.K., McGuire, J.G., Pitas, R.E., Eckel, R.H., and Farese, R.V. (2002). Increased insulin and leptin sensitivity in mice lacking acyl CoA:diacylglycerol acyltransferase 1. J Clin Invest *109*, 1049-1055.

Coleman, R.A., and Mashek, D.G. (2011). Mammalian triacylglycerol metabolism: synthesis, lipolysis, and signaling. Chem Rev *111*, 6359-6386.

Ekelund, L., Arvidson, G., and Astedt, B. (1973). Amniotic fluid lecithin and its fatty acid composition in respiratory distress syndrome. J Obstet Gynaecol Br Commonw *80*, 912-917.

Ferré, C., Callaghan, W., Olson, C., Sharma, A., and Barfield, W. (2016). Effects of Maternal Age and Age-Specific Preterm Birth Rates on Overall Preterm Birth Rates - United States, 2007 and 2014. MMWR Morb Mortal Wkly Rep *65*, 1181-1184.

Galal, M., Symonds, I., Murray, H., Petraglia, F., and Smith, R. (2012). Postterm pregnancy. Facts Views Vis Obgyn *4*, 175-187.

Gross, G.A., Imamura, T., Luedke, C., Vogt, S.K., Olson, L.M., Nelson, D.M., Sadovsky, Y., and Muglia, L.J. (1998). Opposing actions of prostaglandins and oxytocin determine the onset of murine labor. Proc Natl Acad Sci U S A *95*, 11875-11879.

Hamilton, B.E., Martin, J.A., Osterman, M.J., Curtin, S.C., and Matthews, T.J. (2015). Births: Final Data for 2014. Natl Vital Stat Rep *64*, 1-64.

Harrison, T.R., and Braunwald, E. (1987). Harrison's principles of internal medicine. (New York: McGraw-Hill).

Kota, S.K., Gayatri, K., Jammula, S., Krishna, S.V., Meher, L.K., and Modi, K.D. (2013). Endocrinology of parturition. Indian J Endocrinol Metab *17*, 50-59.

Liu, L., Johnson, H.L., Cousens, S., Perin, J., Scott, S., Lawn, J.E., Rudan, I., Campbell, H., Cibulskis, R., Li, M., et al. (2012). Global, regional, and national causes of child mortality: an updated systematic analysis for 2010 with time trends since 2000. Lancet *379*, 2151-2161.

Mendelson, C.R., and Condon, J.C. (2005). New insights into the molecular endocrinology of parturition. J Steroid Biochem Mol Biol *93*, 113-119.

Murphy, D. (1993). Caesarean section and fostering. Methods Mol Biol *18*, 177-178.

Murray, S.A., Morgan, J.L., Kane, C., Sharma, Y., Heffner, C.S., Lake, J., and Donahue, L.R. (2010). Mouse gestation length is genetically determined. PLoS One *5*, e12418.

Nelson, D.W., Gao, Y., Spencer, N.M., Banh, T., and Yen, C.L. (2011). Deficiency of MGAT2 increases energy expenditure without high-fat feeding and protects genetically obese mice from excessive weight gain. J Lipid Res *52*, 1723-1732.

Nelson, D.W., Gao, Y., Yen, M.I., and Yen, C.L. (2014). Intestine-specific deletion of acyl-CoA:monoacylglycerol acyltransferase (MGAT) 2 protects mice from diet-induced obesity and glucose intolerance. J Biol Chem *289*, 17338-17349.

Nomura, D.K., Morrison, B.E., Blankman, J.L., Long, J.Z., Kinsey, S.G., Marcondes, M.C., Ward, A.M., Hahn, Y.K., Lichtman, A.H., Conti, B., et al. (2011). Endocannabinoid hydrolysis generates brain prostaglandins that promote neuroinflammation. Science *334*, 809-813.

Sanchez-Alavez, M., Nguyen, W., Mori, S., Moroncini, G., Viader, A., Nomura, D.K., Cravatt, B.F., and Conti, B. (2015). Monoacylglycerol Lipase Regulates Fever Response. PLoS One *10*, e0134437.

Schildknecht, S., Daiber, A., Ghisla, S., Cohen, R.A., and Bachschmid, M.M. (2008). Acetaminophen inhibits prostanoid synthesis by scavenging the PGHS-activator peroxynitrite. FASEB J *22*, 215-224.

Schmitz, G., and Müller, G. (1991). Structure and function of lamellar bodies, lipid-protein complexes involved in storage and secretion of cellular lipids. J Lipid Res *32*, 1539-1570.

Silver, L.M. (1995). Mouse genetics : concepts and applications. (New York: Oxford University Press).

Smith, S.J., Cases, S., Jensen, D.R., Chen, H.C., Sande, E., Tow, B., Sanan, D.A., Raber, J., Eckel, R.H., and Farese, R.V. (2000). Obesity resistance and multiple mechanisms of triglyceride synthesis in mice lacking Dgat. Nat Genet *25*, 87-90.

Sun, X., and Dey, S.K. (2012). Endocannabinoid signaling in female reproduction. ACS Chem Neurosci *3*, 349-355.

Virgo, B.B., and Bellward, G.D. (1974). Serum progesterone levels in the pregnant and postpartum laboratory mouse. Endocrinology *95*, 1486-1490.

Wang, H., Xie, H., Sun, X., Kingsley, P.J., Marnett, L.J., Cravatt, B.F., and Dey, S.K. (2007). Differential regulation of endocannabinoid synthesis and degradation in the uterus during embryo implantation. Prostaglandins Other Lipid Mediat *83*, 62-74.

Yen, C.L., Cheong, M.L., Grueter, C., Zhou, P., Moriwaki, J., Wong, J.S., Hubbard, B., Marmor, S., and Farese, R.V. (2009). Deficiency of the intestinal enzyme acyl CoA:monoacylglycerol acyltransferase-2 protects mice from metabolic disorders induced by high-fat feeding. Nat Med *15*, 442-446.

Yen, C.L., and Farese, R.V. (2003). MGAT2, a monoacylglycerol acyltransferase expressed in the small intestine. J Biol Chem *278*, 18532-18537.

Yen, C.L., Stone, S.J., Cases, S., Zhou, P., and Farese, R.V. (2002). Identification of a gene encoding MGAT1, a monoacylglycerol acyltransferase. Proc Natl Acad Sci U S A *99*, 8512-8517.

Loss of acyl-CoA: monoacylglycerol acyltransferase (MGAT) 2 impairs mammary gland functions in mice

Ting-Ni Huang, Mei-I Yen, Feng-Chun Miao, and Chi-Liang E Yen*

Department of Nutritional Sciences, University of Wisconsin–Madison, WI 53706

*Address for correspondence:

C.-L. Eric Yen

Department of Nutritional Sciences, University of Wisconsin–Madison

1415 Linden Drive

Madison, WI 53706

Fax: (608) 262-5860

E-mail: yen@nutrisci.wisc.edu

Running title: MGAT2 and milk production

Abstract

Acyl-CoA: monoacylglycerol acyltransferase (MGAT) 2 mediates dietary fat absorption by catalyzing triacylglycerol synthesis in the enterocytes. Mammary epithelia also synthesize triacylglycerol, which accounts for more than 95% of milk fat. In this study, to test the hypothesis that MGAT2 is required for milk fat production in mice, we collected and analyzed milk from MGAT2 deficient dams and wildtype dams that had suckling pups – we observed that loss of MGAT2 in female mice reduces pregnancy rate, have prolonged gestation, smaller litter size, and a high neonatal mortality of offspring. At early lactation, compared to that from wildtype dams, milk expressed from MGAT2 deficient dams contained 26% lower levels of triacylglycerol. Interestingly, at mid-lactation, compared to milk from wildtype dams, their milk was low not only in triacylglycerol but also in lactose and protein. From cross-fostering experiments, in which pups born on the same day to wildtypes and MGAT2 deficient dams were mixed and evenly distributed, we found that MGAT2 deficient dams produced less quantity of milk at mid-lactation and the pups they nursed weighed less at weaning. The defects in milk production at mid-lactation were associated with reduced differentiation markers, including α-casein, β-casein, and whey acidic protein, which is related to early involution. We found that *Mogat2*, the gene codes for MGAT2, is expressed in the adipocytes but not in the milk producing mammary epithelial cells and that adipose-specific MGAT2 deficient dams had normal milk fat production. These findings reveal a novel physiological role of MGAT2 in mammary gland functions through yet unidentified mechanisms.

Key words: lipid metabolism, milk, mammary glands

Introduction

Triacylglycerol (TAG) is the most energy rich nutrient in the body and plays a pivotal role in cellular and systemic metabolism. The synthesis of TAG in cells is essential for multiple processes including milk fat production. TAG accounts for over 98% milk fat (Anderson et al., 2007), providing fatty acids for growing mammalian neonates and a condensed energy source (Uauy and Castillo, 2003). It can also act as a carrier of other essential nutrients such as lipid soluble vitamins.

There are two main pathways mediating TAG synthesis in mammals: glycerol-3-phosphate (G3P) pathway (Kennedy, 1961) and the monoacylglycerol (MAG) pathway (Lehner and Kuksis, 1996). Different from G3P pathway, which is involved in ubiquitous lipid synthesis, the MAG pathway is well-characterized in the small intestine performing the TAG repackage for dietary fat absorption (Phan and Tso, 2001; Yen and Farese, 2003). Acyl-CoA: monoacylglycerol acyltransferase (MGAT) 2 is the isoform responsible for this physiological function. Mice lacking a functional MGAT2 globally have greatly reduced intestinal MGAT activity and delayed fat absorption (Yen et al., 2009). It therefore affects systemic energy balance with increased energy expenditure and protects mice from diet-induced obesity and related comorbidities (Nelson et al., 2011; Yen et al., 2009). We also reported that MGAT2 is required for female reproduction, although the physiological mechanisms and biochemical significance are not clear (Chapter 3). Other than dietary fat absorption and female reproduction, the physiology of MGAT2 has not been characterized.

In this study, we used genetically engineered mice to test the hypothesis that MGAT2 is required for milk production.

Materials & Methods

Mice

All animal studies were approved by the University of Wisconsin-Madison Animal Care and Use Committee and were performed in accordance with the Public Health Service Policy on Human Care and Use of Laboratory Animals.

Mice globally deficient in *Mogat1* (*M1*$^{-/-}$) (Agarwal et al., 2016), *Mogat2* (*M2*$^{-/-}$) (Yen et al., 2009), and *Dgat1* (*D1*$^{-/-}$) (Smith et al., 2000) were generated at the Gladstone Institutes, University of California at San Francisco, as previously described. These lines of mice used in our studies have been backcrossed into the C57BL/6J genetic background for 10 or more generations. The experimental mice and their wildtype littermate controls were generated by intercrossing heterozygous mice of each genotype. *M1*$^{-/-}$, *M2*$^{-/-}$, and *D1*$^{-/-}$ mice were born at Mendelian ratios, as reported.

To generate mice without a functional *Mogat2* specifically in the enterocytes (*M2*^{IKO}) or in the adipocytes (*M2*^{AKO}) as well as their littermate controls (*M2*$^{f/f}$), mice possessing the “floxed” *Mogat2* allele (*M2*$^{f/f}$) were bred with mice expressing the Cre transgene under the control of villin 1 (Nelson et al., 2014) or aP2 promoter (B6.Cg-Tg(Fabp4-cre)1Rev/J; The Jackson Laboratory), respectively. Both *M2*^{IKO} and *M2*^{AKO} mice were born at Mendelian ratios.

Mice were housed at 23ºC on a 12 hr light / 12 hr dark cycle where the dark phase was from 6 pm to 6 am. They were fed a standard chow diet (8604, Teklad, Madison, WI) after weaning.

Genotyping

Genotypes of mice were determined by PCR. To determine the *Mogat1* genotypes, three primers were used: forward primer between exon 1 and exon 2 of *Mogat1*, 5'-CTGGAGCAAGCAGGGCCAGAATGAG-3'; reverse primer between exon 2 and exon 3 of *Mogat1*, 5'-GGACCTAAGGCACGTTCTGTCTG-3'; reverse primer on *neo* cassette which replaces the deleted exon 2, 5'-CGTTGACTCTAGAGGATCCGAC-3'. The PCR reaction produced a 586-bp amplicon and a ~300-bp amplicon for the wildtype and the *Mogat1*-targeted allele, respectively. To determine the *Mogat2* genotypes, three primers were used: forward primer, 5'-CCTTTAGCCTGGTCTAGGCAGAG-3'; reverse primer, 5'-CAGCAAAGCCCCCTCCTGAATCTCTC-3'; reverse primer on *neo* cassette which replaces the deleted exon 1, 5'-CGTTGACTCTAGAGGATCCGAC-3'. The PCR reaction produced a 381-bp amplicon and a ~200-bp amplicon for the wildtype and the *Mogat2*-targeted allele, respectively. To determine the *Dgat1* genotypes, three primers were used: forward primer, 5'-ACTCCTGTCTCAATGCTGTGG-3'; reverse primers, 5'-TGTGCACGGGGATATTCCAG-3' and 5'-TACCGGTGGATGTGGAATGTGTGC-3'. The PCR reaction produced a 194-bp amplicon and a ~300-bp amplicon for the wildtype and the *Dgat1*-targeted allele, respectively.

To determine the presence of Cre recombinase transgene and an internal control (*Mogat1*), four primers were used: forward primer for Cre, 5'-CCCGGCAAAACAGGTAGTTA-3'; reverse primer for Cre, 5'-TGCCAGGATCAGGGTTAAG-3'; forward and reverse primers for *Mogat1*, as described above. The PCR reaction produced a 374-bp amplicon and a 586-bp amplicon for transgene and internal control, respectively. To determine the presence of the floxed *Mogat2* allele, two primers were used: forward for *Mogat2*, 5'-GTATGCCACCTGGTGGTAC-3'; reverse for *Mogat2*, 5'-GCAGTCCTATACCAGTACAG-3'. The PCR reaction produced a 478-bp amplicon and a 512-bp amplicon for the wildtype allele and the allele with the addition of a 34-bp *loxP* site, respectively.

Milk collection

The date of birth was considered lactation day 0. Milk was collected at lactation day 2 and 12 to represent early and mid-lactation, respectively. One hour before collection, the dam was separated from her litter by covering the pups with a container with ventilation holes. The dam was left inside the same cage to avoid additional stress from leaving her litter. After the separation, the dam was anesthetized using isoflurane gas and injected intraperitoneally with 0.3-0.6-unit oxytocin (Osborn 1OXY016). Her mammary glands were massaged and milk was collected with a capillary tube. 50-100 μL milk was collected for macronutrient analyses. After milk collection, the dam was allowed to recover from anesthesia and then reunited with her pups. Most dams reared their litters normally after milk collection.

Milk composition

Milk composition was assessed for three macronutrients: lactose, protein, and triacylglycerol (TAG). Fatty acid composition from the milk fat was analyzed to delineate the source of substrates. Milk lactose was determined by a lactose assay kit (Roche 10 986 119 035). Milk protein was quantified by the BCA method (ThermoScientific 23225). For TAG and fatty acid composition, lipid was extracted from 30 μL milk with 3 mL chloroform: methanol (2:1, v/v, containing 0.1 mg/mL butylated hydroxytoluene, BHT, to avoid the oxidation of fatty acids) and 1 mL ddH_2O. 17:0 TAG (Nu-Chek Prep T-155) was added to the milk as an internal standard before lipid extraction. The lipid extract was dried under N_2. To determine milk TAG, 10% lipid extract was resuspended with chloroform containing 1% Triton X-100 to help dissolve in water-soluble reagents for TAG assay and evaporated to dryness. Dried lipid extract was resuspended in ddH_2O for TAG analysis by an enzymatic and colorimetric assay (Infinity™ Triglycerides Reagent (ThermoScientific TR22321)). To analyze milk fatty acid composition, boron trifluoride

(BF_3) methanol (Sigma B1252) solution was added to the other 10% lipid extract, and the mixture was heated at 100ºC for 30 min. Fatty acid methyl esters (FAME), the products after methylation, were extracted using 1 mL hexane and 0.5 mL ddH_2O and analyzed by gas chromatography, as previously described (Miyazaki et al., 2001), using 15:0 FAME as an internal standard.

Milk quantity and the growth of pups

Milk quantity was assessed by weigh-suckle-weigh method (Hernandez et al., 2012). Litter size was standardized at birth by cross-fostering the pups born to one wildtype (WT) and one *M2*$^{-/-}$ dam on the same day. The number of pups that survived from each genotype of dams was calculated at birth. The original litter from each mother was gently removed. Equal numbers of pups and similar numbers from each genotype of mother were given for nursing. The new litter for fostering was placed in a nest after mixing them with bedding from the cage used to house the litter from the foster mom. During early and mid-lactation, pups were moved out of the cages and stayed on a heat pad for 4 hours in the early morning, were weighed, and were returned to their mother at noon. The pups were allowed to suckle for 2 hours, then body weight difference of the litter before and 2 hours after suckling was taken as an indicator of milk quantity. Body weight of pups was recorded when cross-fostering, at lactation day 9, and weaning at 3 weeks of age.

When studying the effect of MGAT2 deficiency in dams on milk production, we paired the *M2*$^{-/-}$ females and their WT littermate controls with WT and *M2*$^{-/-}$ males, respectively. With this breeding scheme, all pups had the same genotype so the effect on growth of pups is specifically from the genotype of the nursing dams.

Fatty acid synthesis in the mammary glands

Fatty acid synthesis was evaluated on dams at lactation day 12 (Harwood et al., 1993). Dams were fasted for 4 hours and refed after lights off at 6 pm. Two hours after refeeding, 10 mCi tritiated H_2O was injected intraperitoneally. One hour after injection, mice were euthanized. Blood was collected to determine the specific activity and corrected for residual blood contamination in organs. Five pairs of mammary glands, liver, and kidneys were then collected and digested in 2.5 M KOH overnight. Lipids were then extracted sequentially with 80% ethanol, hexane, 50 mM H_2SO_4, and 3 M H_2SO_4. The incorporation of radioactive substrate into lipid products was quantified from the lipid extracts after re-dissolving in chloroform using a scintillation counter (Packard Tri-Carb 2200 CA liquid scintillation counter analyzer).

Gene expression level in the mammary glands

Total RNA was isolated from the whole mammary glands (Bio-Rad 732-6820) from virgin females, pregnant, and lactating dams. 1 μg RNA was reversed transcribed to cDNA (Bio-Rad 170-8891). Relative levels of mRNA expression were assessed by quantitative PCR using SYBR Green Master Mix (Bio-Rad 172-5124) and the ABI 7700 PRISM sequence detection system. Ribosomal protein S15 (*Rps15*) was taken as a housekeeping gene, and its expression level was not different between genotypes. The $2^{-\Delta\Delta Ct}$ method was used to calculate the fold change in gene expression. Primer information is listed in Table 4-1.

Mammary gland whole mount, histology, and immunohistochemistry

Mice were euthanized and their 4th pair (inguinal fat pad) of mammary glands were collected and fixed in 4% paraformaldehyde overnight. One gland was taken for whole mount stain. After washing out the formalin and rehydrating sequentially through 70% ethanol, 50% ethanol, and ddH_2O, whole mount stain was performed in carmine solution (0.2% carmine stain (Fischer Scientific C579) and 0.5% aluminum potassium sulfate (Fischer Scientific S70459)) until the stain penetrated through the fat pad. The mammary gland was then dehydrated sequentially through 70%, 90%, and 100% ethanol. Xylenes were used to wash out the fat and clear the glands. The gland was stored in glycerol afterwards. The other gland was taken for histological evaluation. It was embedded in paraffin and sectioned (5 μm). The sectioned mammary gland was stained with hematoxylin and eosin (H&E), proliferation marker Ki-67 (Abcam 15580, 1:200), apoptosis marker caspase-3 (Cell signaling 9661, 1:200), or epithelial cell marker E-Cadherin (BD Biosciences 610181, 1:250). Briefly, sectioned mammary gland was deparaffinized in xylenes, epitope-recovered by 10 mM citric acid (pH=6.0) at 95℃, immunoblotted with the primary antibody overnight at 4°C, detected with fluorescent secondary antibody for 1 hour at room temperature, and mounted using antifade mountant with DAPI (Life Technologies P36962) for fluorescence maintenance and nuclei staining. Alexa Fluor 488 goat anti-mouse antibody (Life Technologies A11001, 1:250) and Alexa Fluor 546 goat anti-rabbit antibody (Life Technologies A11010, 1:250) were used as secondary antibodies.

Statistical analysis

All data are presented as mean ± SEM. For determining the effects of MGAT2 deficiency – our primary research goal – data were compared between two groups, *i.e*. *M2*$^{-/-}$ mice and their WT littermates; tissue specific MGAT2 deficient mice and their *M2*$^{f/f}$ littermates, by the

Student's *t*-test. When additional genotypes were included for comparison, one-way ANOVA was first used to determine if there is a genotype effect. If so, the Dunnett's post hoc test was used to determine if the data from each group were different compared to WT. When time in addition to genotype was involved, two-way ANOVA was used to determine the effects of time, genotype, and interaction, followed by the Bonferroni post-test to assess differences between groups (Prism 5.01, GraphPad Inc.; La Jolla, CA). $p<0.05$ is considered statistically significant.

Results

Loss of MGAT2 impairs milk production

To test if MGAT2 is required for milk fat synthesis in the mammary glands, we analyzed the milk produced by dams with global MGAT2 deficiency (*Mogat2*$^{-/-}$; *M2*$^{-/-}$) and their wildtype (*Mogat2*$^{+/+}$; WT) littermate controls. These first-time dams were mated with male mice of the opposite genotype, so that their pups were the same genotype (*Mogat2*$^{+/-}$; *M2*$^{+/-}$). We noted that *M2*$^{-/-}$ mice have a reduced pregnancy rate, prolonged gestation, smaller litter size, and high neonatal mortality in their offspring (Chapter 3). Because lactation ceases without suckling pups, we only collected and analyzed milk from those dams with surviving offspring. In WT mice, milk TAG levels were maintained (Fig 4-1A), while milk lactose and protein levels significantly increased (Fig 4-1B and C, the effect of lactating stage, $p<0.05$) in the milk collected during early lactation (L2), as compared to that collected during mid-lactation (L12). At mid-lactation, milk from *M2*$^{-/-}$ dams contained 19% less TAG (Fig 4-1A), and 18% less lactose (Fig 4-1B) compared to the milk from WT counterparts, suggesting MGAT2 is required for maintaining normal levels of fat, and unexpectedly, lactose in the milk.

To determine whether MGAT2 deficiency affects the amount of milk produced, we used the weigh-suckle-weigh method. Litter size affects the amount of milk produced (Morag et al., 1975). Since *M2*$^{-/-}$ dams often gave birth to fewer pups with a higher mortality rate than those from WT dams (Chapter 3), in this experiment, litter size was specifically standardized at the day of birth by cross-fostering an equal number of pups from *M2*$^{-/-}$ and WT dams that gave birth on the same day. From early to mid-lactation, milk yield significantly increased (Fig 4-2A, the effect of lactating stage, $p<0.05$). At mid-lactation, milk yield of *M2*$^{-/-}$ dams was 44% less than those of WT dams (Fig 4-2A), suggesting that MGAT2 is required not only for producing normal quality of milk but also normal quantity.

To evaluate the effect of low milk quality and quantity from *M2*$^{-/-}$ dams, we equalized the number and body weight of pups at birth and monitored the growth of pups cross-fostered by *M2*$^{-/-}$ or WT dams. In this study, we only analyzed data from dam pairs that had similar litter size throughout the lactation period (litter size at weaning: 6.5 ± 0.6 nursed by *M2*$^{-/-}$ dams vs 6.5 ± 0.5 nursed by WT dams). Pups nursed by *M2*$^{-/-}$ dams were weaned with 24% lower body weight compared to those nursed by WT dams (Fig 4-2B), consistent with the idea that impaired milk production in *M2*$^{-/-}$ dams is insufficient to support the growth of pups.

To determine if the effect on milk production is specific to the loss of MGAT2, milk was analyzed from dams lacking a functional *Mogat1* (*Mogat1*$^{-/-}$; *M1*$^{-/-}$), an enzyme that shares 52% amino acid sequence homology with *Mogat2* (Yen et al., 2002) and also catalyzes MGAT activity *in vitro*. Milk produced from *M1*$^{-/-}$ dams contained similar macronutrient levels as the milk produced from WT dams (Fig 4-1), suggesting that *Mogat1* does not modulate milk production.

Mice lacking both copies of the *Dgat1* gene have defects in mammary gland development and fail to produce milk (Cases et al., 2004). However, heterozygous mice (*Dgat1*$^{+/-}$; *D1*$^{+/-}$) with only one functional *Dgat1* gene do produce milk and can support pups to weaning. To test whether DGAT1-mediated TAG synthesis is essential for milk fat synthesis, we analyzed the milk collected from *D1*$^{+/-}$ dams. Milk from *D1*$^{+/-}$ dams contained 20% less TAG at mid-lactation (Fig 4-1A), suggesting that, like MGAT2, DGAT1 is also involved in milk fat production.

Milk fat from MGAT2 deficient dams contains less medium-chained fatty acids (MCFAs)

To determine if loss of MGAT2 impairs incorporation of preformed fatty acids from dietary fat into milk fat, we analyzed the fatty acid composition in the milk. Mammary glands are active in

de novo synthesis of fatty acids – mostly medium-chained fatty acids (MCFAs, C8:0-C14:0) due to thioesterase II, unique to the mammary epithelium (Barber et al., 1997), hydrolyzing the thioester bond from the elongating acyl chains in the fatty acid synthase (FAS) prematurely and releasing MCFAs. From early to mid-lactation, MCFAs by percentage significantly increased in the milk (C<16 fatty acids; Table 4-2), suggesting that the milk fat production shifts from utilizing existing long-chained unsaturated fatty acids from dietary fat or from stored fat in the adipose tissue and liver to fatty acids synthesized in the mammary glands. MCFAs in the milk of *M2*$^{-/-}$ dams also displayed such a shift but not to the level as those of WT dams, with 18% less MCFAs by percentage specifically at mid-lactation (C<16 fatty acids; Table 4-2). These data suggest that MGAT2 deficiency may impair endogenous fatty acid synthesis in the mammary glands.

MGAT2 deficient dams have smaller mammary glands with normal capacity for fat synthesis

To determine if endogenous fat synthesis is impaired in the mammary glands of *M2*$^{-/-}$ dams, we examined expression levels of fatty acid synthesis related genes by qPCR and measured fatty acid synthesis *in vivo* by labeling newly synthesized fatty acids with tritiated H_2O. We performed the experiments using the whole mammary glands collected at mid-lactation, when we observed the decreases in milk fat (Fig 4-1A) and MCFAs (Table 4-2). We first noted that the mass of mammary glands at mid-lactation was 16% lower in *M2*$^{-/-}$ dams than in WT dams (Fig 4-3A). However, the mRNA expression levels of genes involved in endogenous fatty acid synthesis, including ATP citrate lyase (*Acly*), acetyl-CoA carboxylase 1 (*Acc1*), fatty acid synthase (*Fas*), and stearoyl-CoA desaturase 1 (*Scd1*), were not different between the mammary glands from *M2*$^{-/-}$ and WT dams (Fig 4-3B). Functionally, fatty acids were predominately synthesized in the mammary glands compared to in the liver, another tissue

performing lipogenesis (Fig 4-3C) during the lactation period, as expected. When comparing between the two genotypes, fatty acid synthesis level was not different when normalizing by the mass of mammary glands (Fig 4-3C). These data suggest that the mammary glands in MGAT2 deficient dams may not have impaired endogenous fat synthesis. However, with the decreased size of mammary glands, MGAT2 deficient dams may reduce the amount of milk produced.

MGAT2 is required for mammary gland development

To examine if loss of MGAT2 impairs mammary gland development, we examined mammary glands from virgin, pregnant, and lactating mice by whole mount stains. We found that mammary epithelial ducts filled the margin of fat pads in the 50-day old mammary glands of WT mice (Fig 4-4A), suggesting that the mammary glands reached the state of a mature virgin mouse. However, the mammary glands of *M2*$^{-/-}$ females exhibited fewer ductal branches and fewer buds than the ones of WT (Fig 4-4A), indicating that these mice had delayed mammary gland development before pregnancy. At early pregnancy, the ductal branching accelerates, resulting in the exhibition of more highly dense branches in the mid-pregnant mammary glands (P15) than in virgin ones (Fig 4-4B). Perinatally, the alveolar buds appeared to differentiate, as we observed secretory lobes at pregnancy day 19 (Fig 4-4C) and lactation day 2 (Fig 4-4D). After pregnancy, we did not observe a difference between genotypes in the density of mammary glands using whole mount stain (Fig 4-4B~D).

Histological sections of mammary glands collected at late pregnancy (P19) and mid-lactation (L12) showed, as expected, that the epithelial compartment relative to adipose tissue and lumen size gradually expanded (Fig 4-5) in both genotypes. When comparing the mammary glands of *M2*$^{-/-}$ dams to those of WT dams, mammary gland H&E stain appeared highly variable at either stage (Fig 4-5) and we were not able to detect the difference.

At the molecular level, we examined markers of proliferation, differentiation, and apoptosis in the mammary glands. During late pregnancy (P19), mammary glands of both genotypes had more Ki67-positive cells than during mid-lactation (L12) (Fig 4-6), suggesting more proliferating cells during pregnancy than during lactation. When comparing the two genotypes, mammary glands from *M2*$^{-/-}$ dams appeared to have normal numbers of proliferating cells at both stages (Fig 4-6). Mature mammary glands express α-*casein* (Fig 4-7A), β-*casein* (Fig 4-7B), and whey acidic protein (*WAP*) (Fig 4-7C). We found expression levels of these differentiation markers gradually increased from virgin (V50), to pregnancy (P19), to lactation (L12), as expected, in the mammary glands collected from WT mice. Mammary glands from *M2*$^{-/-}$ dams, however, did not increase their β-*casein* gene expression from pregnancy to lactation (Fig 4-7B). At mid-lactation, *M2*$^{-/-}$ mammary glands showed a significant decrease in the expression level of all three genes compared to WT mammary glands (Fig 4-7). Associated with the reduced differentiation markers, mid-lactating *M2*$^{-/-}$ mammary glands also exhibited an increase in apoptotic cells, as suggested by the caspase 3 staining (Fig 4-8). These data suggest that *M2*$^{-/-}$ mammary gland development fails at mid-lactation, specifically in differentiation, which is associated with early involution.

Mogat2 is not expressed in the mammary epithelium

To determine if MGAT2 may function locally in the mammary glands, we measured *Mogat2* mRNA expression in the mouse whole mammary glands at various stages of development. *Mogat2* expression levels in the mature virgin (V50), pregnant (P19), and lactating (L12) mammary glands were relatively low compared to jejunum, kidney, and inguinal fat pads in male mice (IWAT, which is the 4th pair of mammary glands if collected in females), with a progressive reduction in mammary glands from virgin, to pregnancy, to lactation (Fig 4-9). *Mogat2* mRNA is

not detected in the lactating mammary glands when they were filled with epithelial cells and their adipose tissues were almost depleted (Fig 4-9), suggesting that *Mogat2* is expressed in the adipocytes but not in the epithelial cells of the mammary glands.

Neither tissue-specific loss of MGAT2 in the adipose tissue nor in the intestine decreases milk fat

To determine if MGAT2 in the adipocytes is required for milk fat production, we analyzed the milk from dams in which adipose *Mogat2* is deleted in a tissue-specific manner, (*Mogat2*^{AKO}; *M2*^{AKO}). Milk from *M2*^{AKO} dams contained similar amounts of TAG and lactose at both early and mid-lactation (Fig 4-10A and B), but 13% less protein at mid-lactation (Fig 4-10C), compared to the milk of their respective *M2*$^{f/f}$ controls. Likewise, when we analyzed the milk from intestine-specific MGAT2 deficient dams (*Mogat2*^{IKO}; *M2*^{IKO}), their milk contained similar amounts of macronutrients, compared to the milk of *M2*$^{f/f}$ dams (Fig 4-11). Taken together, these data suggest that MGAT2 in tissues other than adipose and intestine are required for milk production.

Discussion

Since the gene codes for MGAT2, *Mogat2*, has been cloned (Cases et al., 2001) and identified (Yen and Farese, 2003), the only well-established physiological function is TAG repackage for dietary fat absorption in the enterocyte, which in turn, affects systemic energy metabolism (Nelson et al., 2011; Yen et al., 2009). We recently reported that MGAT2 is required for female reproduction, although the mechanisms remain unclear (Chapter 3). In this study, we observed that those MGAT2 deficient dams that delivered and nursed pups successfully have reduced milk quality and quantity. The failures in milk production were associated with impaired mammary gland development, specifically in differentiation, which is related to the early involution. For the first time, we identified MGAT2 is required for mammary gland functions.

Mammary gland is composed of two major tissue compartments, the stroma and the epithelium (Anderson et al., 2007; Hennighausen and Robinson, 2005). The stroma is composed of mostly adipocytes that may locally secrete hormones and growth factors to coordinate systemic signals to support mammary gland development (Anderson et al., 2007; Hennighausen and Robinson, 2005). Milk production, which occurs in mammary epithelial cells, requires a successful mammary gland development switching from pregnancy to lactation, when genes involved in milk fat synthesis are mostly up-regulated (Anderson et al., 2007). Interestingly, *Mogat2*, which also involved in TAG esterification, is expressed in adipocytes but not in mammary epithelium (Fig 4-9) yet MGAT2 deficiency impairs milk production (Fig 4-1 and 4-2). The associated failures in mammary gland development (Fig 4-7 and 4-8) prompt us to test whether the defect is contributed by adipose MGAT2. Loss of MGAT2 specifically in the adipose tissue, however, does not affect milk production as loss of MGAT2 globally. Therefore, the regulation of MGAT2 in mammary gland functions may not come from the local mammary epithelium or adipocytes.

Lactating mothers need a remarkably high calorie intake for milk production. The deficiency of TAG synthesis enzymes, GPAT4 and DGAT1, exhibit not only metabolic inefficiency (Smith et al., 2000; Vergnes et al., 2006) but also failures in milk production (Beigneux et al., 2006; Cases et al., 2004). GPAT4 is highly expressed in the mammary epithelium but not in the surrounding adipose tissues. Lacking a functional GPAT4 globally, mouse mammary glands are underdeveloped with reduced size and number of alveoli in the lactating mammary glands. This results in the depletion of TAG in the milk and pups nursed by GPAT4 deficient dams die perinatally (Beigneux et al., 2006). DGAT1 is expressed in both mammary epithelium and adipose tissues, and its expression in both compartments is required for mammary gland functions. Lacking a functional DGAT1 globally, mouse mammary glands exhibit less mammary ducts at pregnancy, and reduced epithelium and small lumen at peripartum. Therefore, these dams cannot produce milk (Cases et al., 2004).

Similarly, we observed global MGAT2 deficient dams also exhibited both metabolic inefficiency and failures in milk production specifically at mid-lactation. At this stage, *M2*$^{-/-}$ dams exhibited lower body weight and feed efficiency than the respective WT dams (data not shown) and impaired mammary gland development (Fig 4-7 and 4-8). Despite the intestinal specific MGAT2 deficient dams, another metabolic inefficient mouse model, exhibited normal milk production (Fig 4-11), we may argue that their energy imbalance is not to the same level as that of global MGAT2 deficient dams (Nelson et al., 2014).

In addition to impaired systemic energy metabolism, failures in hormonal regulation may also be one of the causes in defective mammary gland functions. From pregnancy to lactation, the withdrawal of progesterone and the subsequent release of prolactin are required for the lactation switch in milk production (Anderson et al., 2007). High progesterone circulation during pregnancy has been reported to block the milk production (Kuhn, 1969; Neville et al., 2002; Silberstein et al., 1996) and associated with the downregulation of prolactin response (Djiane

and Durand, 1977). *M2*$^{-/-}$ dams exhibit high circulating progesterone at late pregnancy (Chapter 3), which may cause the failures in milk production.

In summary, we have identified MGAT2 as being required for mammary gland functions, including mammary gland development and milk production. Despite MGAT2 may not function locally in the mammary epithelium or adipocytes, it may regulate mammary gland functions through systemic metabolism, which needs further characterization. Nonetheless, this study may highlight a potential genetic selection markers of efficient milk production for dairy science.

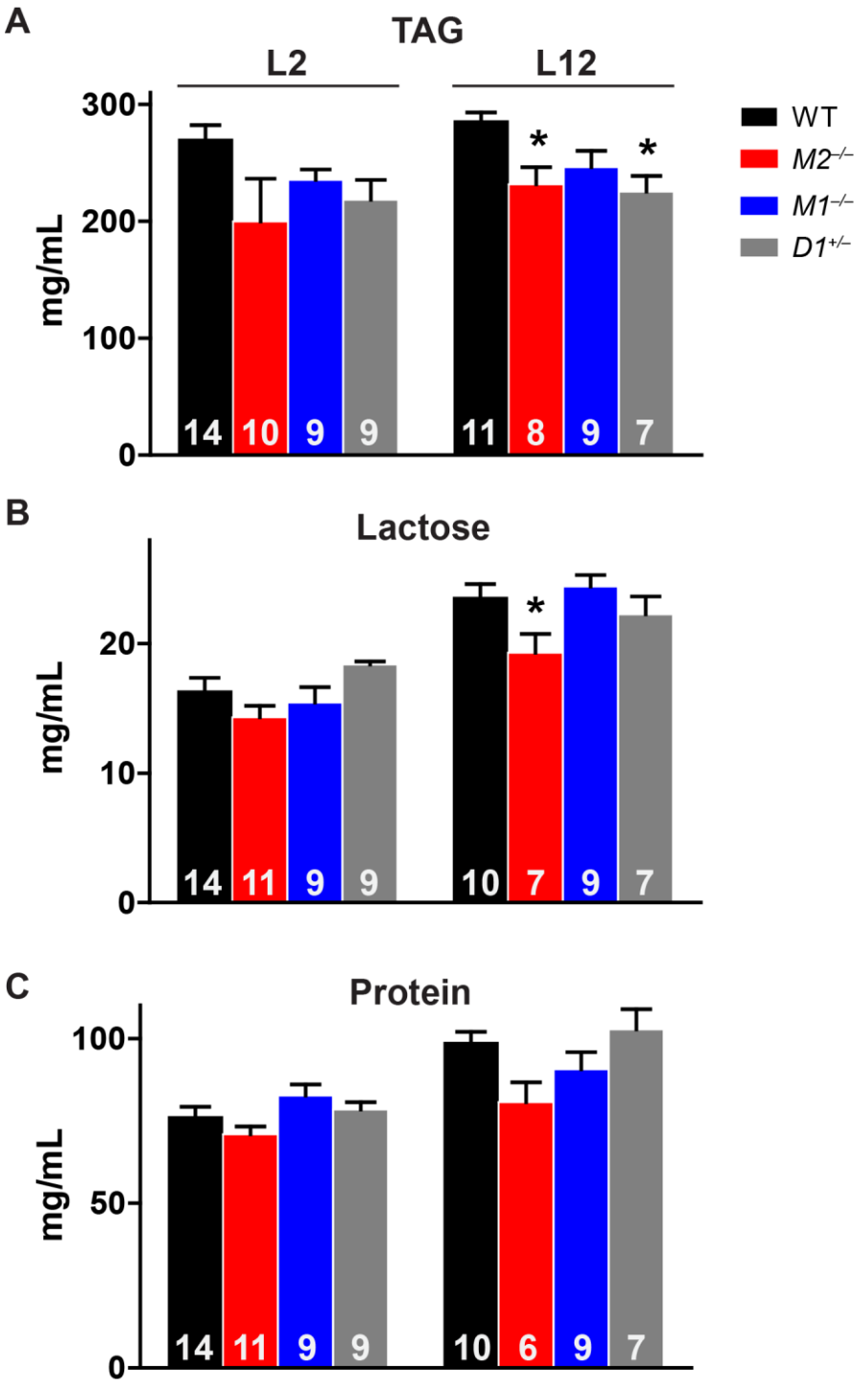
A
TAG
L2
L12
300
200
100
0
mg/mL
14 10 9 9
11 8 9 7
*
*
WT
M2−/−
M1−/−
D1+/−
B
Lactose
20
10
0
mg/mL
14 11 9 9
10 7 9 7
*
C
Protein
100
50
0
mg/mL
14 11 9 9
10 6 9 7

Figure 4-1. Loss of MGAT2 impairs milk quality.

Milk A. TAG, B. Lactose, and C. Protein at lactation day 2 and 12 to represent early and mid-lactation, respectively. Milk was collected from those dams had surviving pups to nurse without standardizing the litter size. Milk fat was extracted by chloroform: methanol (2:1, v/v). Data are presented as mean ± SEM. The sample size of milk collected was indicated as the number written on the bar. Milk from WT dams, black bars; $M2^{-/-}$ dams, red bars; $M1^{-/-}$ dams, blue bars; $M1^{+/-}$ dams, grey bars. One-way ANOVA was used to determine if there is a genotype effect at specific lactating stage. If so, Dunnett's post hoc test was used to determine if the data from each group were different from WT controls. *p<0.05 is considered statistically significant. Two-way ANOVA was used to determine the effect of lactating stage, which is statistically significant in milk lactose and protein but not in milk TAG.

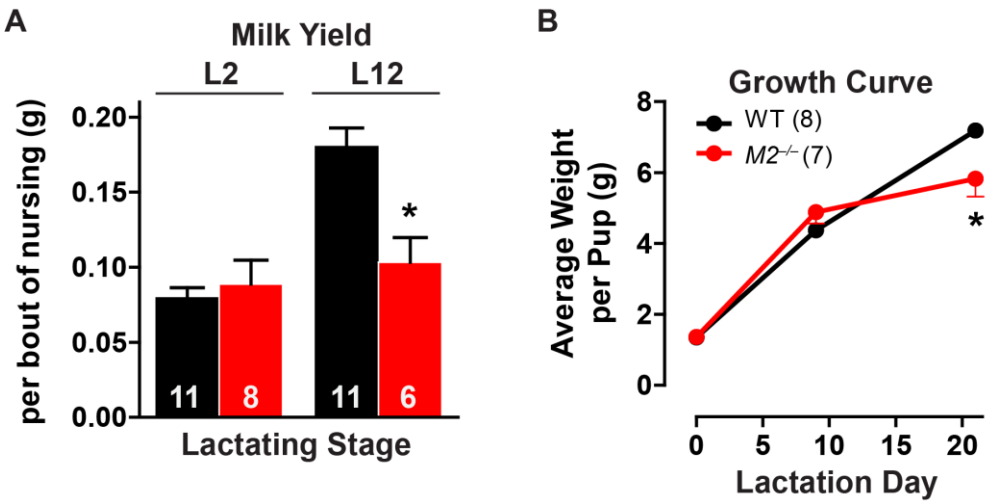

Figure 4-2. Loss of MGAT2 impairs not only milk quality but also milk yield. As a result, it is insufficient to support the growth of pups.

A. Milk yield of *M2*$^{-/-}$ and WT dams at lactation day 2 and 12 to represent early and mid-lactation, respectively. B. Growth of pups nursed by *M2*$^{-/-}$ and WT dams. Milk yield was assessed by weigh-suckle-weigh method. In these two experiments, litter size was specifically standardized at the day of birth by cross-fostering an equal number of pups from *M2*$^{-/-}$ and WT dams that gave birth on the same day, and the litter size at weaning were similar between the two genoptypes (6.5 ± 0.6 nursed by *M2*$^{-/-}$ dams vs 6.5 ± 0.5 nursed by WT dams). Data are presented as mean ± SEM. The sample size of milk yield measured was indicated as the number written on the bar. The number of litters observed for growth was indicated as the number written in the parentheses next to the genotype of dams. Milk from and litters nursed by WT dams, black bars/circles/lines; milk from and litters nursed by *M2*$^{-/-}$ dams, red bars/circles/lines. Two-way ANOVA was used to determine the effects of lactating stage or lactation day, genotype, and interaction, followed by the Bonferroni post-test to assess differences between groups. *p<0.05 is considered statistically significant. The effects of lactating stage or lactation day, genotype, and interaction are statistically significant in both milk yield and the growth of pups.

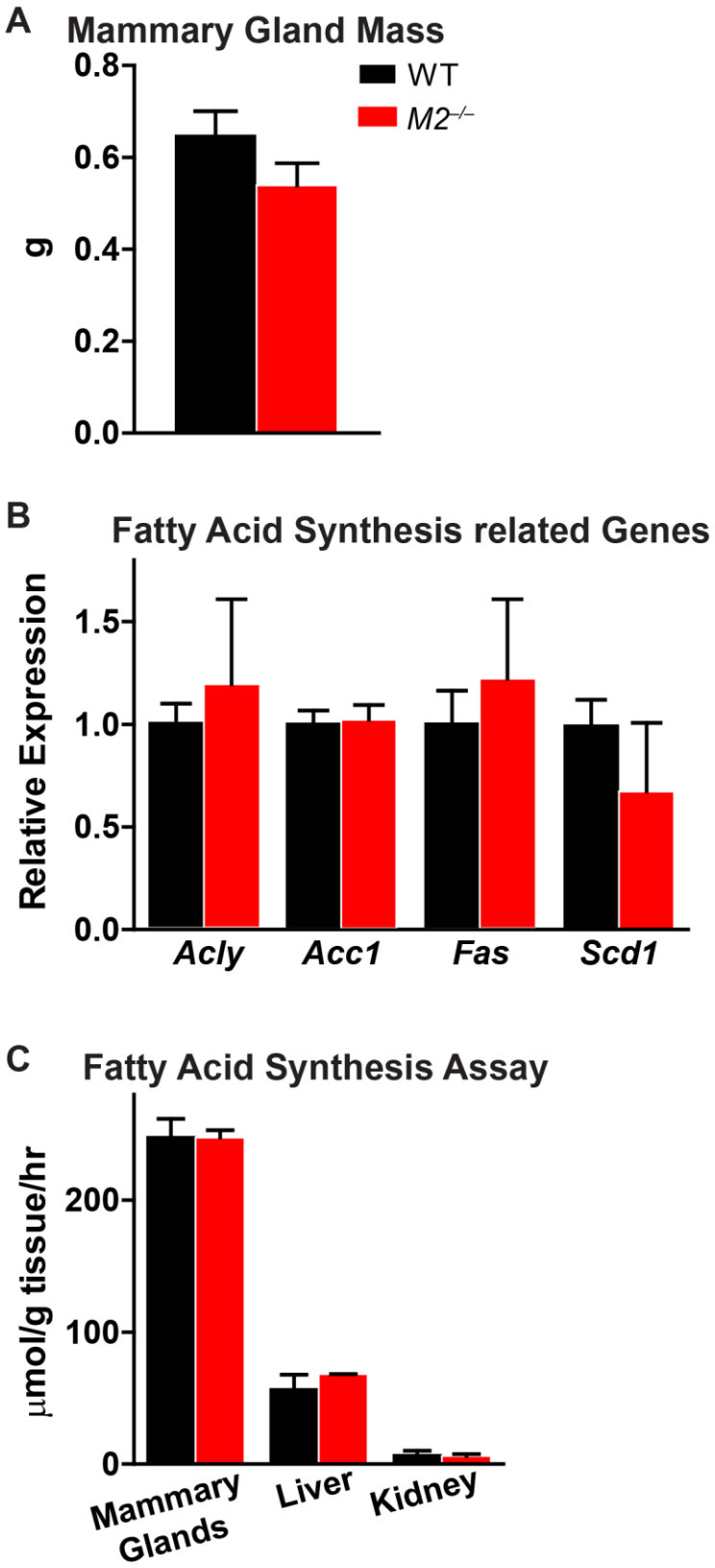
A
Mammary Gland Mass
WT
M2-/-
g
0.8
0.6
0.4
0.2
0.0
B
Fatty Acid Synthesis related Genes
Relative Expression
1.5
1.0
0.5
0.0
Acly
Acc1
Fas
Scd1
C
Fatty Acid Synthesis Assay
µmol/g tissue/hr
200
100
0
Mammary Glands
Liver
Kidney

Figure 4-3. MGAT2 deficient dams have smaller mammary glands with normal capacity for fat synthesis.

A. Mass, B. mRNA expression level of genes related to fatty acid synthesis, and C. fatty acid synthesis assay in the mid-lactating mammary glands. Lactation day 12 represents mid-lactation. The gene expression levels and fatty acid synthesis assay were analyzed with the whole mammary glands. *Acly*, ATP-citrate lyase; *Acc1*, acetyl-CoA carboxylase 1; *Fas*, fatty acid synthase; *Scd1*, stearoyl-CoA desaturase 1. WT is taken as 1 for each gene. Fatty acid synthesis was performed using tritiated H_2O injected intraperitoneally at fed state. n=2-9/genotype. Data are presented as mean ± SEM. WT mammary glands, black bars; *M2*$^{-/-}$ mammary glands, red bars.

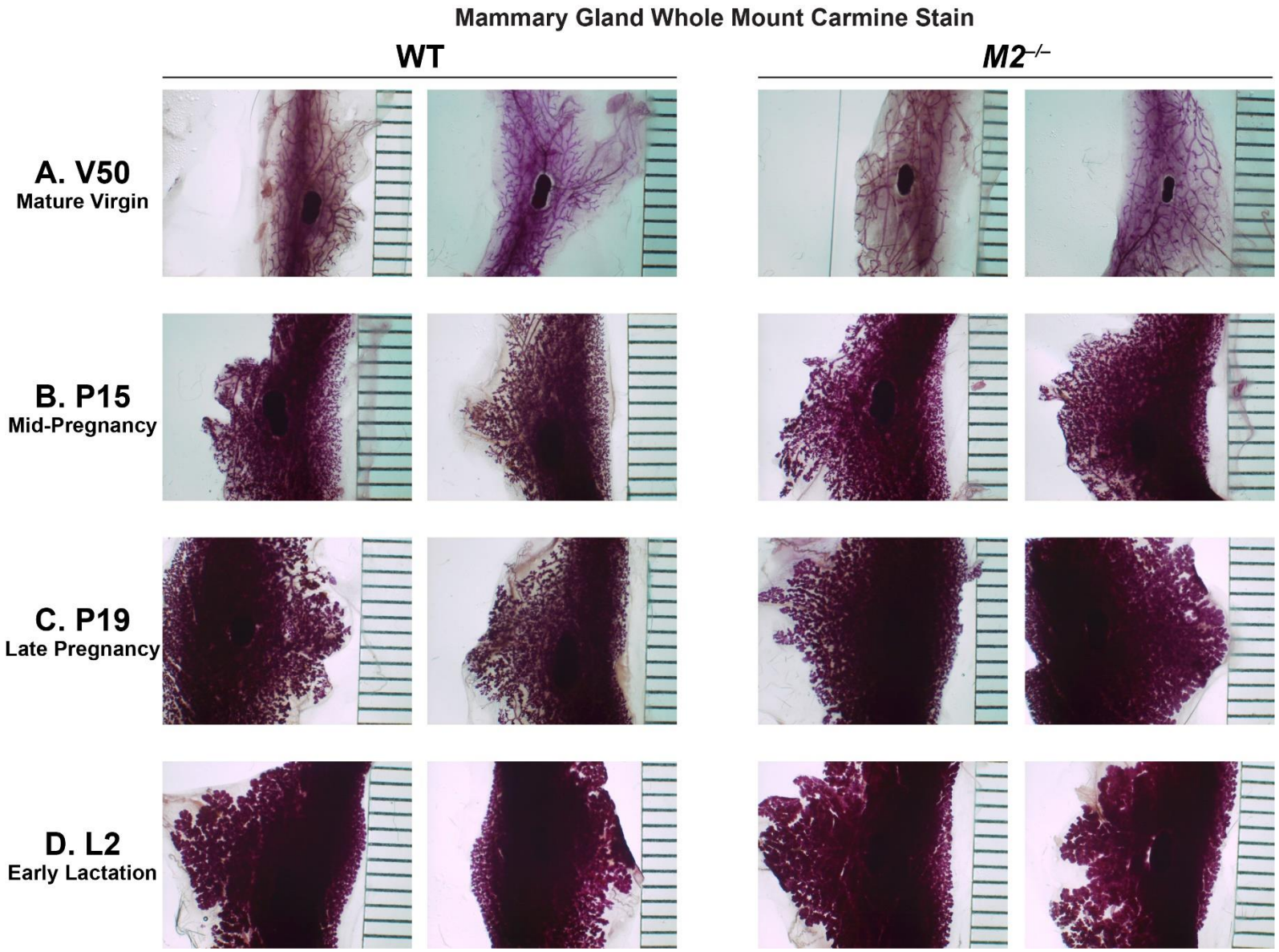
Mammary Gland Whole Mount Carmine Stain
WT
M2−/−
A. V50
Mature Virgin
B. P15
Mid-Pregnancy
C. P19
Late Pregnancy
D. L2
Early Lactation

Figure 4-4. *M2*$^{-/-}$ virgin females exhibit delayed mammary gland development with fewer ductal branches.

Whole mount carmine stain for the 4th pair of mammary glands. A. V50, virgin females at 50 days old, represents mature virgin; B. P15, and C. P19, 15 and 19 days of gestation, represent mid- and late gestation; D. L2, lactation day 2, represents early lactation. The width of the pictures is 1.2 cm.

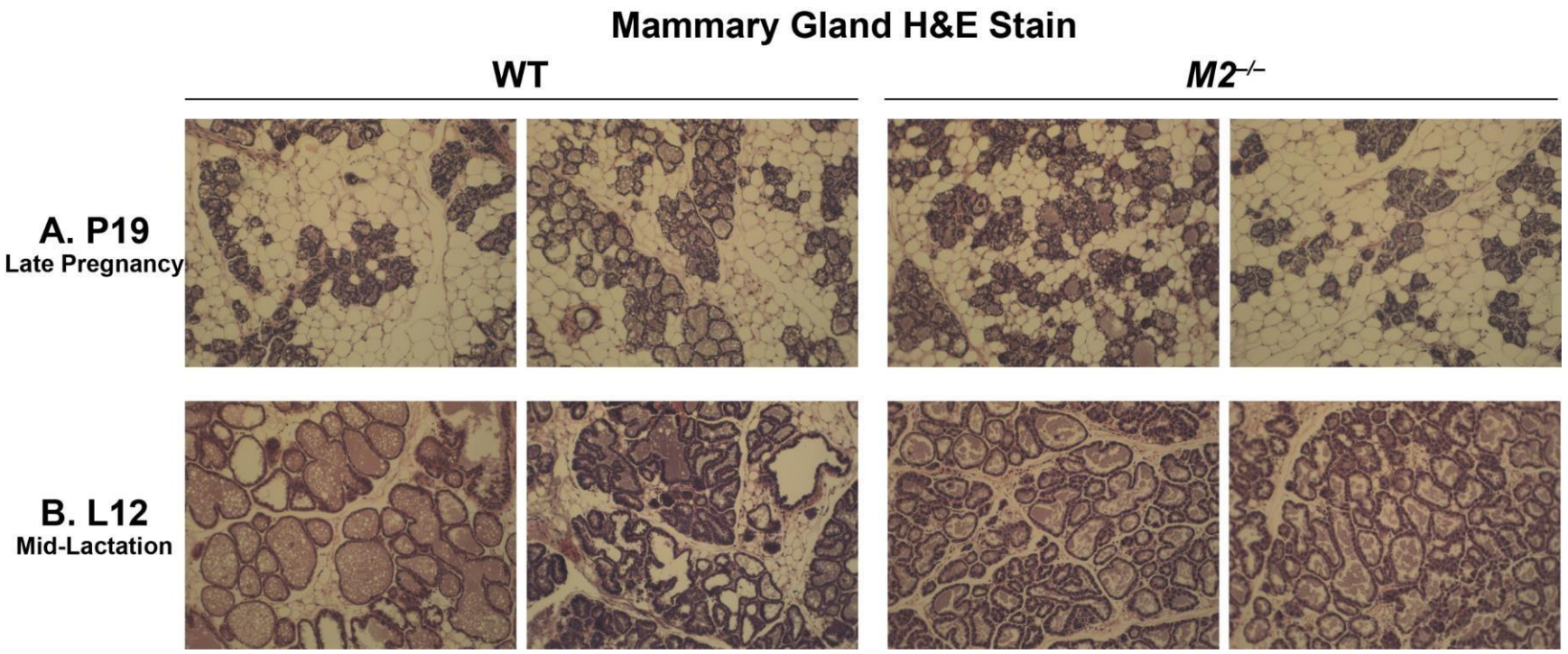

Figure 4-5. Mammary glands from WT and MGAT2 deficient dams appear highly variable at both late pregnancy and mid-lactation.

H&E stains for the 4th pair of mammary glands. A. P19, 19 days of gestation, represents late pregnancy; (B) L12, lactation day 12, represents mid-lactation. 100X images are shown.

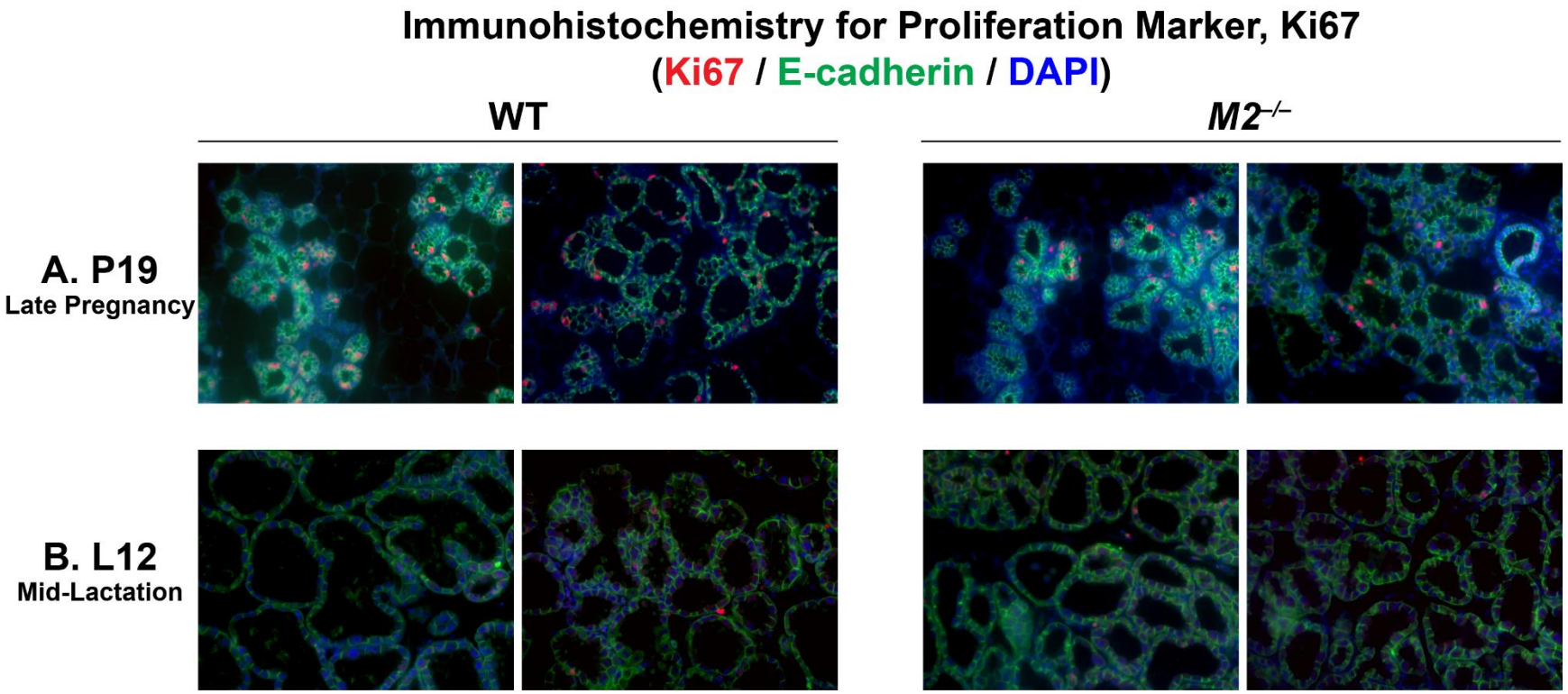

Figure 4-6. WT and MGAT2 deficient dams exhibit similar proliferation in the mammary glands.

Immunohistochemistry for Ki67, the marker for proliferation, on the 4th pair of mammary glands. E-cadherin stains mammary epithelium and DAPI stains for nuclei. A. P19, 19 days of gestation, represents late pregnancy; B. L12, lactation day 12, represents mid-lactation. 200X images are shown.

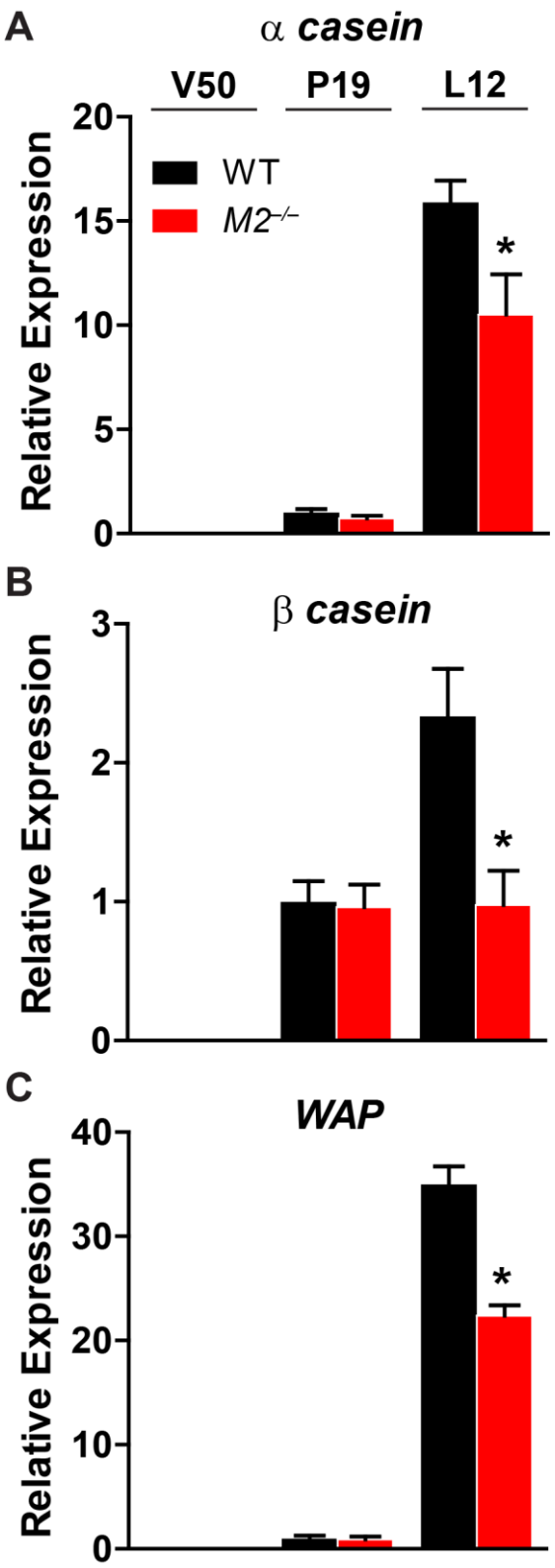
A
α casein
V50
P19
L12
WT
M2-/-
Relative Expression
20
15
10
5
0
*
B
β casein
Relative Expression
3
2
1
0
*
C
WAP
Relative Expression
40
30
20
10
0
*

Figure 4-7. MGAT2 deficient dams exhibit failures in differentiation in the mammary glands.

mRNA expression levels of differentiation markers in the whole mammary glands: A. α casein, B. β casein, and C. WAP, whey acidic protein. V50, virgin females at 50 days old, represents mature virgin; P19, 19 days of gestation, represents late pregnancy; L12, lactation day 12, represents mid-lactation. For each gene, WT at P19 is taken as 1. n=3-6/genotype. Data are presented as mean ± SEM. WT mammary glands, black bars; *M2*$^{-/-}$ mammary glands, red bars. Two-way ANOVA was used to determine the effects of developmental stage, genotype, and interaction, followed by the Bonferroni post-test to assess differences between groups. *p<0.05 is considered statistically significant. The effect of developmental stage is statistically significant in all the three genes tested.

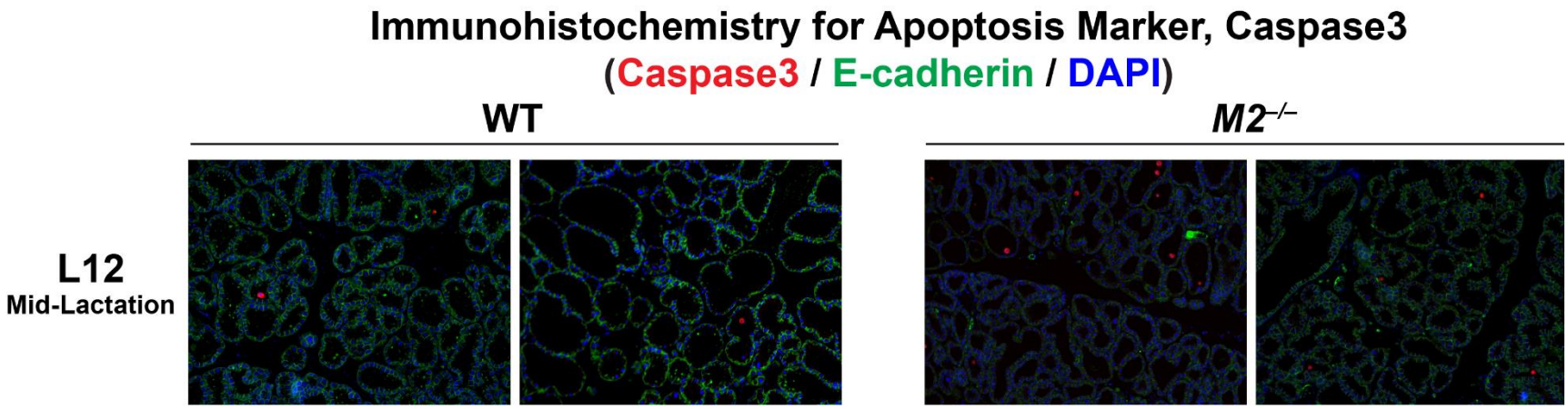

Figure 4-8. *M2*$^{-/-}$ mammary glands exhibit early involution.

Immunohistochemistry for caspase3, the marker for apoptosis, on the 4th pair of mammary glands. E-cadherin stains mammary epithelium and DAPI stains for nuclei. nuclei. L12, lactation day 12, represents mid-lactation. 100X images are shown.

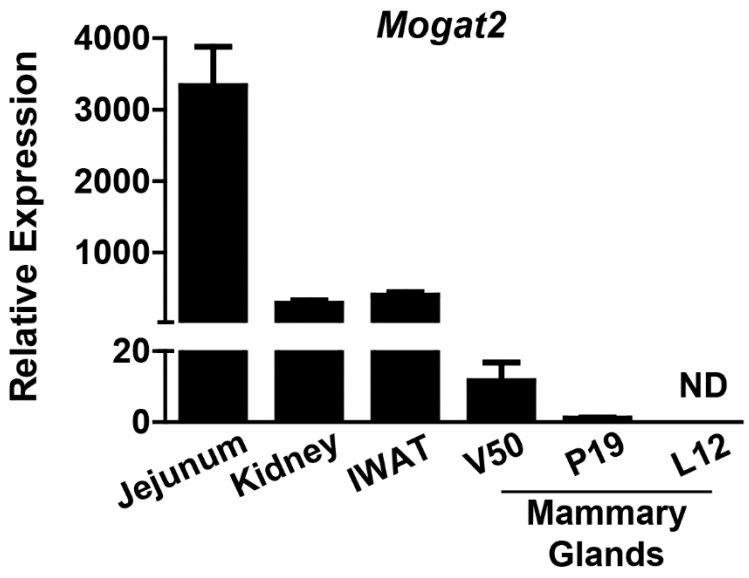

Figure 4-9. *Mogat2* is not expressed in the mammary epithelium.

mRNA expression level of *Mogat2* in the whole mammary glands at various stages of development and male tissues. *Mogat2* expression level at P19 is taken as 1. IWAT, inguinal fat pads, which is the 4th pair of mammary glands if collected in females. V50, virgin females at 50 days old, represents mature virgin; P19, 19 days of gestation, represents late pregnancy; L12, lactation day 12, represents mid-lactation. Data are presented as mean ± SEM. n=3-5/tissue. ND, not detected.

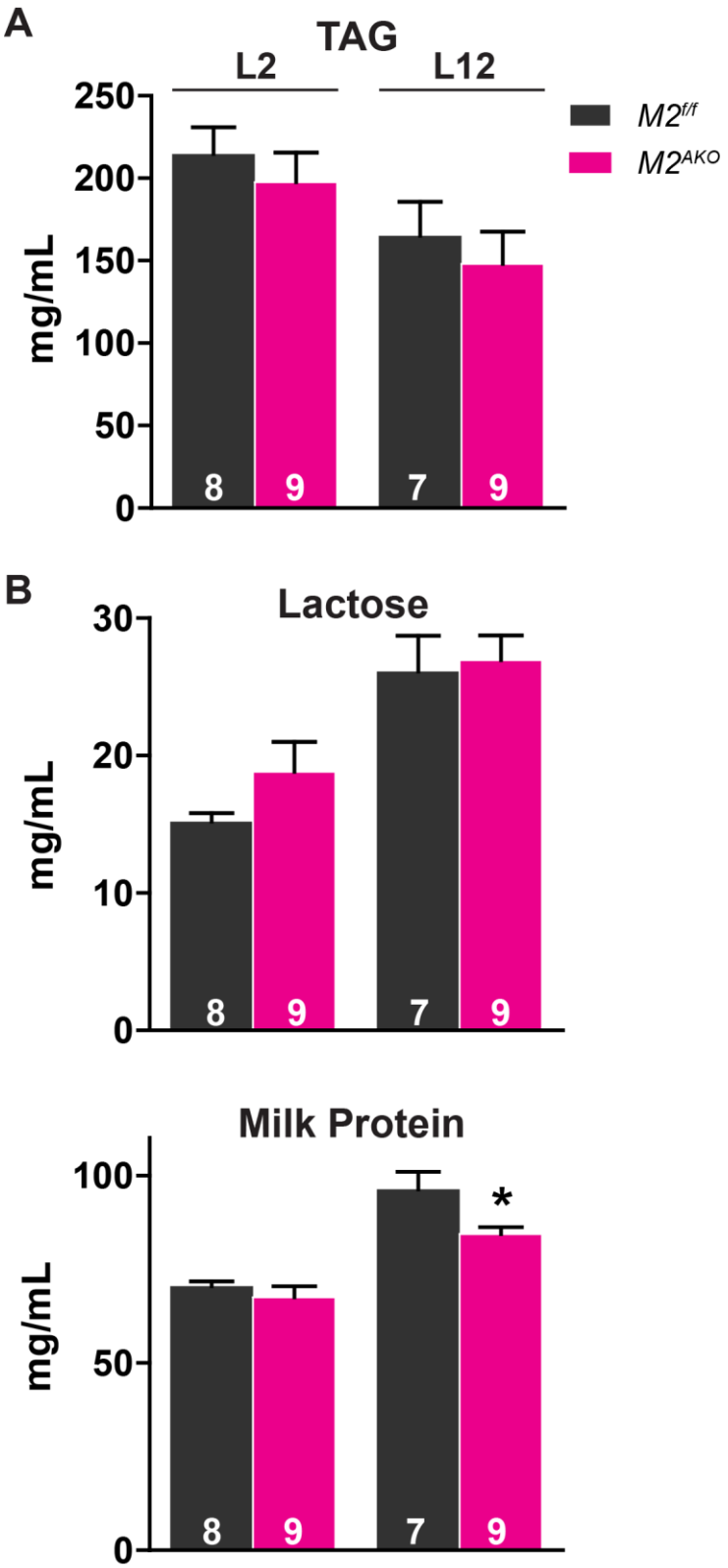
A
TAG
L2
L12
250
200
150
100
50
0
mg/mL
M2f/f
M2AKO
8
9
7
9
B
Lactose
30
20
10
0
mg/mL
8
9
7
9
Milk Protein
100
50
0
mg/mL
*
8
9
7
9

Figure 4-10. Loss of MGAT2 specifically in the adipose tissue does not reduce milk fat production.

Milk A. TAG, B. Lactose, and C. Protein at lactation day 2 and 12 to represent early and mid-lactation, respectively. Milk was collected without standardizing the litter size. Milk fat was extracted by chloroform: methanol (2:1, v/v). Data are presented as mean ± SEM. The sample size of milk collected was indicated as the number written on the bar. Milk from $M2^{f/f}$ dams, dark grey bars; milk from $M2^{AKO}$ dams, pink bars. Student's *t*-test was used to determine the difference in macronutrients at the same stage between the two genotypes. *$p<0.05$ is considered statistically significant. Two-way ANOVA was used to determine the effect of lactating stage. The effect of lactating stage is statistically signficant in all three macronutrients.

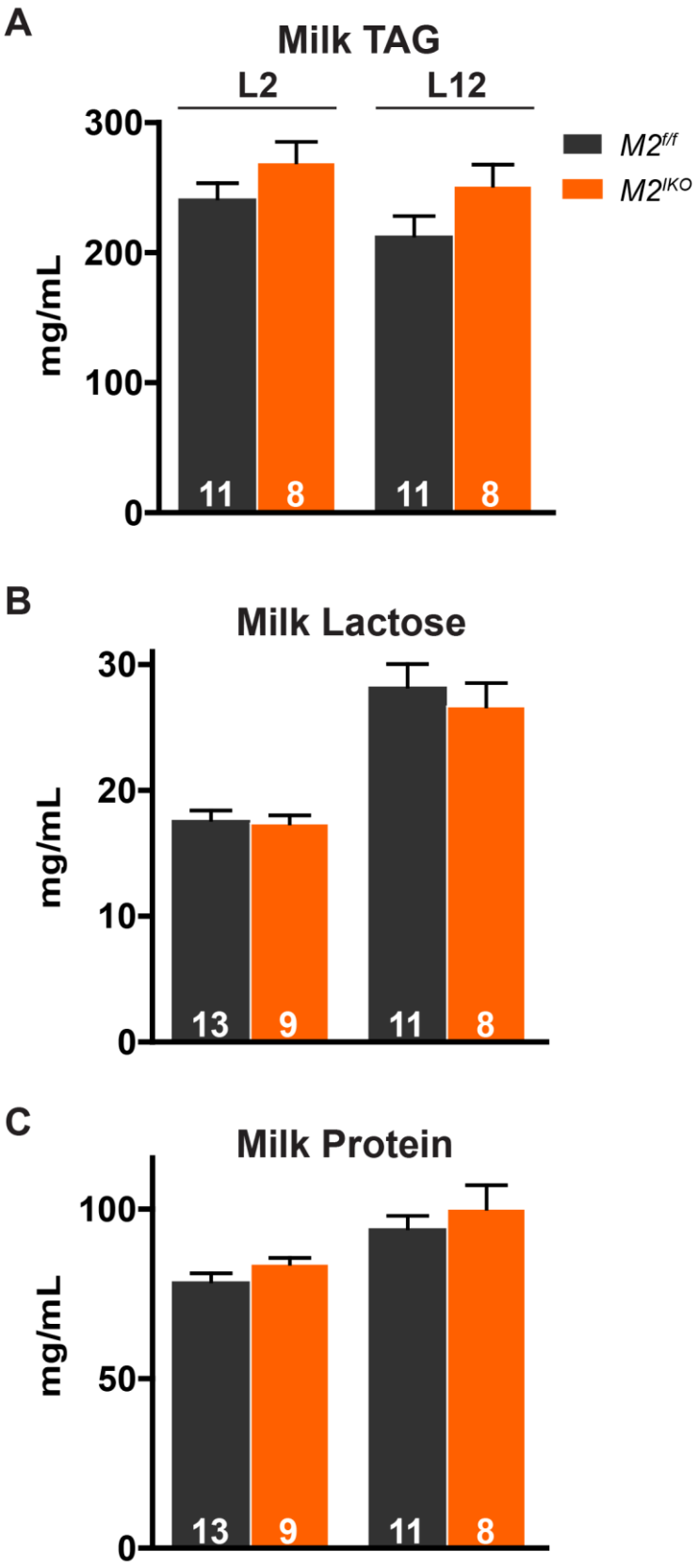
A
Milk TAG
L2
L12
300
200
100
0
mg/mL
11
8
11
8
M2f/f
M2lKO
B
Milk Lactose
30
20
10
0
mg/mL
13
9
11
8
C
Milk Protein
100
50
0
mg/mL
13
9
11
8

Figure 4-11. Loss of MGAT2 specifically in the intestine does not reduce milk production.

Milk A. TAG, B. Lactose, and C. Protein at lactation day 2 and 12 to represent early and mid-lactation, respectively. Milk was collected without standardizing the litter size. Milk fat was extracted by chloroform: methanol (2:1, v/v). Data are presented as mean ± SEM. The sample size of milk collected was indicated as the number written on the bar. Milk from $M2^{f/f}$ dams, dark grey bars; milk from $M2^{IKO}$ dams, orange bars. Two-way ANOVA was used to determine the effect of lactating stage. $p<0.05$ is considered statistically significant. The effect of lactating stage is statistically significant in milk lactose and protein but not in milk TAG.

Table 4-1. Primer sequences for quantitative PCR

Gene	Forward	Reverse	Accession No.
α-casein	GACATCTCTCAGGAACTCCACA	TCCATAGAATGAATAGAGAGACATGAG	NM_001286016
Acc1	TGGACAGACTGATCGCAGAGAAAG	TGGAGAGCCCCACACACA	NM_133360
Acly	GCCAGCGGGAGCACATC	CTTTGCAGGTGCCACTTCATC	NM_134037.2
β-casein	GGTGAATCTCATGGGACAGC	TGACTGGATGCTGGAGTGAA	NM_001286020
Fas	GGAGGTGGTGATAGCCGGTAT	TGGGATATCCATAGAGCCCAG	NM_007988.2
Mogat2	TGGGAGCGCAGGTTACAGA	CAGGTGGCATACAGGACAGA	NM_177448
Rps15	GTTGAAGGTCTTGCCGTTGT	TTGAGAAAGGCCAAAAAGGA	NM_009091
Scd1	CCTTCCCCTTCGACTACTCTG	GCCATGCAGTCGATGAAGAA	NM_009127.2
WAP	TGACATGTACACCCCCAGTG	CTGGTCACTCCCGACAGG	NM_011709

To avoid detecting genomic sequences, primer pairs spanning large introns are mostly used. The specificity of the primers is confirmed by dissociation curve. *Acc1*, acetyl-CoA carboxylase 1. *Acly*, ATP citrate lyase. *Fas*, fatty acid synthase. *Mogat*, acyl-CoA: monoacylglycerol acyltransferase. *Rps15,* ribosomal protein S15. *Scd1*, stearoyl-CoA desaturase 1. *WAP*, whey acidic protein.

Table 4-2. Relative amount of fatty acids in the milk of WT and *M2*$^{-/-}$ dams at early and mid-lactation

	Early lactation day 2		Mid-lactation day 12	
%	WT (14)	*M2*$^{-/-}$ (10)	WT (11)	*M2*$^{-/-}$ (7)
10:0	1.43 ± 0.32	1.53 ± 0.29	3.80 ± 1.07	2.28 ± 0.46
12:0	6.62 ± 0.43	7.77 ± 0.57	13.17 ± 0.87	11.28 ± 0.99
14:0	12.56 ± 0.46	13.53 ± 0.98	18.62 ± 0.83	15.62 ± 0.85*
C<16	20.61 ± 1.06	22.83 ± 1.49	35.64 ± 1.63	29.19 ± 2.10*
16:0	32.87 ± 0.97	34.19 ± 1.05	30.45 ± 1.13	28.63 ± 0.84
16:1	6.08 ± 0.29	4.86 ± 0.43*	1.95 ± 0.14	3.03 ± 0.45*
C=16	38.95 ± 0.81	39.05 ± 0.75	32.40 ± 1.12	31.67 ± 0.86
18:0	1.94 ± 0.06	2.28 ± 0.11*	2.99 ± 0.16	2.80 ± 0.28
18:1 (n-9)	17.22 ± 0.84	16.81 ± 0.84	13.41 ± 0.61	15.99 ± 0.82
18:1 (n-7)	1.80 ± 0.13	1.70 ± 0.13	1.97 ± 0.21	1.79 ± 0.17
18:2 (n-6)	15.19 ± 0.77	12.54 ± 1.03*	10.22 ± 1.06	14.35 ± 1.65*
18:3 (n-6)	0.49 ± 0.02	0.40 ± 0.03*	0.22 ± 0.02	0.30 ± 0.03*
18:3 (n-3)	0.82 ± 0.13	0.76 ± 0.10	0.50 ± 0.11	0.96 ± 0.17*
20:0	0.10 ± 0.01	0.13 ± 0.02	0.60 ± 0.13	0.10 ± 0.00
20:1 (n-9)	0.56 ± 0.05	0.66 ± 0.09	0.47 ± 0.12	0.75 ± 0.24
20:3 (n-6)	0.81 ± 0.02	1.05 ± 0.19	0.58 ± 0.02	0.71 ± 0.03*
20:4 (n-6)	0.79 ± 0.18	0.87 ± 0.22	0.66 ± 0.07	0.72 ± 0.26
20:5 (n-3)	0.55 ± 0.03	0.37 ± 0.33*	0.26 ± 0.03	0.37 ± 0.04
22:0	0.06 ± 0.01	0.15 ± 0.01*	0.09 ± 0.02	0.03 ± 0.00
22:1 (n-9)	0.07 ± 0.01	0.12 ± 0.03	0.12 ± 0.02	0.05 ± 0.01
22:6 (n-3)	0.84 ± 0.08	0.81 ± 0.13	0.32 ± 0.03	0.63 ± 0.13*

24:0	0.13 ± 0.00	0.16 ± 0.02	0.07 ± 0.01	0.08 ± 0.00
C>16	40.45 ± 1.50	38.12 ± 1.87	31.95 ± 1.39	39.15 ± 2.29*

Animals were maintained on a regular chow diet through the breeding process. Milk was collected from those dams had surviving pups to nurse without standardizing the litter size. Lactation day 2 and 12 represent early and mid-lactation, respectively. Milk fat was extracted by chloroform: methanol (2:1, v/v) and methylated by BF_3 methanol. FAMEs produced were analyzed by gas chromatography. The sample size of milk collected was indicated as the number written in the parentheses next to the genotype of dams. Data are presented as mean ± SEM. Student's *t*-test was used to determine the difference in fatty acids at the same stage between the two genotypes. *p<0.05 is considered statistically significant. Two-way ANOVA was used to determine the effect of lactating stage specifically for C<16, C=16, and C>16 fatty acids. The effect of lactating stage is statistically significant in all three categories.

Acknowledgement

We thank Nicole M. Spencer and Tessa N. Warner for pioneering this study. The authors' responsibilities were as follows–TNH and EY: designed the research and wrote the manuscript; TNH and FCM: conducted breeding experiments and milk collection; TNH and MIY: conducted measurements for milk composition and analyzed the data; TNH conducted most of the experiments and had primary responsibility for the final content of the manuscript. This work was funded by U.S. National Institutes of Health (DK088210) and U.S. Department of Agriculture (WIS01442).

References

Agarwal, A.K., Tunison, K., Dalal, J.S., Yen, C.L., Farese, R.V., Horton, J.D., and Garg, A. (2016). Mogat1 deletion does not ameliorate hepatic steatosis in lipodystrophic (Agpat2-/-) or obese (ob/ob) mice. J Lipid Res *57*, 616-630.

Anderson, S.M., Rudolph, M.C., McManaman, J.L., and Neville, M.C. (2007). Key stages in mammary gland development. Secretory activation in the mammary gland: it's not just about milk protein synthesis! Breast Cancer Res *9*, 204.

Barber, M.C., Clegg, R.A., Travers, M.T., and Vernon, R.G. (1997). Lipid metabolism in the lactating mammary gland. Biochim Biophys Acta *1347*, 101-126.

Beigneux, A.P., Vergnes, L., Qiao, X., Quatela, S., Davis, R., Watkins, S.M., Coleman, R.A., Walzem, R.L., Philips, M., Reue, K., et al. (2006). Agpat6--a novel lipid biosynthetic gene required for triacylglycerol production in mammary epithelium. J Lipid Res *47*, 734-744.

Cases, S., Stone, S.J., Zhou, P., Yen, E., Tow, B., Lardizabal, K.D., Voelker, T., and Farese, R.V. (2001). Cloning of DGAT2, a second mammalian diacylglycerol acyltransferase, and related family members. J Biol Chem *276*, 38870-38876.

Cases, S., Zhou, P., Shillingford, J.M., Wiseman, B.S., Fish, J.D., Angle, C.S., Hennighausen, L., Werb, Z., and Farese, R.V. (2004). Development of the mammary gland requires DGAT1 expression in stromal and epithelial tissues. Development *131*, 3047-3055.

Djiane, J., and Durand, P. (1977). Prolactin-progesterone antagonism in self regulation of prolactin receptors in the mammary gland. Nature *266*, 641-643.

Harwood, H.J., Chandler, C.E., Pellarin, L.D., Bangerter, F.W., Wilkins, R.W., Long, C.A., Cosgrove, P.G., Malinow, M.R., Marzetta, C.A., and Pettini, J.L. (1993). Pharmacologic consequences of cholesterol absorption inhibition: alteration in cholesterol metabolism and reduction in plasma cholesterol concentration induced by the synthetic saponin beta-tigogenin cellobioside (CP-88818; tiqueside). J Lipid Res *34*, 377-395.

Hennighausen, L., and Robinson, G.W. (2005). Information networks in the mammary gland. Nat Rev Mol Cell Biol *6*, 715-725.

Hernandez, L.L., Grayson, B.E., Yadav, E., Seeley, R.J., and Horseman, N.D. (2012). High fat diet alters lactation outcomes: possible involvement of inflammatory and serotonergic pathways. PLoS One *7*, e32598.

KENNEDY, E.P. (1961). Biosynthesis of complex lipids. Fed Proc *20*, 934-940.

Kuhn, N.J. (1969). Progesterone withdrawal as the lactogenic trigger in the rat. J Endocrinol *44*, 39-54.

Lehner, R., and Kuksis, A. (1996). Biosynthesis of triacylglycerols. Prog Lipid Res *35*, 169-201.

Miyazaki, M., Kim, H.J., Man, W.C., and Ntambi, J.M. (2001). Oleoyl-CoA is the major de novo product of stearoyl-CoA desaturase 1 gene isoform and substrate for the biosynthesis of the Harderian gland 1-alkyl-2,3-diacylglycerol. J Biol Chem *276*, 39455-39461.

Morag, M., Popliker, F., and Yagil, R. (1975). Effect of litter size on milk yield in the rat. Lab Anim *9*, 43-47.

Nelson, D.W., Gao, Y., Spencer, N.M., Banh, T., and Yen, C.L. (2011). Deficiency of MGAT2 increases energy expenditure without high-fat feeding and protects genetically obese mice from excessive weight gain. J Lipid Res *52*, 1723-1732.

Nelson, D.W., Gao, Y., Yen, M.I., and Yen, C.L. (2014). Intestine-specific deletion of acyl-CoA:monoacylglycerol acyltransferase (MGAT) 2 protects mice from diet-induced obesity and glucose intolerance. J Biol Chem *289*, 17338-17349.

Neville, M.C., McFadden, T.B., and Forsyth, I. (2002). Hormonal regulation of mammary differentiation and milk secretion. J Mammary Gland Biol Neoplasia *7*, 49-66.

Phan, C.T., and Tso, P. (2001). Intestinal lipid absorption and transport. Front Biosci *6*, D299-319.

Silberstein, G.B., Van Horn, K., Shyamala, G., and Daniel, C.W. (1996). Progesterone receptors in the mouse mammary duct: distribution and developmental regulation. Cell Growth Differ *7*, 945-952.

Smith, S.J., Cases, S., Jensen, D.R., Chen, H.C., Sande, E., Tow, B., Sanan, D.A., Raber, J., Eckel, R.H., and Farese, R.V. (2000). Obesity resistance and multiple mechanisms of triglyceride synthesis in mice lacking Dgat. Nat Genet *25*, 87-90.

Uauy, R., and Castillo, C. (2003). Lipid requirements of infants: implications for nutrient composition of fortified complementary foods. J Nutr *133*, 2962S-2972S.

Vergnes, L., Beigneux, A.P., Davis, R., Watkins, S.M., Young, S.G., and Reue, K. (2006). Agpat6 deficiency causes subdermal lipodystrophy and resistance to obesity. J Lipid Res *47*, 745-754.

Yen, C.L., Cheong, M.L., Grueter, C., Zhou, P., Moriwaki, J., Wong, J.S., Hubbard, B., Marmor, S., and Farese, R.V. (2009). Deficiency of the intestinal enzyme acyl CoA:monoacylglycerol acyltransferase-2 protects mice from metabolic disorders induced by high-fat feeding. Nat Med *15*, 442-446.

Yen, C.L., and Farese, R.V. (2003). MGAT2, a monoacylglycerol acyltransferase expressed in the small intestine. J Biol Chem *278*, 18532-18537.

Yen, C.L., Stone, S.J., Cases, S., Zhou, P., and Farese, R.V. (2002). Identification of a gene encoding MGAT1, a monoacylglycerol acyltransferase. Proc Natl Acad Sci U S A *99*, 8512-8517.

Chapter 5 Summary and Future Directions

In this dissertation, I identified various novel physiological functions of MGAT, including MGAT1 in systemic energy metabolism and MGAT2 in female reproduction and mammary gland functions. *Mogat1* deficiency in mice reduces energy expenditure and promotes adiposity in response to excess calories. These findings in mice highlight a potential target for treating obesity in humans, as a human genome wide association study also shows an inverse correlation between adipose *MOGAT1* expression levels and adiposity. *Mogat2* deficiency in female mice impairs the processes of achieving pregnancy, parturition, low numbers and a high neonatal mortality of offspring, and milk production. These findings in mice highlight a potential side effect of MGAT2 inhibitors on women, as MGAT2 is an important pharmaceutical target for treating obesity.

Mice lacking *Mogat1* exhibit reduced energy expenditure, which is associated with increased thermal insulation in a cold environment or decreased physical activity at room temperature and thermoneutrality. The mechanisms underlying thermal insulation is established, as these mice accumulate fat in various depots, including a layer of adipose tissue in the skin. However, it is not clear if the reduced physical activity is due to systemic or tissue-specific factors, because *Mogat1* expression is low yet detectable in the calf. Thus, I cannot exclude the possibility that local muscle *Mogat1* deficiency impairs muscle functions and causes the decrease in physical activity, which in turn results in reduced energy expenditure and increased adiposity. It warrants further investigation and may be delineated by tissue-specific *Mogat1* deficient mouse model.

Although both *Mogat1* and *Mogat2* coded enzymes catalyze MGAT activity in the test tube, they play divergent roles in systemic energy metabolism. While *Mogat2* deficiency increases energy expenditure and protects mice from metabolic disorders, *Mogat1* deficiency reduces energy expenditure and promotes adiposity in response to excess calories. Additionally, mice

lacking a functional *Mogat1* do not show a reduction in MGAT activity in any tissues examined. These raise the possibility that *Mogat1* coded enzyme may not catalyze MGAT activity yet other biochemical reactions *in vivo*. Indeed, this enzyme catalyzes various potential acyltransferase activities *in vitro*, despite the levels are not as striking as MGAT activity. In fact, various significant physiological functions are contributed by a tiny level of signaling lipids. Whether *Mogat1* coded enzyme regulates systemic energy metabolism by providing a lipid product from a novel yet unidentified biochemical reaction worth further characterization, and may be delineated by lipidomic analysis.

Mice lacking *Mogat2* exhibit impaired female reproduction. For parturition specifically, MGAT2 deficient dams have dysregulated progesterone metabolism and uterine prostaglandin synthesis. Although MGAT2 may limit prostaglandin synthesis indirectly by competing with monoacylglycerol lipase for 2-arachidonoylglycerol or promote prostaglandin synthesis by providing membrane phospholipids as substrates, neither can explain the lack of specific prostaglandins $PGF_{2\alpha}$ and PGE_2 in the uterus of MGAT2 deficient dams near parturition. It is likely that the dysregulated prostaglandin synthesis is the secondary effect of progesterone, as the effects of progesterone must be overcome by factors that coordinate myometrial contraction for successful parturition. Bypassing the potential impaired maternal myometrial contraction using Caesarean section delivery cannot rescue the pups, suggesting that the pups born to MGAT2 deficient dams may not be fully developed. Whether the impaired myometrial contraction is the result of dysregulated progesterone metabolism or the effect of failed fetal maturation signals needs further delineation and may highlight the potential effect of lipid metabolism on maternal-fetal communication.

Mice lacking *Mogat2* exhibit impaired mammary gland functions, including development and milk production. These failures may not result from local effect in the mammary glands, as *Mogat2* is not expressed in the milk producing mammary epithelium, and adipose-specific

MGAT2 deficiency do not cause impaired milk fat production. The failures may come from systemic inefficiency since other similar mouse model including GPAT4 and DGAT1 deficient females also exhibit the impaired mammary gland functions. The other underlying mechanism is dysregulated progesterone metabolism, as high progesterone circulation during pregnancy in MGAT2 deficient dams may block the milk production. Taken together with the parturition failure, it is likely that the functional progesterone metabolism regulated by MGAT2 may be the key to the success in both female reproduction and mammary gland functions. It may lead to another question in how MGAT2 modulates this hormonal regulation.

Various gaps remain in the delineation of underlying mechanisms in these newly identified MGAT functions. Nonetheless, these studies open new areas of research in lipid metabolism.